

HIGH SPEED EDGEWISE ROTOR COMPUTATIONAL ANALYSIS AND OPTIMIZATION AT  
HIGH INFLOW VELOCITIES ACHIEVED THROUGH FORWARD MAST TILT

by

CORY MICHAEL HITTE

Presented to the Faculty of the Graduate School of  
The University of Texas at Arlington in Partial Fulfillment  
of the Requirements  
for the Degree of

MASTER OF SCIENCE IN AEROSPACE ENGINEERING

THE UNIVERSITY OF TEXAS AT ARLINGTON

DECEMBER 2011

Copyright © by Cory Hitte 2011

All Rights Reserved

## ACKNOWLEDGEMENTS

I would like to thank my advisor, Dr. Don Wilson, for supporting me throughout my graduate education, for his guidance, and for his patient accommodation of the unique needs of “distance” students. I would like to thank my co-advisor, Dr. Dudley Smith, for his guidance and support, as well as being a constant source of knowledge both historical and technical. I would also like to thank Dr. Brian Dennis for serving on my committee and providing insight during my time as a student.

I would like to acknowledge Mark Dreier, Kirk Groninga, Dan Robertson, Brent Ross, and Steve Ivans for assisting me in various capacities during the multiple years of development and research that this project required. I would like to thank Bell Helicopter and Textron for the financial assistance made available to me in pursuit of this degree.

I would like to thank my amazing wife, Lauren, for her constant support and encouragement as I continued my education. Also, I would like to thank my parents for the many sacrifices they have made to provide opportunities for their children. Finally, I would like to thank the many family members and friends who have continually encouraged me to strive for that which is not easily achieved but always worthwhile.

November 22, 2011

## ABSTRACT

### HIGH SPEED EDGEWISE ROTOR COMPUTATIONAL ANALYSIS AND OPTIMIZATION AT HIGH INFLOW VELOCITIES ACHIEVED THROUGH FORWARD MAST TILT

Cory Hitte, M.S.

The University of Texas at Arlington, 2011

Supervising Professor: Don Wilson

Increased forward flight speed has long been the desire of the rotorcraft industry. Novel designs, such as compounds and tilt rotors have allowed for speed envelope expansion, but not without incurring performance hindrances unique to each configuration. Designs that utilize low disc loading edgewise rotors, which offer efficient flight at high speeds while maintaining hover performance, are desirable. Such designs require increased flapping capability and/or mast tilt in order to achieve the necessary thrust orientation required for overcoming aircraft drag. The combination of speed and thrust vector inclination yields a relatively undocumented region of rotorcraft performance. In particular, the effects of forward mast inclination, and the subsequent high airflow ingestion or “inflow”, requires further analysis for accurate performance prediction.

This thesis presents a recently developed analytical tool meant to capture rotor aerodynamic performance throughout the flight regime with particular attention paid to analysis of the effects of mast angle inclination and subsequent inflow at high speed. MATLAB<sup>®</sup> Version 7 was used in conjunction with wind tunnel generated compressible NACA airfoil tables to create a modified Blade Element Model (BEM). The BEM is capable of conducting compressible rotor analysis at all speeds, ambient air conditions, mast angles, and geometries. Model validation to known historical data is presented.

A baseline rotor geometry was selected and subjected to sweeps of mast angle from 0 to 30 degrees and speed from 0 to 250 knots and the performance was determined. The degradation of available baseline rotor thrust as a function of speed is illustrated. Power coefficients (profile, induced, and total), H-force coefficient, peak blade torsional moments, and required control inputs as a function of thrust coefficient are presented. Additionally, a design parameter trade study is presented illustrating the concurrent effects on high speed performance of varying tip speed, solidity, number of blades, and radius.

## TABLE OF CONTENTS

ACKNOWLEDGEMENTS .....	iii
ABSTRACT .....	iv
LIST OF ILLUSTRATIONS.....	viii
LIST OF TABLES .....	x
NOMENCLATURE .....	xi
Chapter .....	Page
1. INTRODUCTION.....	1
1.1 Introduction .....	1
1.2 Background and Motivation .....	1
1.3 Edgewise Rotor Performance Review .....	3
1.4 Objectives .....	4
1.5 Thesis Contributions .....	5
1.6 Historical Study and Literature Survey .....	6
2. METHODOLOGY .....	7
2.1 Overview .....	7
2.2 Mathematical Model – Blade Element Method .....	7
2.3 Computational Methodology .....	16
2.4 Notable Assumptions and Omissions .....	19
2.5 Fundamental and Preliminary Expectations .....	21
2.6 Model Validation .....	23

2.7 Baseline Rotor Design and Operational Setting .....	29
2.8 Test Matrix Description .....	31
3. RESULTS AND DISCUSSION.....	32
3.1 Overview .....	32
3.2 Baseline Rotor Study – Performance Effects due to Variation of Aircraft Velocity.....	32
3.3 Baseline Rotor Study – Performance Effects due to Variation of Forward Mast Tilt...	41
3.4 Baseline Rotor Study – Parameter Variation Study.....	47
4. CONCLUSION .....	50
APPENDIX	
A. BASELINE ROTOR ANALYSIS STUDY DATA.....	52
B. ROTOR PARAMETER VARIATION STUDY DATA .....	87
C. ROTOR ANALYSIS TOOL SOURCE CODE .....	98
REFERENCES.....	112
BIOGRAPHICAL INFORMATION .....	113

## LIST OF ILLUSTRATIONS

Figure	Page
2.1-Rotor Tip Path Plane ( $\alpha_{TPP}$ ) Relationship to Long. Flapping ( $a_{1s}$ ) and Mast Tilt ( $\alpha_m$ ).....	8
2.2-Velocity Transformation from Aircraft Axes to Rotor Shaft Axes .....	10
2.3-Velocity Transformation from Rotor Shaft Axes to Rotor Blade Axes .....	11
2.4-Velocity Transformation from Rotor Blade Axes to Blade Element Axes .....	13
2.5-TSTM Sensitivity Matrix .....	17
2.6-Rotor Mesh Azimuthal and Radial Distribution .....	18
2.7-Computational Tool Program Logic Flow Chart.....	19
2.8- $C_T$ vs $C_P$ Model Validation Case (Teetering Rotor, $\mu=.85$ , $M=.9$ ) .....	24
2.9- $C_T$ vs $C_H$ Model Validation Case (Teetering Rotor, $\mu=.85$ , $M=.9$ ) .....	25
2.10- $C_T$ vs $\theta_o$ Model Validation Case (Teetering Rotor, $\mu=.85$ , $M=.9$ ) .....	25
2.11- $C_T$ vs $B_1$ Model Validation Case (Teetering Rotor, $\mu=.85$ , $M=.9$ ).....	26
2.12- $C_T$ vs $C_P$ Model Validation Case (Articulated Rotor, $\mu=.86$ , $M=.92$ ) .....	26
2.13- $C_T$ vs $C_H$ Model Validation Case (Articulated Rotor, $\mu=.86$ , $M=.92$ ) .....	27
2.14- $C_T$ vs $\theta_o$ Model Validation Case (Articulated Rotor, $\mu=.86$ , $M=.92$ ) .....	27
2.15- $C_T$ vs $B_1$ Model Validation Case (Articulated Rotor, $\mu=.86$ , $M=.92$ ).....	28
2.16-Baseline Rotor Blade .....	30
2.17-Baseline Rotor System Design .....	30
3.18-Advancing Tip Mach Number as a Function of $V_f$ and $\alpha_m$ .....	33
3.19-Advance Ratio, $\mu$ , as a Function of $V_f$ and $\alpha_m$ .....	34
3.20-Percent Rotor Area in Reversed Flow as a Function of $V_f$ and $\alpha_m$ .....	35
3.21- $C_T$ vs $C_P$ as a Function of $V_f$ ( $\alpha_m = 20\text{deg}$ ).....	36
3.22- $C_T$ vs $C_{P_{ind}}$ and $C_{P_{pro}}$ as a Function of $V_f$ ( $\alpha_m = 20\text{deg}$ ) .....	37



3.23- $C_T$ vs $C_H$ as a Function of $V_f$ ( $\alpha_m = 20\text{deg}$ ) .....	38
3.24- $C_T$ vs $M_{\text{Torsion}}$ as a Function of $V_f$ ( $\alpha_m = 20\text{deg}$ ) .....	39
3.25- $C_T$ vs $\theta_o$ as a Function of $V_f$ ( $\alpha_m = 20\text{deg}$ ) .....	40
3.26- $C_T$ vs $B_1$ as a Function of $V_f$ ( $\alpha_m = 20\text{deg}$ ) .....	40
3.27-Advancing Blade Inflow Angle (.75 Radius) as a Function of $V_f$ and $\alpha_m$ .....	41
3.28- $C_T$ vs $C_P$ as a Function of $\alpha_m$ ( $V_f = 200\text{kt}$ ) .....	42
3.29- $C_T$ vs $C_{P_{\text{pro}}}$ and $C_{P_{\text{ind}}}$ as a Function of $\alpha_m$ ( $V_f = 200\text{kt}$ ) .....	43
3.30- $C_T$ vs $C_H$ as a Function of $\alpha_m$ ( $V_f = 200\text{kt}$ ) .....	44
3.31- $C_T$ vs $M_{\text{Torsion}}$ as a Function of $\alpha_m$ ( $V_f = 200\text{kt}$ ) .....	45
3.32- $C_T$ vs $\theta_o$ as a Function of $\alpha_m$ ( $V_f = 200\text{kt}$ ) .....	46
3.33- $C_T$ vs $B_1$ as a Function of $\alpha_m$ ( $V_f = 200\text{kt}$ ) .....	46

LIST OF TABLES

Table	Page
2.1-Model Validation-Historical Data Test Geometries .....	24
2.2-Baseline Rotor Geometric and Operational Description .....	29
2.3-Study Test Matrix .....	31
3.4-Parameter Variation Performance Deltas Compared to Baseline Rotor .....	48

## NOMENCLATURE

$a$	Ambient Speed of Sound
$a_{1s}$	Blade Longitudinal Flapping Angle
$A_1$	Blade Lateral Cyclic Angle
$b$	Number of Blades Per Rotor
$b_{1s}$	Blade Lateral Flapping Angle
$B_1$	Blade Longitudinal Cyclic Angle
$C_P$	Rotor Total Power Coefficient
$C_{P\_ind}$	Rotor Induced Power Coefficient
$C_{P\_Pro}$	Rotor Profile Power Coefficient
$C_H$	H-force Coefficient
$C_T$	Thrust Coefficient
$c$	Rotor Blade Chord
$c_l$	Blade Element Lift Coefficient
$c_d$	Blade Element Drag Coefficient
$c_m$	Blade Element Moment Coefficient
$D$	Airfoil Drag
$D_{pro}$	Rotor Profile Drag
$D_{ind}$	Rotor Induced Drag
$D_{inp}$	Inplane Drag
$h$	Iteration Step Size (trapezoid method)
$H$	H-force
$kt$	Knot
$L$	Blade Lift

$M$	Local Blade Element Mach Number
$M_{\text{Torsion}}$	Blade Aerodynamic Torsional Moment
$M_{\text{lat}}$	Rotor Lateral (rolling) Aerodynamic Moment
$M_{\text{long}}$	Rotor Longitudinal (pitching) Aerodynamic Moment
$P$	Rotor Total Power Required
$P_{\text{pro}}$	Rotor Profile Power Coefficient
$P_{\text{ind}}$	Rotor Induced Power
$Q$	Rotor Torque
$Q_{\text{pro}}$	Rotor Torque due to Profile Power
$Q_{\text{ind}}$	Rotor Torque due to Induced Power
$r$	Blade Radial Increment
$r_e$	Equivalent Blade Radius
$\text{rpm}$	Revolutions Per Minute
$R$	Blade Radius
$T$	Rotor Thrust
$U_{\text{perp}}$	Blade Element Perpendicular Velocity Component
$v$	Rotor Induced Velocity
$v_o$	Rotor Hover Induced Velocity
$V_{\text{Tip}}$	Blade Tip Speed
$V_f$	Aircraft Flight Velocity
$V_c$	Aircraft Climb Velocity
$V_{\text{ho}}$	Aircraft Horizontal Velocity
$V_{\text{ax}}$	Disc Axial Velocity
$V_{\text{inp}}$	Disc Inplane Velocity
$V_{\text{b\_perp}}$	Rotor Blade Perpendicular Velocity
$V_{\text{b\_parallel}}$	Rotor Blade Spanwise Velocity
$V_{\text{ax\_tot}}$	Total Disc Perpendicular (Axial) Velocity

$\alpha_b$	Blade Element Angle of Attack
$\alpha_c$	Control Plane Angle
$\alpha_m$	Mast Tilt Angle
$\beta$	Blade Flapping Angle
$\rho$	Ambient Density
$\varphi$	Blade Element Inflow Angle
$\theta_{tot}$	Total Blade Geometric Pitch
$\theta_T$	Blade Twist Angle
$\theta_o$	Blade Collective Angle
$\sigma$	Rotor Solidity
$\mu$	Advance Ratio
$\omega$	Rotor RPM
$\psi$	Blade Azimuth Angle

## CHAPTER 1

### INTRODUCTION

#### 1.1 Introduction

The rotorcraft industry has long pursued increased speed. Speed allows for quicker ingress into and egress from hostile territory for the military, greater operator productivity in the commercial arena, and a more rapid response in the medical EMS industry. The complex aerodynamic phenomena that present themselves when a rotor is subjected to high speeds are difficult to correctly capture in closed form performance methods. Furthermore, establishing such data through wind-tunnel testing or flight test is costly in terms of time, equipment, and capital. Thus, computational modeling is desirable in order to predict thrust, power, and required control input in the analysis of rotors in an accurate, cost-effective, and timely manner. This study utilizes a classic blade element model, developed by the author in MATLAB®. The model captures rotor aerodynamic performance characteristics and is specifically modified to represent the effects of forward mast tilt and compressibility during high speed edgewise rotor operation. The primary goal of this study is to develop and calibrate a design tool to establish the aerodynamic performance and design sensitivities of high speed edgewise rotors, particularly under the influence of high inflow due to forward mast tilt.

#### 1.2 Background and Motivation

While efficient hovering performance is inherent in the classic edgewise rotor configuration, high speed capability comes with increasingly stiff performance penalties. As speed increases, main rotor thrust and subsequent control input must be continually increased to maintain altitude and velocity. Velocity dissymmetry across the rotor, compressibility effects, and retreating blade stall create cumulative effects that causes the available thrust capability of

the main rotor to diminish with increasing speed. Furthermore, oscillatory loading from these dissymmetries introduce destructive vibratory forces, corresponding occupant discomfort, and empty weight penalties from fatigue considerations. When combined with the aforementioned thrust limitations, these define the “effective speed limit” for conventional rotorcraft. The standard approach to overcoming these hurdles and expanding the rotorcraft speed envelope has been to alter the operating physics of the standard helicopter edgewise rotor by incorporating auxiliary sources of lift and propulsive thrust, i.e. compounding. As a result, the main rotor’s thrust requirements are reduced, allowing it to be operated at higher speeds without incurring the aforementioned limits. However, these compound configurations introduce their own issues: weight, drag, download, and power penalties which diminish their desirable performance effects.

To achieve forward velocity with an edgewise rotor, the main rotor thrust vector must be oriented such that necessary lift is maintained while aircraft drag is overcome. This can be accomplished through flapping of the individual blades, forward inclination of the rotor mast, or a combination of the two. Historically, rotorcraft have utilized flapping as the preferred method, due to mechanical simplicity and the relatively low design cruise speeds which require only minor tilt of the rotor’s thrust vector. At high speeds, mast tilt allows for greater inclination of the thrust vector to provide necessary propulsive force while limiting to some degree the oscillatory load issues that would result from high degrees of flapping to achieve a similar inclination. At these high angles of mast tilt, the normal velocity component of the freestream into the rotor results in an operating condition similar to a rotor in climb. This high rotor “inflow” velocity when coupled with the high edgewise velocities is a relatively unexplored field for high speed edgewise flight.

Unfortunately, the availability of data for high speed edgewise rotors inclined to mast angles greater than approximately 10 degrees is limited. Most closed form performance models complicate the matter by minimizing or negating the effect of forward mast tilt by applying small angle assumptions. Additionally, many models omit the effects of compressibility and non-linear

aerodynamics, further enforcing the accepted speed limitations of conventional rotorcraft. Subsequently, there is great motivation for the creation of analytical models capable of predicting performance of edgewise rotors at high speed and high forward mast inclination. A computational tool which allows for high fidelity, rapid performance prediction and sensitivity analysis would aid designers of high speed rotorcraft in their initial configuration trade studies as well as detailed design.

### 1.3 Edgewise Rotor Performance Review

Analysis of edgewise rotors at speeds below 170 knots and tip path plane angles of approximately 10 degrees or less is relatively well understood. At such conditions, closed form performance equations accurately capture rotor performance and subsequent modeling of the rotor physics is not computationally involved (Ref 6). As speed and the rotor tip path angle increase beyond this range, the effects of compressibility, reversed flow, stall, and high inflow complicate analysis. Closed form equations will overestimate available thrust while power required will be overly optimistic. Consequently, a higher fidelity methodology analysis must be used.

Blade element analysis is one such method. Blade element analysis models each rotor blade as a series of individual airfoil segments. The velocity conditions prescribed by the rotor rpm and aircraft flight condition are computed as a function of the radial station along the blade and the azimuthal position of the blade in its rotation. Radial and azimuthal variations due to the collective input, cyclic input, blade twist, and resulting inflow angles are further assessed for each segment. As a result, each airfoil segment, or blade element, is subjected to its own unique velocity and angle of attack. With airfoil type, angle of attack, and velocity known, it is possible to assign lift, drag, and moment coefficients to each blade element. The availability of compressible airfoil tables which sweep through an angle of attack range of -180 degrees to +180 degrees allows for highly accurate prediction of the resulting element forces and Mach



effects. With forces and moment contributions of each differential element known, simple integration in the radial and azimuthal dimensions yield total rotor forces, moments, and torque.

For the purposes of this analysis, the normal to the rotor tip path plane is defined coincident to the mast. Thus, it is necessary for the rotor flapping contribution in the rotor tip path plane be eliminated, while the rotor aerodynamic pitching and rolling moments at the hub are trimmed to zero. Perturbation of the lateral and longitudinal cyclic allows for creation of an invertible sensitivity matrix that upon iteration yields the requisite trim control inputs.

As the rotor model is swept through the range of speeds, mast angles and available thrust performance data is recorded. Items of interest include rotor H-force, profile power, induced power, torque, and requisite control inputs. This data allows one to map the available area of rotor operation and visualize the effects of speed and forward mast inclination on the performance of the rotor. Additionally, designers may assess the sensitivities to parameter variation, allowing for rotor optimization.

#### 1.4 Objectives

The main objectives of this thesis are:

1. Affirm accuracy of the aforementioned blade element analysis software by correlating to known historical wind tunnel results. The desired wind tunnel data to be tested against should present high speed conditions with multiple degrees of forward mast tilt such that compressibility and inflow calculations can be validated.
2. Illustrate edgewise rotor performance characteristics of a selected baseline rotor design throughout a speed range of 0 to 250 knots and mast tilt from 0 to 30 degrees forward.
3. Illustrate the effects of rotor parameter variation at a prescribed high speed and high inflow flight condition such that design sensitivities and rotor performance trends may be attained.

All data will result from numerical simulation using a blade element analysis code modified to reflect the effects of compressibility and high inflow realized during high speed edgewise rotor operation at forward mast tilt. Experimental results would serve to validate all predicted data as well as provide a calibration metric for similar analytical tools.

A literature survey concerning the historical development of the high speed rotorcraft field, analytical approaches to blade element analysis, as well as available experimental data regarding high speed rotor performance at various degrees of mast tilt is presented in Section 1.6. A description of the mathematical blade element model, a thorough presentation of the previously mentioned analytical tool, as well as a detailed illustration of the validation of said tool are presented in Chapter 2. Results of the performance analysis and parameter variation of the baseline rotor are given in Chapter 3. Conclusions are then presented in Chapter 4. Appendices A and B detail the source code of the analytical tool and present all relevant performance charts.

### 1.5 Thesis Contributions

The analytical tool which is the basis for this thesis is a modified version of traditional blade element analytical methods presented in numerous rotorcraft texts. The descriptions provided by Stepniewski and Keys as well as Prouty proved extremely instructional (Ref 6, 7). Compressible wind tunnel test data for the NACA 0012 airfoil is utilized to provide accurate compressibility, stall, and reversed flow results (Ref 1). Tip loss estimation models developed by Wald were utilized within the blade element model (Ref 7). The MATLAB<sup>®</sup> Help files contributed extensively to the development of the computational tool used for all subsequent analysis (Ref 5). Finally, rotor wind tunnel test data provided by NASA are utilized in the validation of the computational tool (Ref 4).

### 1.6 Historical Study and Literature Survey

The origination of rotorcraft can be traced back to Chinese bamboo flying toys in 400 BC and later, da Vinci's aerial screw in the early 1480's (Ref 2). Since then, rotorcraft development continued as scientists and engineers pursued the unique flight capabilities not inherent to rotorcraft's fixed wing brethren. The ability to take off and land vertically, hover for extended periods of time, reach remote locations, and land on undeveloped terrain provided a niche by which the rotorcraft industry was born. While hovering will always be the reason for the existence of rotorcraft, forward flight capability is the metric by which future platform advancement is and will be driven. The ability to overcome the physical impediments inherent to rotor aerodynamics at high speed has spurred innovative approaches to configuration modification and analysis. With the application and extension of present-day technology, higher speed and increased range can be achieved (Ref 3). The key to increased rotorcraft speed capability is and has always been the offloading of the main rotor through either ancillary lift and/or propulsion i.e. compounding. Tiltrotors and other present day configurations exist solely to expand the rotorcraft speed envelope while maintaining efficient VTOL capability.

Increased forward flight requirements have also driven the need for higher fidelity rotor performance analysis with respect to the effects of speed and increased inflow. The ability of closed form equations using classical assumptions diminishes as compressibility, retreating blade stall, and inflow begin to create previously unaccounted for phenomena (Ref 6). Computational analysis and physical testing (wind tunnel, flight test) provide a means by which new equations and estimation techniques can be validated. Available high speed, high inflow test data from NASA and other sources allows for the development and calibration of a new series of tools that can rapidly predict the performance of new rotorcraft concepts (Ref 4).

## CHAPTER 2

### METHODOLOGY

#### 2.1 Overview

In order to analyze the aerodynamic characteristics of rotors in high speed edgewise operation, an adequate mathematical model must be employed. Notably, the model must be capable of capturing the effects of compressibility and forward mast tilt. Several mathematical methods exist for the accurate reproduction of rotor aerodynamics (Ref 2, 6, 7). Momentum, vortex-lattice, and the blade element method are among the most commonly used. The blade element method was chosen for its ability to utilize compressible tabular airfoil data, availability of instructional resources, as well as ease of computation. Once a suitable mathematical model is defined, a computational program of the model needs to be created and validated. Such a computational tool allows for the rapid, high fidelity experimentation and parameter variation required for the attainment of physical characteristics and sensitivity trends. The details pertaining to the mathematical model and computational tool developed for this study are explained in the following sections.

#### 2.2 Mathematical Model – Blade Element Method

The blade element method provides the ability to accurately predict the forces and moments acting on a rotor during high speed flight. As its name states, the method requires division of the rotor blade into sections or elements defined radially along the span of the blade. Each increment corresponds to a blade airfoil section which is subjected to the local flight conditions. The operating flight condition varies for each combination of radial and azimuthal location of the segment. The following explanation of a blade element model is detailed in

Reference 7 with the exception of modifications made to better capture compressibility and mast tilt effects. In order to generate respective flight conditions for each element, the overall rotor flight condition i.e. speed and orientation must be transformed from the inertial axes to the blade element axes. The aircraft velocity is defined by  $V_i$ , which has components  $V_c$ , climb velocity, and  $V_{ho}$ , horizontal velocity. The inclination of the disc relative to the aircraft axes is defined as  $\alpha_m$ , or mast angle. Equation 2.1 details the relationship between longitudinal flapping,  $a_{1s}$ , and  $\alpha_m$  to the rotor tip path plane angle,  $\alpha_{TPP}$ . Figure 2.1 further illustrates this relationship.

$$\alpha_{TPP} = \alpha_m - a_{1s} \quad (2.1)$$

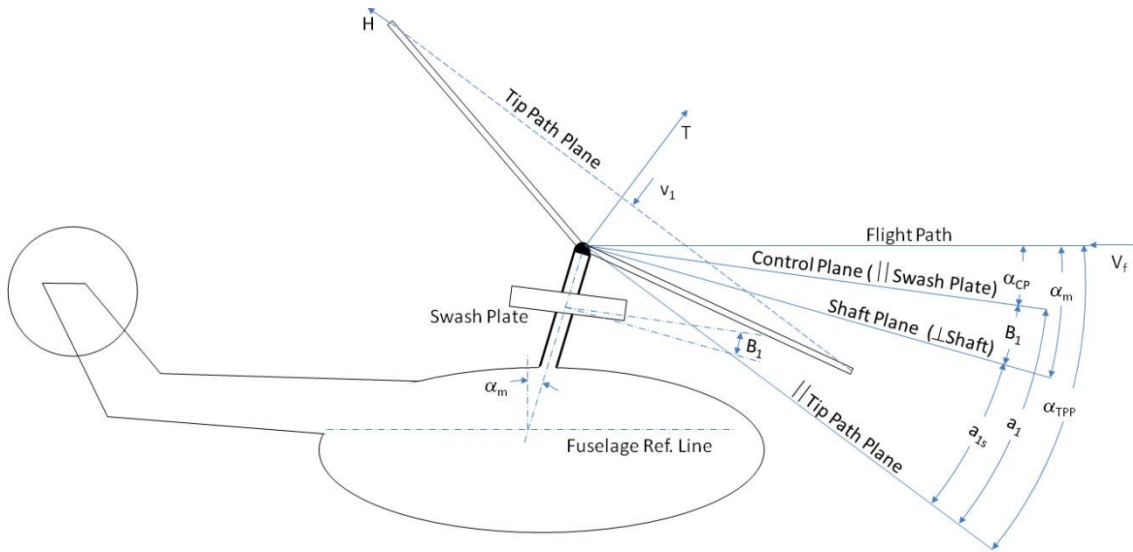


Figure 2.1-Rotor Tip Path Plane ( $\alpha_{TPP}$ ) Relationship to Long. Flapping ( $a_{1s}$ ) and Mast Tilt ( $\alpha_m$ )

For the purposes of this study, mast angle will equal the tip path plane orientation as well, i.e. all points will be trimmed to zero steady state flapping. Ironically, forward mast tilt is given a “-” designation due to the method's origination in auto-gyro analysis. For the purposes of this study, all mast angles presented here are positive and refer to forward tilt. The first

velocity transformation occurs through  $\alpha_m$ , resulting in disc-perpendicular (axial) velocity,  $V_{ax}$ , and disc-parallel (inplane) velocity,  $V_{inp}$ . In addition to the axial flow due to  $V_i$ , rotor induced velocity,  $v$ , and axial velocities due to flapping must be calculated and further combined to yield the total disc perpendicular (axial) velocity,  $V_{ax\_tot}$ . Flapping velocities are negated since the rotor will be trimmed to zero flapping for all test cases. Rotor induced velocity is most notably a function of rotor thrust,  $T$ , and diminishes at high speeds. Reference 7 provides a simple method for estimating the change in  $v$  due to speed. Furthermore, it will be assumed that  $v$  is uniform both radially and azimuthally across the rotor disc, the consequences of which are discussed later. Equations 2.2-2.6 detail the transformation from aircraft to rotor shaft axes through  $\alpha_m$  as well as the calculation of rotor induced velocity in both hover ( $v_o$ ) and forward flight ( $v$ ). Figure 2.2 further illustrates this transformation.

$$V_{ax} = -V_c \cos \alpha_m + V_{ho} \sin \alpha_m \quad (2.2)$$

$$V_{inp} = -V_{ho} \cos \alpha_m + V_c \sin \alpha_m \quad (2.3)$$

$$v_o = \sqrt{\frac{T}{2\rho\pi R^2}} \quad (2.4)$$

$$v = v_o \left[ \sqrt{-\frac{\left(\frac{V_f}{v_o}\right)^2}{2} + \sqrt{\frac{\left(\frac{V_f}{v_o}\right)^2}{4} + 1}} \right] \quad (5)$$

$$V_{ax\_tot} = V_{ax} - v - r\dot{\beta} - V_{ho}\beta \cos \psi \quad (2.6)$$

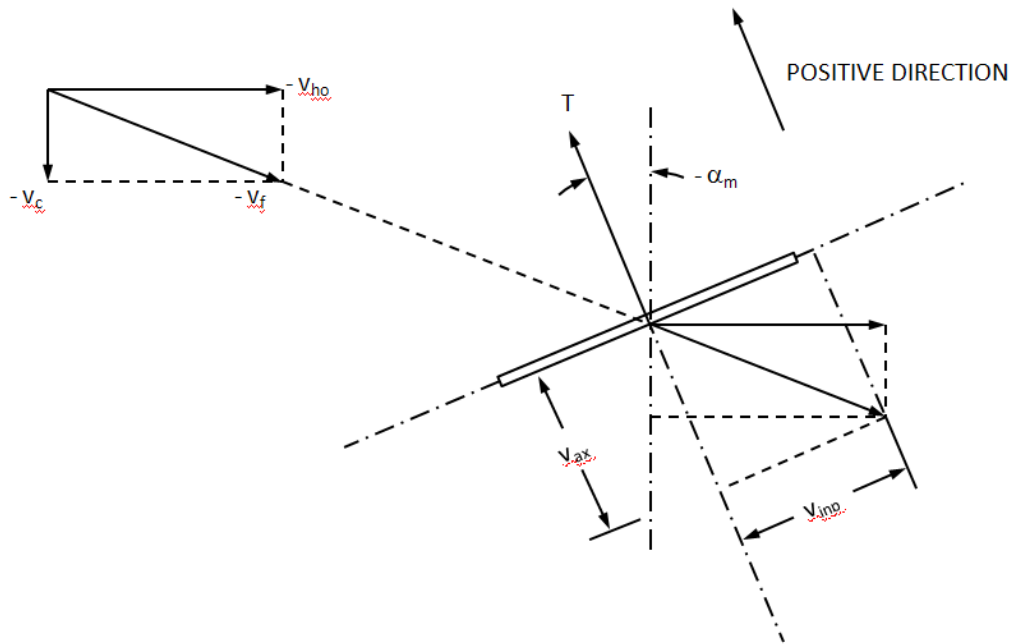


Figure 2.2-Velocity Transformation from Aircraft Axes to Rotor Shaft Axes

The next step involves transforming the velocity components from rotor shaft axes to rotor blade axes.  $V_{inp}$  is decomposed through  $\psi$  into radial,  $V_{b\_parallel}$ , and tangential,  $V_{b\_perp}$ , rotor blade velocity components. Equations 2.7-2.8 detail the transformation from rotor shaft to rotor blade axes through the mast tilt angle. Figure 2.3 further illustrates this transformation.

$$V_{b\_parallel}(\psi) = V_{inp} \cos \psi \quad (2.7)$$

$$V_{b\_perp}(\psi) = V_{inp} \sin \psi \quad (2.8)$$

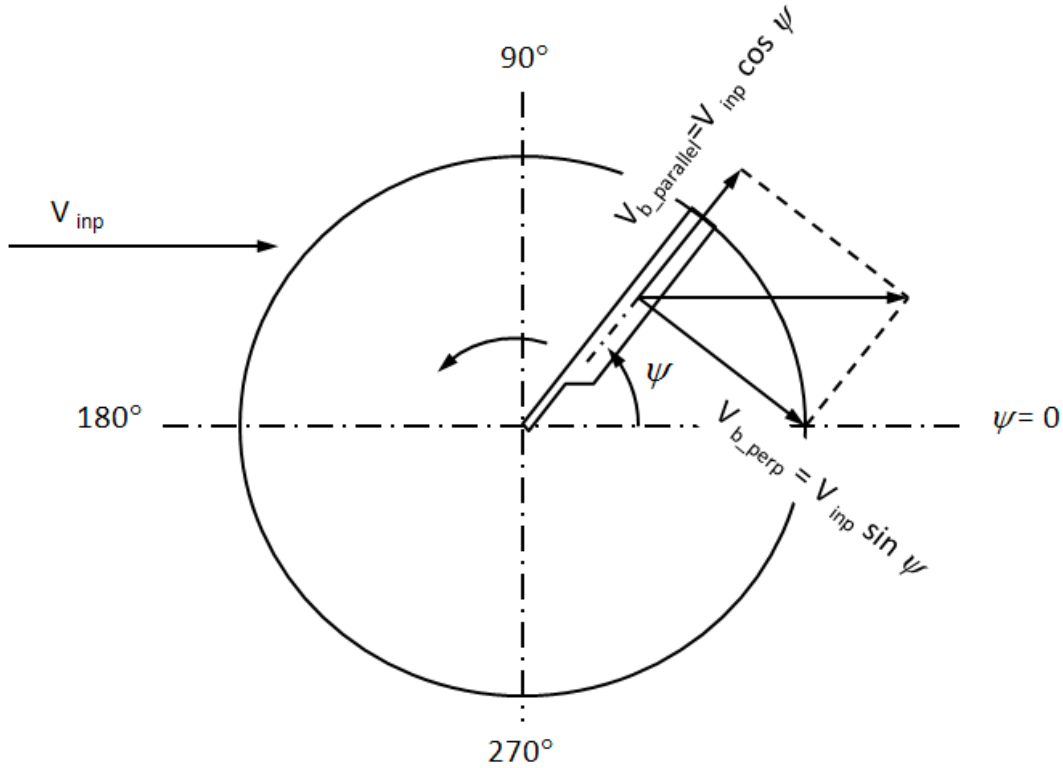


Figure 2.3-Velocity Transformation from Rotor Shaft Axes to Rotor Blade Axes

$V_{b\_perp}$  must now be combined with the rotor tip speed,  $V_{tip}$ , of the rotor due to operational rotor RPM,  $\omega$ , in order to accurately represent perpendicular rotor velocity distribution along the radial span of the blade. Equations 2.9-2.10 illustrate the perpendicular blade element velocity,  $U_{perp}$  as a function of azimuth and blade radius.

$$V_{tip} = R\omega \quad (2.9)$$

$$U_{perp}(r, \psi) = V_{tip}r + V_{b\_perp} \quad (2.10)$$

With the velocities occurring both axially through the disc and perpendicular to the blade as a function of radius and azimuth position known, it is now possible to model the unique environment of each differential blade element. In order to estimate the forces and moments



using compressible airfoil wind-tunnel data tables, one must know the local angle of attack,  $\alpha_b$ , and Mach number,  $M$  as functions of radius and azimuth position. The angle of attack on each differential blade element results from two separate entities: geometric pitch and inflow angle. The geometric pitch,  $\theta_{tot}$ , of the blade is defined as the angular displacement of the blade relative to the hub as a function of blade radius and azimuth position. Design blade twist,  $\theta_t$ , collective,  $\theta_o$ , longitudinal cyclic,  $B_1$ , and lateral cyclic input,  $A_1$ , all contribute to the total geometric pitch. The inflow angle,  $\varphi$ , is defined as the change in angle of attack due to the influence of axial inflow velocity through the rotor disc. Equations 2.11-2.13 detail the calculation of  $\alpha_b$  and its subsequent components.

$$\theta_{tot}(r, \psi) = \theta_t(r) + \theta_o(r, \psi) + A_1(r, \psi) \cos \psi + B_1(r, \psi) \sin \psi \quad (2.11)$$

$$\varphi(r, \psi) = \tan^{-1} \left( \frac{V_{ax\_tot}}{U_{perp}} \right) \quad (2.12)$$

$$\alpha_b(r, \psi) = \theta_{tot} - \varphi \quad (2.13)$$

Local Mach number is a function of ambient speed of sound,  $a$ ,  $U_{perp}$ , and  $V_{ax\_tot}$ . Equation 2.14 details the calculation of local blade element Mach number.

$$M(r, \psi) = \frac{\sqrt{U_{perp}^2 + V_{ax\_tot}^2}}{a} \quad (2.14)$$

With local  $\alpha_b$  and Mach numbers known, it is possible to retrieve values of lift, drag, and moment coefficients ( $c_l$ ,  $c_d$ ,  $c_m$ ) from tabular wind tunnel airfoil tables (Ref. 1). Ideally, these tables will present data covering an entire angular rotation (-180 to +180 degrees) and Mach number sweep of the airfoil (0 to >1 preferred). The output lift, drag, and moment coefficients

are used to calculate differential forces and moments for each blade element. For this study, the term induced drag is related to the drag caused by the inflow angle on the local blade elements rather than that of the traditional induced velocity of the entire rotor disc as described in Reference 7. Figure 2.4 illustrates the orientation of velocity components, angles, and forces relative to the differential blade element axes.

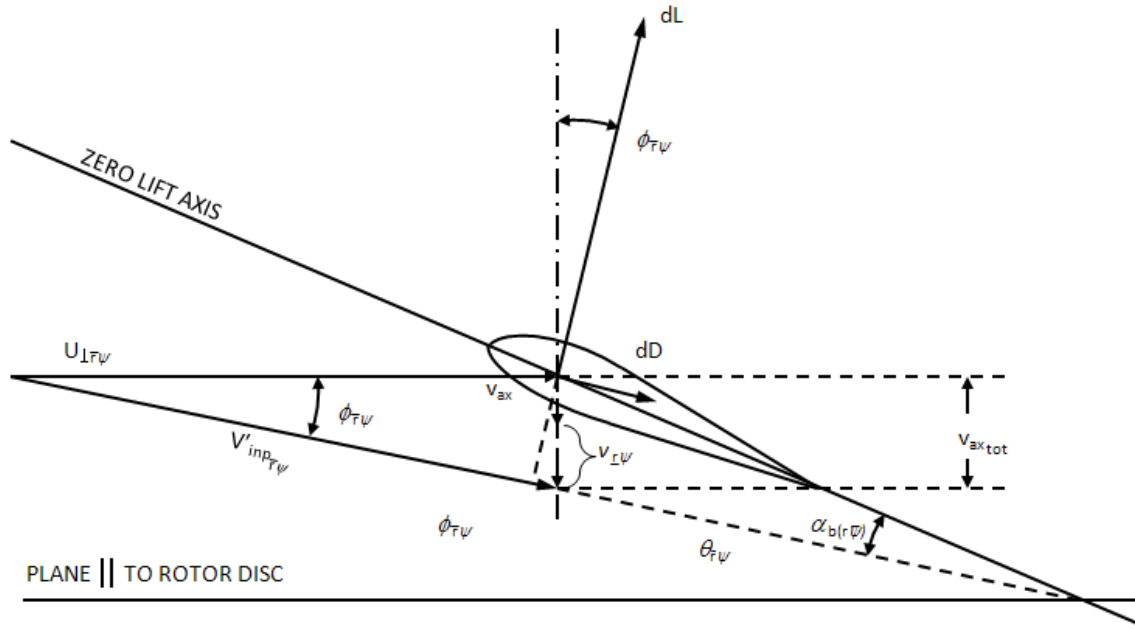


Figure 2.4-Velocity Transformation from Rotor Blade Axes to Blade Element Axes

The blade element forces can be manipulated such that total blade forces, torques, and powers are calculated. For example, the differential blade element induced and profile drag can be transformed into the inplane blade drag which can then be converted into total blade H-force. Additionally, blade element lift (L) can be converted to total blade thrust (T). Figure 2.1 details the orientation of total blade thrust (T) and H-force (H) relative to the tip path plane. Equations 2.15-2.17 detail the formulation of blade element lift and drag components. Equations 2.18-2.26 detail the formulation of the differential lift, thrust, total rotor in-plane drag, H-force, torque, lateral aerodynamic blade moment, and longitudinal aerodynamic blade moment as functions of

radius and azimuth position. It should be noted that, contrary to Reference 7, small angle assumption is not applied in order to accurately represent the effects of forward mast tilt,  $\alpha_m$ .

$$dL_{blade}(r, \psi) = \frac{1}{2} R \rho c(r) c_l U_{perp}^2 d\bar{r} \quad (2.15)$$

$$dD_{pro}(r, \psi) = \frac{1}{2} R \rho c(r) c_d U_{perp}^2 \cos \varphi d\bar{r} \quad (2.16)$$

$$dD_{ind}(r, \psi) = dL \sin \varphi d\bar{r} \quad (2.17)$$

$$dD_{inp}(r, \psi) = (dD_{pro} + dD_{ind}) \quad (2.18)$$

$$dH(r, \psi) = dD_{inp} \sin \psi d\bar{r} \quad (2.19)$$

$$dQ(r, \psi) = dD_{inp} R \bar{r} d\bar{r} \quad (2.20)$$

$$dQ_{pro}(r, \psi) = dD_{pro} R \bar{r} d\bar{r} \quad (2.21)$$

$$dQ_{ind}(r, \psi) = dD_{ind} R \bar{r} d\bar{r} \quad (2.22)$$

$$dT(r, \psi) = (dL_{blade} \cos \varphi - dD_{pro} \sin \varphi) \quad (2.23)$$

$$dM_{lat}(r, \psi) = dTR \sin \psi d\bar{r} \quad (2.24)$$

$$dM_{long}(r, \psi) = dTR \cos \psi d\bar{r} \quad (2.25)$$

$$dM_{Torsion}(r, \psi) = \frac{1}{2} R \rho c^2(r) c_m U_{perp}^2 d\bar{r} \quad (2.26)$$

A standard correction is applied to relevant forces due to loss of lift caused by aerodynamic vortex rollup at the blade tips. Wald provides a method by which the “effective” blade radius can be calculated as a function of thrust in order to aptly represent the true lifting span of the blade accounting for the vortex rollup or “tip loss” (Ref 7). Equation 2.27 details this correction for tip loss.

$$r_e = 1 - 1.98\sqrt{C_T/b} \quad (2.27)$$

With the differential blade forces and moments known, two-dimensional integration in the radial and azimuthal directions is applied. This action yields each individual rotor blade’s force and moment contributions to the total rotor disc. Each blade’s forces and moments must then be summed in order to calculate the total rotor output. The conversion of output rotor torque allows for rotor power required to be calculated. Equations 2.28-2.30 details the calculation of total (P), profile ( $P_{pro}$ ), and induced power ( $P_{ind}$ ).

$$P = \frac{Q\omega}{550} \quad (2.28)$$

$$P_{pro} = \frac{Q_{pro}\omega}{550} \quad (2.29)$$

$$P_{ind} = \frac{Q_{ind}\omega}{550} \quad (2.30)$$

### 2.3 Computational Methodology

The computational analysis of edgewise rotor performance focuses on capturing the resulting force, power, and required control input trends for a given rotor as thrust, speed, and mast tilt are varied. Further influential design trends may be captured by studying the rotor performance response to design parameter variation (i.e. twist, solidity, etc.). For the purposes of such a study, a computational blade element analysis tool was created using MATLAB® version 7.0. The tool is composed of the following 5 major modules:

1. Input, Governing, and Post Processor Module (IGPPM)
2. Thrust Sweep and Trim Module (TSTM)
3. Blade Element Analysis Math Module (BEAMM)
4. Airfoil 2D  $c_l$ ,  $c_d$ , and  $c_m$  Interpolation Module (AFIM)
5. 2D Polar Integration Module (2DPIM)

The Input, Governing, and Post Processor Module (IGPPM) conducts the entire analytical operation. Within this module, the user must designate all relevant model assumption, trim logic, flight condition, blade geometry, and rotor operational inputs. Once the test rotor is defined, the user may sweep the rotor through a range of flight velocities and mast angles or conduct a single test case. Once the case has been run, output values are passed to the post processor where they will be formatted and exported in Microsoft Excel format.

The Thrust Sweep and Trim Module (TSTM) accepts the rotor geometry, operational data, and trim logic from the IGPPM. The TSTM first establishes an initial thrust, lateral, and longitudinal rotor moment condition from which the trim routine will attempt to drive to some desired value. For the purposes of this study, it is desirable for the rotor tip path plane to be perpendicular to the rotor shaft i.e., zero steady state rotor flapping. The TSTM accomplishes this by driving lateral and longitudinal rotor moments to zero, allowing the rotor tip path plane to be determined solely by rotor mast inclination. The TSTM attempts to trim to successive levels of thrust until a pre-defined iteration limit is achieved signifying rotor stall. The trim algorithm

used by the TSTM is a three dimensional implementation of the Newton Rhapson Method, using central difference derivatives. In this method, the unique effects on thrust, lateral, and longitudinal moment by  $\theta_o$ ,  $A_1$ , and  $B_1$  are determined. The average (central) differences of forward and backward perturbations serve to populate a 3x3 Jacobian sensitivity matrix. Trim is achieved iteratively by inverting the Jacobian and multiplying it by the error between achieved and desired trim thrust and moments to obtain corrections to control inputs. Figure 2.5 illustrates the sensitivity matrix used to trim.

$$\begin{bmatrix} \frac{\delta T}{\delta \theta_o} & \frac{\delta T}{\delta A_1} & \frac{\delta T}{\delta B_1} \\ \frac{\delta M_{lat}}{\delta \theta_o} & \frac{\delta M_{lat}}{\delta A_1} & \frac{\delta M_{lat}}{\delta B_1} \\ \frac{\delta M_{long}}{\delta \theta_o} & \frac{\delta M_{long}}{\delta A_1} & \frac{\delta M_{long}}{\delta B_1} \end{bmatrix}$$

Figure 2.5-TSTM Sensitivity Matrix

Successful trim will prompt the TSTM to record the relevant performance data and proceed to trim at the next desired thrust level. If the TSTM exceeds the pre-defined iteration limit, it will cancel all subsequent calculations and report a condition of rotor stall to the IGPPM.

In order for the TSTM to gather values for thrust, moments, as well as all other desired performance data, it must pass the input conditions provided by the IGPPM to the Blade Element Analysis Math Module (BEAMM). The BEAMM essentially conducts the mathematical operations detailed in Section 2.2. To reiterate, the BEAMM accepts rotor control inputs and operational parameters that are used to calculate local blade element velocity and angle of attack as a function of radial and azimuthal position. Figure 2.6 illustrates the aforementioned division of the disc.

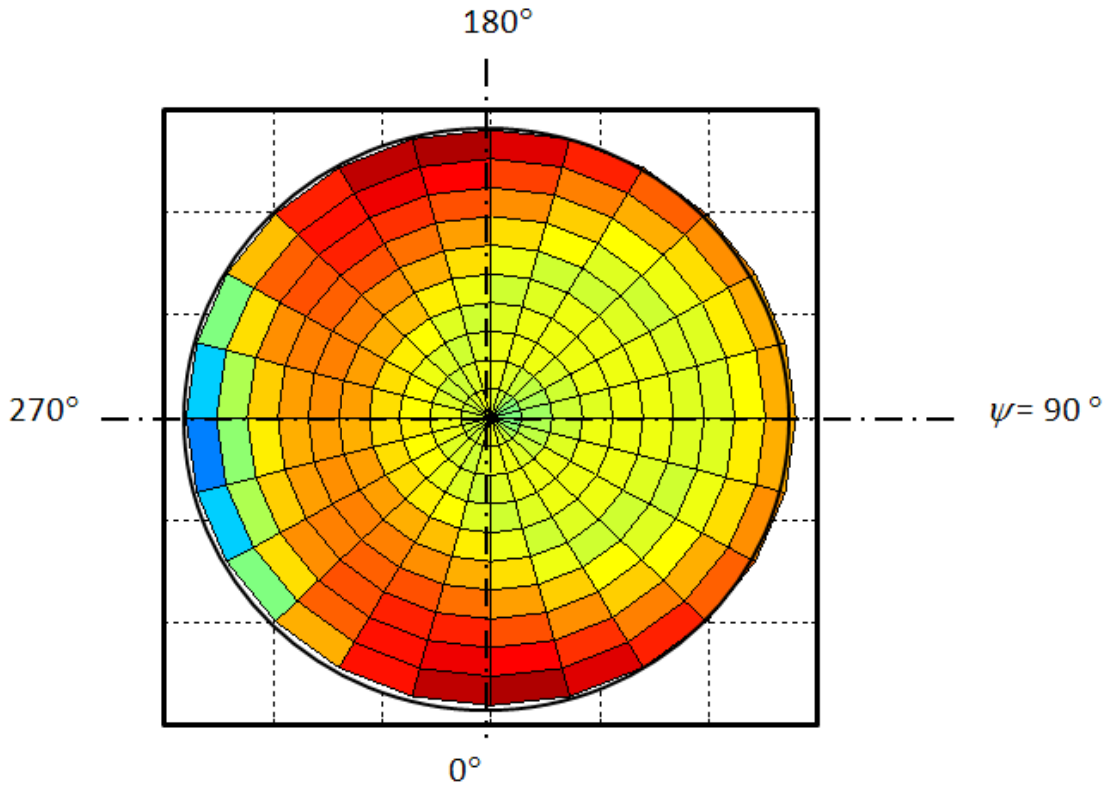


Figure 2.6-Rotor Mesh Azimuthal and Radial Distribution

The angle of attack and Mach number are then passed to the correct Airfoil Interpolation Module (AFIM) designated by the user in the IGPPM. The AFIM uses a 2D interpolation algorithm to find  $c_l$ ,  $c_d$ , and  $c_m$  values from compressible wind tunnel airfoil tables. The resulting coefficients are returned to the BEAMM and used to calculate their respective differential forces and moments. The differential quantities are then passed to the 2D Polar Integration module (2DPIM) where they are integrated to yield steady state rotor blade forces and moments. The 2DPIM utilizes a two dimensional Trapezoidal Integration methodology in order to integrate the differential quantities in the azimuthal and radial directions. Equation 2.31 illustrates the Trapezoidal Integration method where  $h$  represents the incremental step size.

–

(2.31)

The integrated rotor blade values are summed with respect to the number of blades in order to yield the total rotor disc forces, and moments. Finally, the values are passed back to the IGPPM where the aforementioned formatting and post-processing takes place. Figure 2.7 illustrates the program logic flow chart for the computational tool.

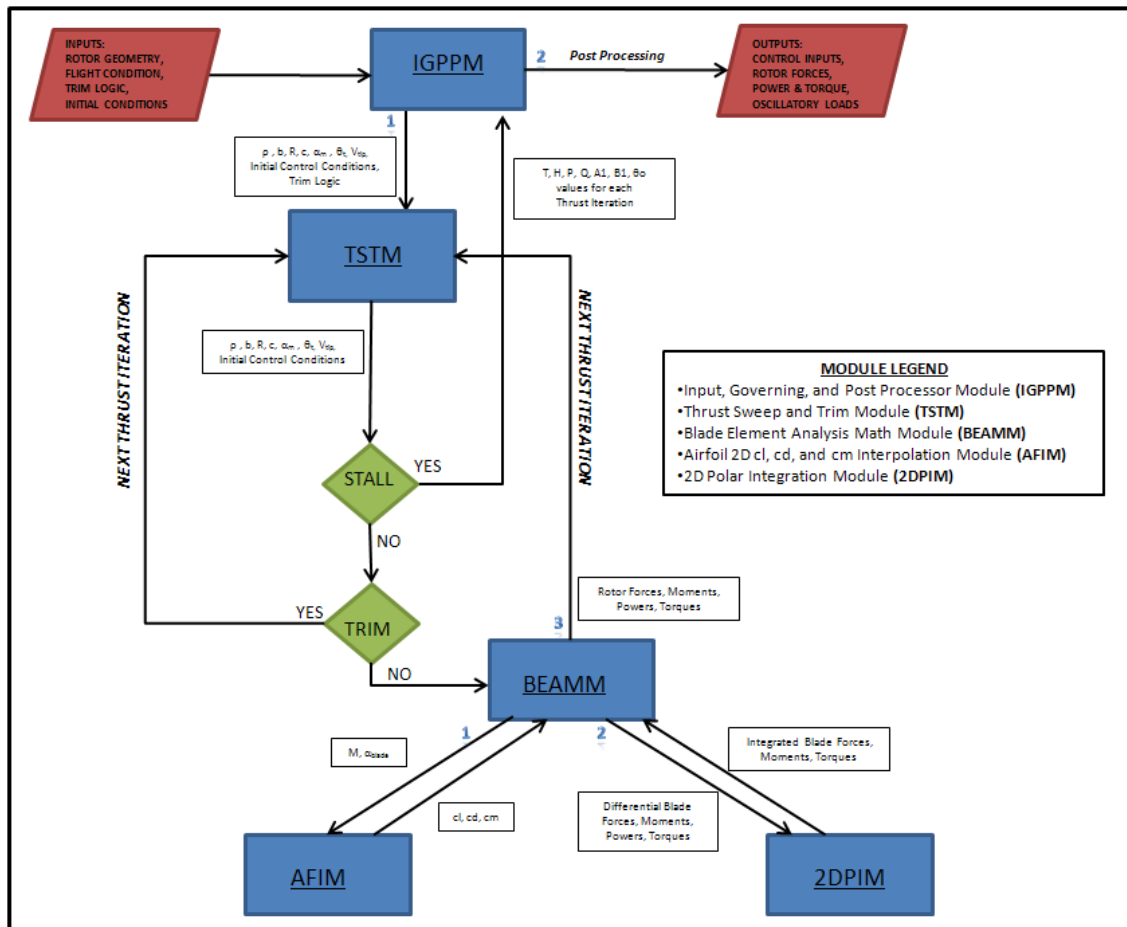


Figure 2.7-Computational Tool Program Logic Flow Chart

#### 2.4 Notable Assumptions and Omissions

At this early stage in the research process, it should be noted that various assumptions and model limitations exist. As the study continues beyond the scope of this thesis, these



assumptions will be analyzed and accounted for through model modification or updated empirical data. The following assumptions exist within the computational model:

1. Zero Flapping Trim
2. Different Hub Dynamics not Specifically Represented
3. Structural Loads and Dynamics Ignored (Rigid Rotor)
4. Steady Aerodynamics/Uniform Inflow/No Free Wake Model

Paramount to the analysis methodology used is the pursuit of zero-flapping trim for all data points. As discussed previously, zero-flapping trim is sought because it allows for isolation of rotor tip path plane augmentation through mast-tilt only. This is highly desirable since edgewise rotor performance at high mast angle is a prime objective of the study. Additionally, zero-flapping trim is thought to yield decreased oscillatory rotor loads at high speed, which will be explored in future studies. The potential negative implications of this trim methodology are limited. Trimming with feathering such that average steady state flapping is driven to zero requires higher than normal cyclic control inputs. This is not a problem for computational tools but may present issues in laboratory/flight tests due to maximum control input limitations of current control set-ups. Additionally, zero-flapping trim is somewhat idealized in that it is a steady state solution thereby ignoring the transient blade flapping which typically exists in any rotor system to some degree. Analysis has shown that even the transient magnitudes can be minimized however, thus any resulting error should be minimal.

Next, there is no specific designation of rotor hub type within the computational tool. In other words, the rotor code makes no differentiation between articulated, teetering, or gimbaled hubs other than the correct representation of the respective blade geometry (i.e. solidity, number blades, radius, etc.). For example, within the computational tool's trim methodology, zero flapping is signified by the zeroing of the rotor pitching and rolling moments. This is somewhat analogous to a gimbaled rotor but most aptly represents a fixed rigid prop. Zero pitching or rolling moments will mean that there is no moment driving the blade to flap, i.e. zero

steady state flapping. Forthcoming model validation illustrates that this computational methodology does not bear significant error variance between different hub types especially when only considering aerodynamic rather than dynamic metrics.

Since the nature of this study pertains specifically to aerodynamic performance analysis, rotor dynamics and loads are ignored. The rotor will be assumed rigid both beam-wise and torsionally (i.e. no structural bending/deflection). While increase in blade torsional moment is presented, the resulting effects of dynamic torsional blade twist resulting from mach effects on the tips are not modeled. Furthermore, lead-lag motion will be assumed negligible. While previous research has shown dynamic loading to be an important factor in defining the high speed edgewise rotor performance envelope, it is beyond the scope of the current analysis. Additionally, generic trends regarding these topics are typically difficult to quantify due to the specific “tailored” rotor/blade design that is required in order to overcome dynamic effects.

Finally, unsteady aerodynamics, non-uniform inflow, and free wake models are not currently utilized within the blade element model. While these tools are highly desirable given the goals of the study, they are still in development with respect to the presented computational tool and as such, are beyond the scope of this thesis. All of the aforementioned assumptions increase the propensity of the model to yield “optimistic” results at high speed. Error between the computational tool results and empirical aerodynamic data that will be presented within forthcoming sections can most aptly be attributed to the omission of these models. However, resulting error is still within limits that are acceptable and it will be shown that resulting trends are analogous to prior testing.

## 2.5 Fundamental and Preliminary Expectations

In order to illustrate the performance characteristics of the validation cases and baseline rotor, several metrics will be presented as functions of thrust. Non-dimensional coefficients of power, H-force, and thrust allow for results to be compared across multiple designs. Equations 2.32-2.36 detail the calculation of these coefficients.

$$C_T = \frac{T}{\rho \pi R^2 V_{Tip}^2} \quad (2.32)$$

$$C_H = \frac{H}{\rho \pi R^2 V_{Tip}^2} \quad (2.33)$$

$$C_P = \frac{P}{\rho \pi R^2 V_{Tip}^3} \quad (2.34)$$

$$C_{P_{pro}} = \frac{P_{pro}}{\rho \pi R^2 V_{Tip}^3} \quad (2.35)$$

$$C_{P_{ind}} = \frac{P_{ind}}{\rho \pi R^2 V_{Tip}^3} \quad (2.36)$$

In addition to the aforementioned coefficients, values for peak torsional blade moment, collective, and cyclic required to trim are presented. Based on Equations 2.15-2.26 presented in Section 2.2, the following trends pertaining to speed and mast angle are expected:

1. Maximum available thrust will diminish proportionally with speed and forward mast tilt due to velocity effects, stall, inflow, and Mach effects.
2. Power required will increase proportionally with speed and forward mast tilt at a given thrust. Profile power will primarily be influenced by speed (i.e. Mach effects) whereas blade induced power required will be driven by mast tilt.
3. Control input required to trim (collective,  $\theta_o$ , and longitudinal cyclic,  $B_1$ ) will increase proportionally with speed and forward mast tilt at a given thrust
4. Increased solidity, radius, and tip speed should have proportional increases in power required and decreases in control inputs required at a given thrust.

## 2.6 Model Validation

Validation of the computational tool is accomplished through comparison to known empirical data. Reference 4 provides high speed test data for both a teetering and articulated rotor at mast angles up to 12 degrees. Each test point represents a full-scale rotor trimmed to zero-flapping which is analogous to the computational methodology of this study, further cementing the validity of the empirical data. Such data is extremely relevant to this study since it provides a metric against which the computational tool can correctly predict the aerodynamic effects of speed and forward mast tilt on edgewise rotor performance. Furthermore, the test data helps define the urgency by which future model modification should commence in order to minimize demonstrated error. In order for validation to commence, the two test data rotor geometries (teetering and articulated) and flight conditions are modeled within the computational tool. Each rotor is then iteratively trimmed to successively higher thrust levels at forward mast angles from 0 to 12 degrees. Power and control input required at each successive thrust level are recorded and compared.

Table 2.1 details the respective rotor geometries to be tested. Figures 2.8-2.11 (Teetering Rotor) and 2.12-2.15 (Articulated Rotor) detail the comparison of the computational model to the empirical data with regard to the aforementioned performance metrics.

Table 2.1-Model Validation-Historical Data Test Geometries

	Teetering Rotor	Fully Articulated Rotor	
Blade Radius, R	17	28	ft
Blade Chord, c	1.75	1.337	ft
Root Cutout	2.04	4.48	ft
Solidity, $\sigma$	0.0656	0.062	N/D
Number of Blades	2	4	N/D
Blade Twist, $\theta_T$	-7.7	-8	deg
Airfoil *	NACA 0012	NACA 0012	N/D

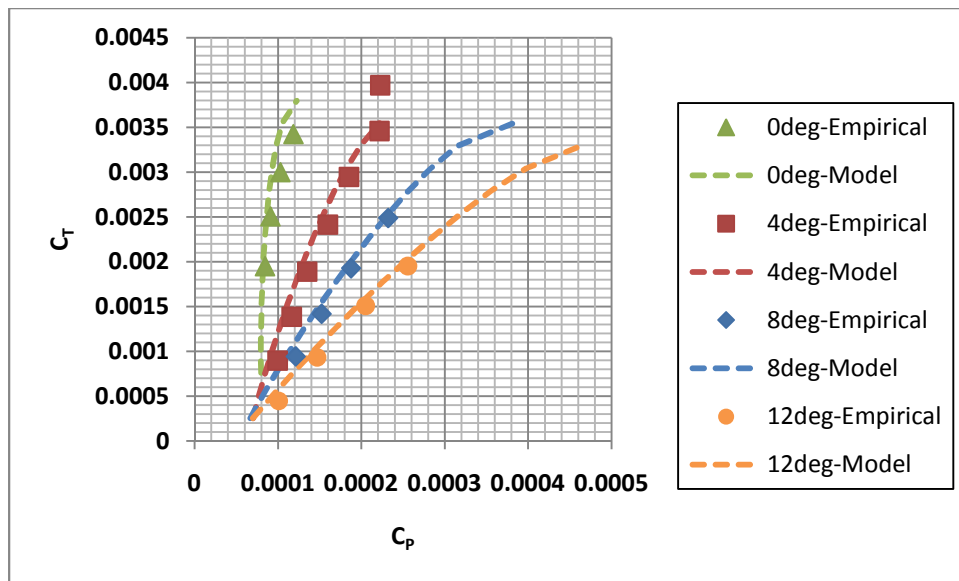


Figure 2.8- $C_T$  vs  $C_P$  Model Validation Case (Teetering Rotor,  $\mu=.85$ ,  $M=.9$ )

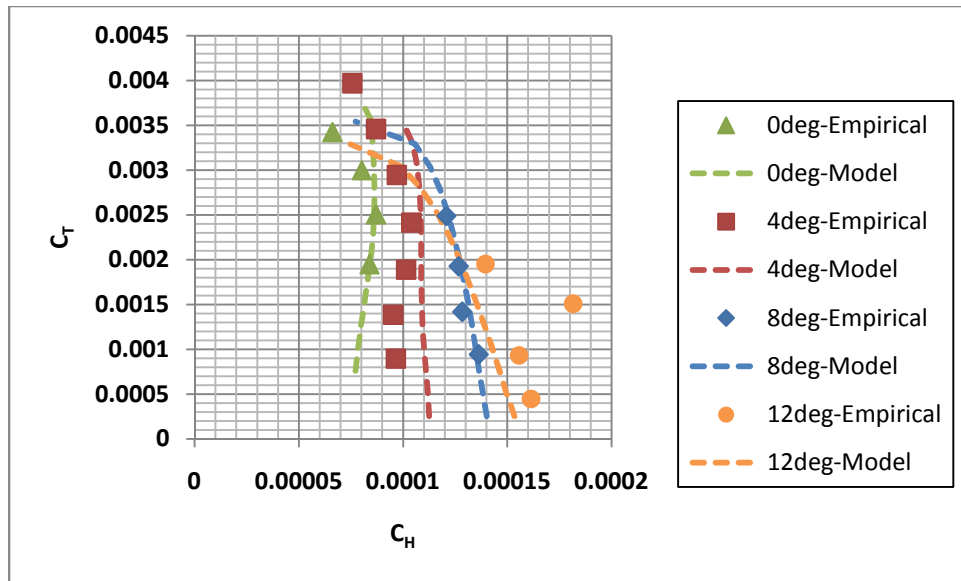


Figure 2.9- $C_T$  vs  $C_H$  Model Validation Case (Teetering Rotor,  $\mu=.85$ ,  $M=.9$ )

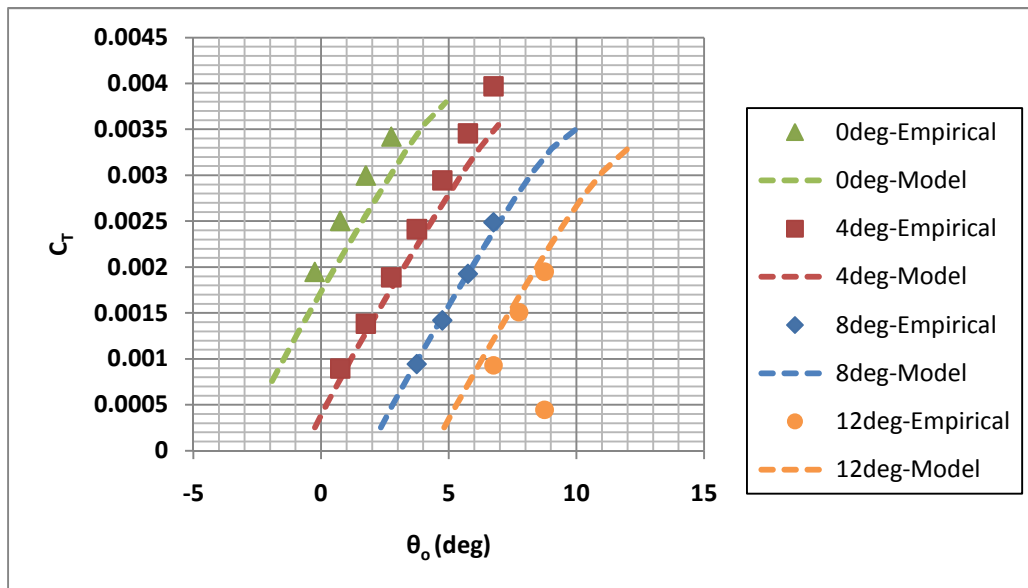


Figure 2.10- $C_T$  vs  $\theta_0$  Model Validation Case (Teetering Rotor,  $\mu=.85$ ,  $M=.9$ )

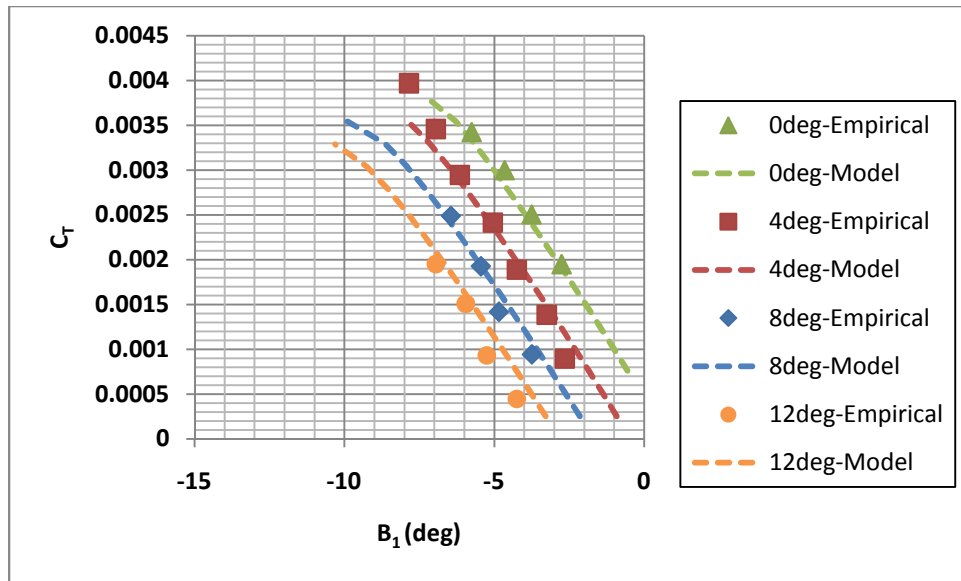


Figure 2.11- $C_T$  vs  $B_1$  Model Validation Case (Teetering Rotor,  $\mu=.85$ ,  $M=.9$ )

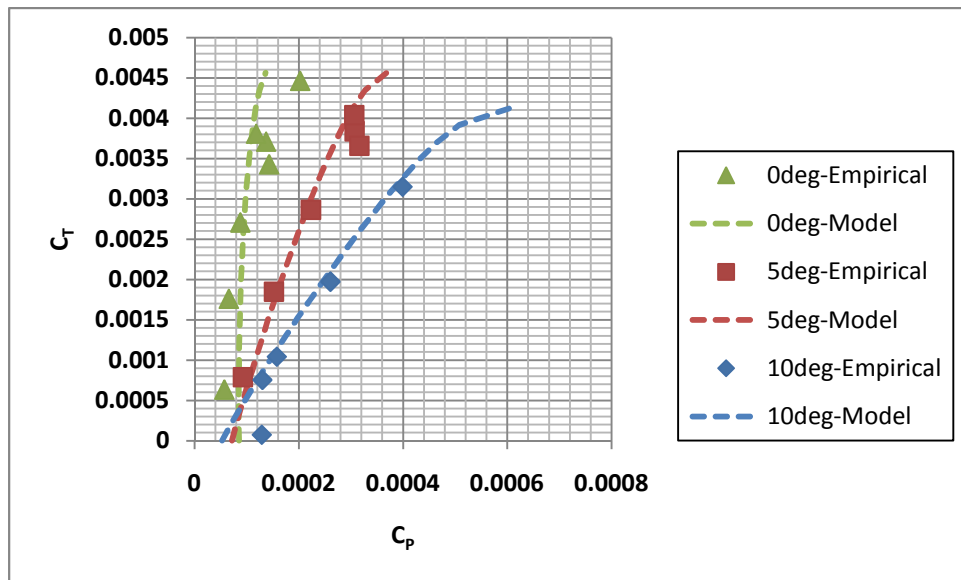


Figure 2.12- $C_T$  vs  $C_p$  Model Validation Case (Articulated Rotor,  $\mu=.86$ ,  $M=.92$ )

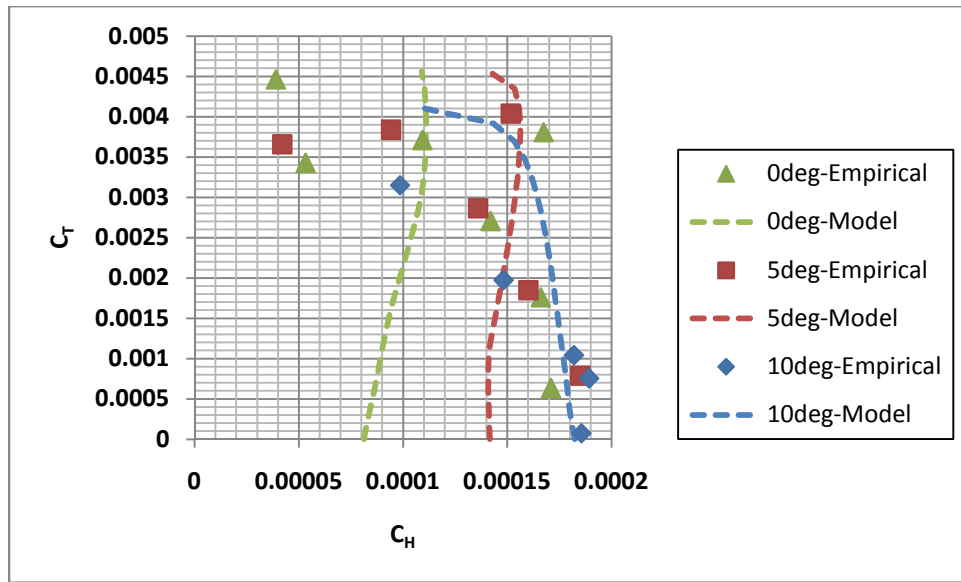


Figure 2.13-  $C_T$  vs  $C_H$  Model Validation Case (Articulated Rotor,  $\mu=.86$ ,  $M=.92$ )

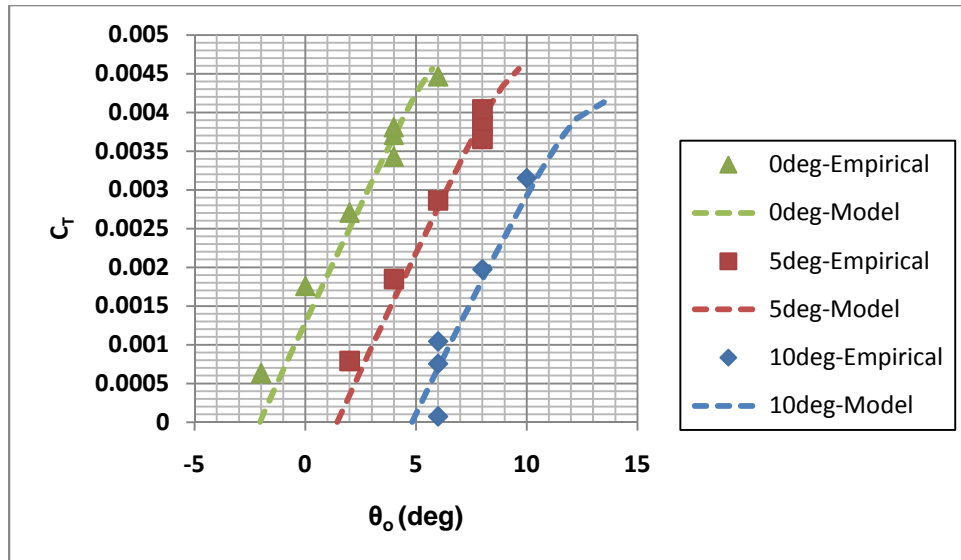


Figure 2.14-  $C_T$  vs  $\theta_0$  Model Validation Case (Articulated Rotor,  $\mu=.86$ ,  $M=.92$ )



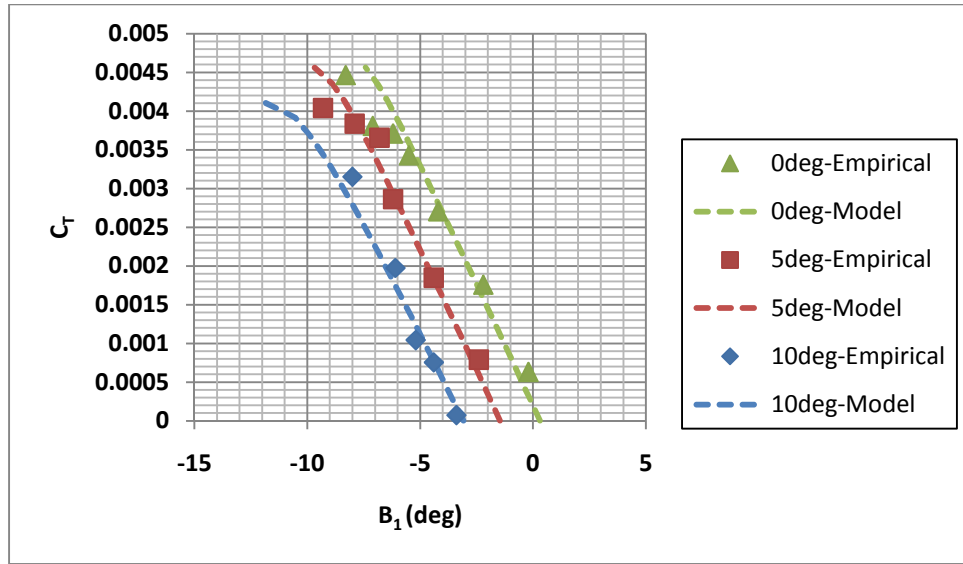


Figure 2.15-  $C_T$  vs  $B_1$  Model Validation Case (Articulated Rotor,  $\mu=.86$ ,  $M=.92$ )

The results of the two model validation cases are highly encouraging. The computational tool correctly reproduces the total power coefficient versus thrust coefficient trends with respect to mast angle at high speed. The results accuracy is within acceptable ranges given methodology assumptions and hub modeling differences (primary reason for data scatter in Figure 2.13). Error reduces with increased mast angle; this inspired confidence in predicting mast angle performance trends in forthcoming experiments. Additionally, control input required trends are analogous between the computational tool and empirical data after being corrected for rigging discrepancies. As a result, computational tool modeling accuracy was validated and further experimentation proceeded with confidence. Model modification through removal of aforementioned assumptions can further improve accuracy. It should be noted that the amount of effort required to further develop the computational tool relative to the improvement of results appears to produce diminishing returns with respect to the aerodynamic parameters of interest.

## 2.7 Baseline Rotor Design and Operational Setting

The baseline rotor design for this study is a four bladed system with standard swash plate control. Root cutout for the inboard 30% of the rotor represents the blade transition to a traditional rotor cuff as well as the expected inefficient inboard lifting sections present in traditional rotor systems. The blades have uniform airfoil distribution with linear twist. As previously mentioned in the Section 2.4, there are no model modifications present to represent hub drag effects. Rotor tip speed is selected such that advancing tip Mach number will remain below supersonic even at maximum model test speeds. All testing occurs at sea level ambient density and temperature.

Table 2.2 describes the baseline rotor geometric and operational parameters. Figure 2.16 and Figure 2.17 illustrate the baseline rotor blade and design of the four bladed system.

Table 2.2-Baseline Rotor Geometric and Operational Description

<b>Baseline Rotor</b>		
Air Density, $\rho$	0.00237	slg/ft <sup>3</sup>
Blade Radius, R	14	ft
Blade Chord, c	1.1875	ft
Root Cutout	0.000711	ft
Solidity, $\sigma$ (Thrust Equiv.)	0.10696	N/D
Number of Blades	4	N/D
Blade Twist, $\theta_T$	-17	deg
$V_{tip}$	640	ft/s
Airfoil *	NACA 0012	

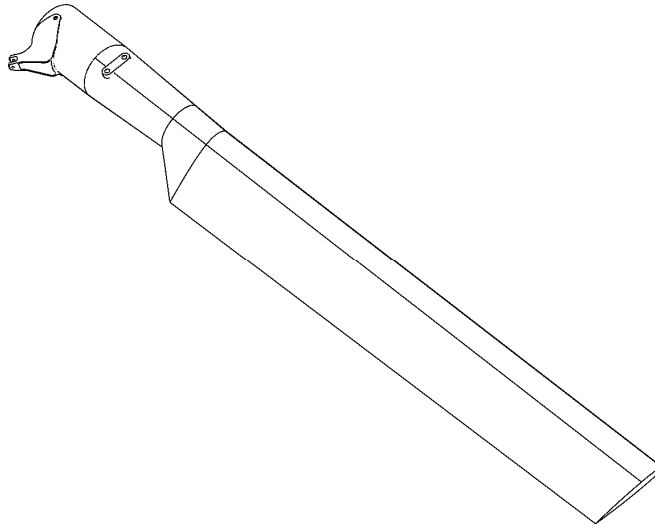


Figure 2.16-Baseline Rotor Blade

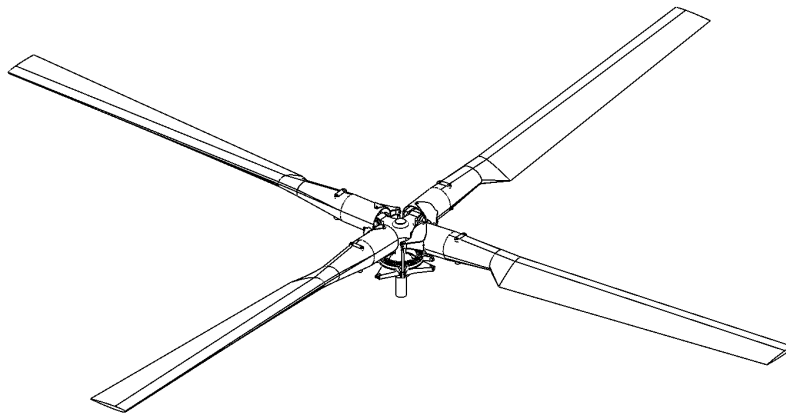


Figure 2.17-Baseline Rotor System Design

## 2.8 Test Matrix Description

This goal of this study is to accurately model the performance of the baseline rotor as it is swept through successive levels of thrust (up to rotor stall), speed, and forward mast tilt. The computational tool will trim the rotor to zero flapping at each point and record relevant performance data. Table 2.3 details the test matrix for all cases analyzed within this study.

Table 2.3-Study Test Matrix

Baseline Rotor Study				
	$\alpha_m$ (deg)			
$V_f$ (kts)	0	10	20	30
0				
50				
100				
150				
200				
250				

\*Target rotor total thrust (T) swept from 0 lbs to stall for each case

Once the baseline rotor performance is defined, a geometric and operational parameter trade study takes place at 250 knots with a mast angle of 30 degrees, the purpose of which is to define design and optimization opportunities in the high speed, high inflow regime.

## CHAPTER 3

### RESULTS AND DISCUSSION

#### 3.1 Overview

The results of the aforementioned baseline rotor and parameter variation studies are presented in the following sections. Emphasis is paid to the effects of aircraft velocity and forward mast tilt on overall rotor performance. The baseline rotor's sensitivity to speed will be discussed through presentation of data for a mast tilt of 20 degrees at multiple speed levels. The reasoning behind presenting results for 20 degrees rather than 0 degrees is that this study is primarily interested in configurations that utilize the main rotor for forward thrust rather than an auxiliary source. Consequently, some amount of forward mast tilt is necessary in order to achieve the speeds of interest. The baseline rotor's sensitivity to mast angle will be discussed through presentation of data for a speed of 200 knots at multiple degrees of forward mast tilt. The entirety of the baseline rotor analysis data for all mast angles and speeds is found in Appendix A. Variation of rotor geometric variables such as blade twist, illustrate possible rotor optimization paths for future high speed configuration development. The optimization study takes place at the 250 knot flight condition at a forward mast tilt of 30 degrees.

#### 3.2 Baseline Rotor Study – Performance Effects due to Variation of Aircraft Velocity

Three important physical phenomena drive edgewise rotor performance at high velocity: Mach effects (compressibility), velocity distribution dissymmetry (reversed flow), and rotor stall. Increased speed causes a large rise in advancing tip Mach number. The advancing tip is of particular interest because it experiences the highest local velocity thus giving it the most

pertinent compressibility influences. Figure 3.18 illustrates the relationship of advancing tip Mach number to speed and forward mast tilt.

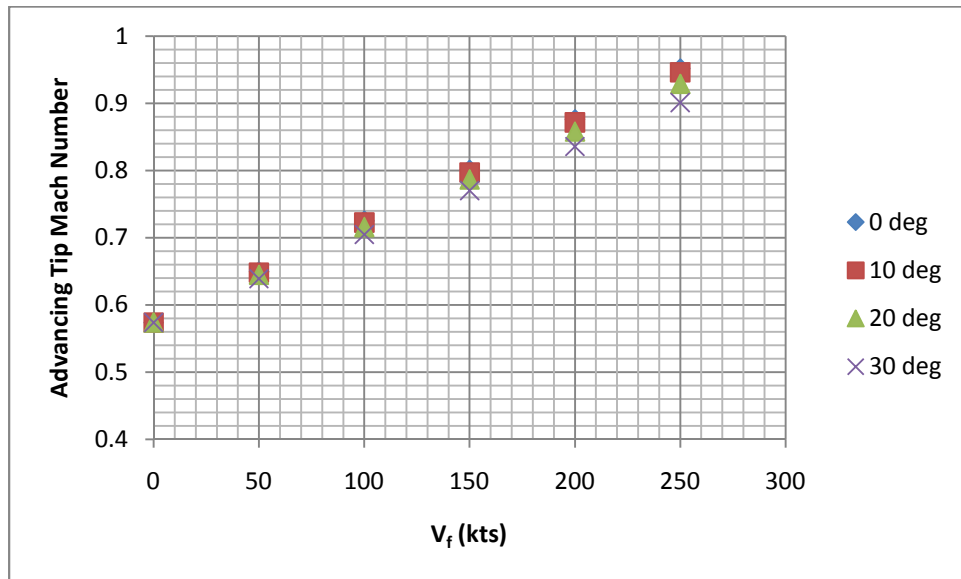


Figure 3.18-Advancing Tip Mach Number as a Function of  $V_f$  and  $\alpha_m$

In the case of the baseline rotor, advancing tip Mach number for the 250 knot condition increases 57% relative to the hover case. As can be seen in the compressible airfoil tables (Ref 1), the result is a reduction in maximum attainable blade element lift coefficient as well as large increases in drag and moment coefficient. Variation of mast angle from 0 to 30 degrees causes a desirable yet minimal 6% reduction in advancing tip Mach number at the 250 knot point.

Dissymmetry of local blade element velocity is a phenomena caused by the rotating of a rotor blade away from the direction of flight. The result is a local blade velocity region that is reversed in the retreating portion of the rotor disc relative to the advancing side. Within this region, the airfoil blade elements experience a negative velocity, resulting in very large angles of attack, reduced lift coefficient, high drag coefficients, and reduced dynamic pressure. The

reversed flow region of a rotor disc is typically defined by the term advance ratio,  $\mu$ . Advance ratio represents the diameter of the circular section of the rotor disc experiencing reversed flow as a function of the true rotor radius,  $R$ . Advance ratio increases proportionally with flight velocity ( $V_f$ ). Equation 3.37 defines the calculation of  $\mu$  while Figure 3.19 demonstrates the growth of advance ratio as a function of speed and forward mast tilt.

$$\mu = \frac{V_f \cos \alpha_m}{V_{Tip}} \quad (3.37)$$

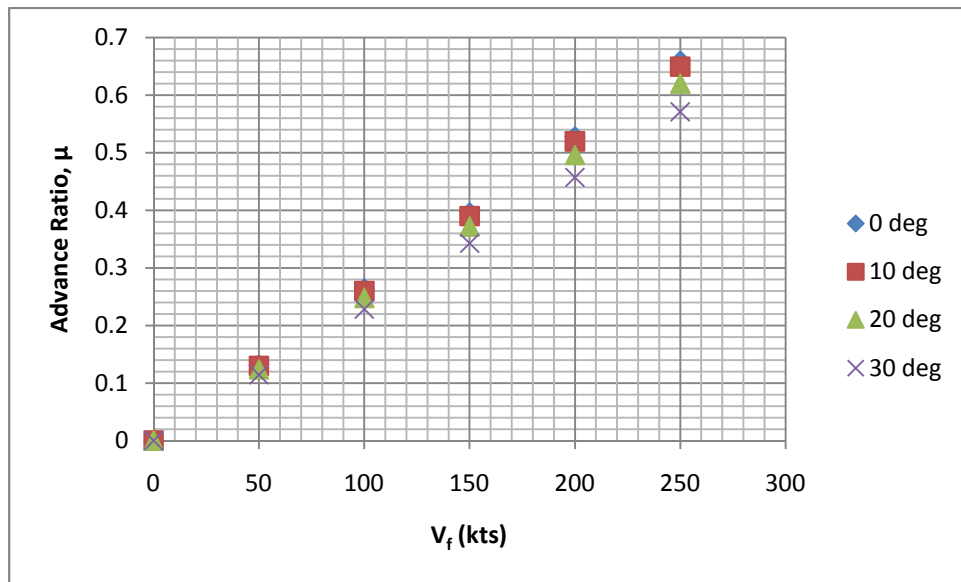


Figure 3.19-Advance Ratio,  $\mu$ , as a Function of  $V_f$  and  $\alpha_m$

Consequently, the area of the rotor undergoing reversed flow can no longer provide lift and exhibits drastically increased drag. Figure 3.20 details the growth of the non-lifting percentage of the baseline rotor area as a function of speed and mast angle.

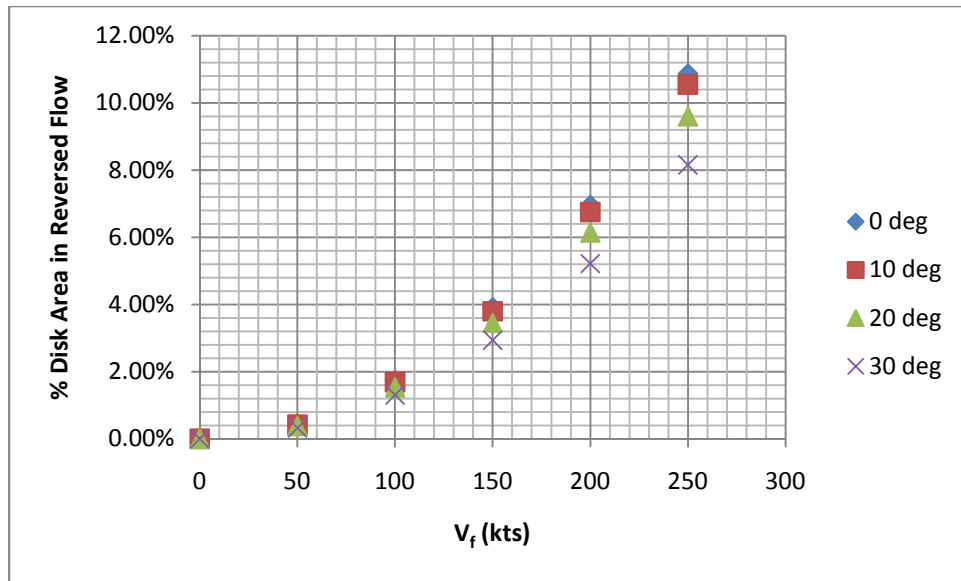


Figure 3.20-Percent Rotor Area in Reversed Flow as a Function of  $V_f$  and  $\alpha_m$

At 250knots, the available lifting area of the baseline rotor is reduced by 11% compared to that at 0 knots. As a result, the remaining section of the rotor disc will incur increased rotor thrust loading as speed rises. Forward mast tilt drives this loss of lifting area at 250 knots down to 8% compared to that at 0 knots. The increased loading on the remaining lifting sections of the rotor will require greater blade element angles of attack in order to achieve the necessary total rotor thrust.

At high speeds, the combined reduction in available rotor lifting area (reversed flow) and loss of max attainable lift coefficient (Mach effects) produce a non-ideal environment for various sections of the rotor disc. Inevitably, these sections will experience stall at increasingly reduced levels of thrust. Furthermore, the increased drag coefficients and angles of attack caused by the aforementioned speed effects will require greater power at a given thrust. Figure 3.21 illustrates the relationships of thrust coefficient ( $C_T$ ) to total power coefficient ( $C_P$ ) as speed increases for the baseline rotor at a mast angle of 20 degrees.



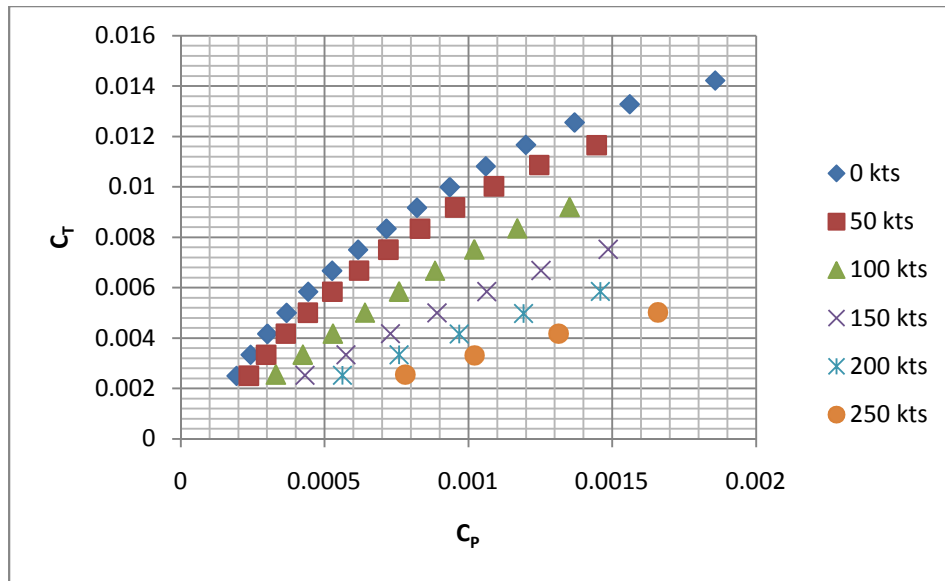


Figure 3.21- $C_T$  vs  $C_P$  as a Function of  $V_f$  ( $\alpha_m = 20^\circ$ )

Maximum achievable  $C_T$  at 250 knots for the provided condition decreases 65% compared to hover. Furthermore, at 250 knots, a 370% higher value of  $C_P$  relative to a speed of 0 knots is required to achieve a  $C_T$  of 0.005.  $C_P$  can be further broken down into blade profile and blade induced contributions. Figure 3.22 illustrates this division of power required.

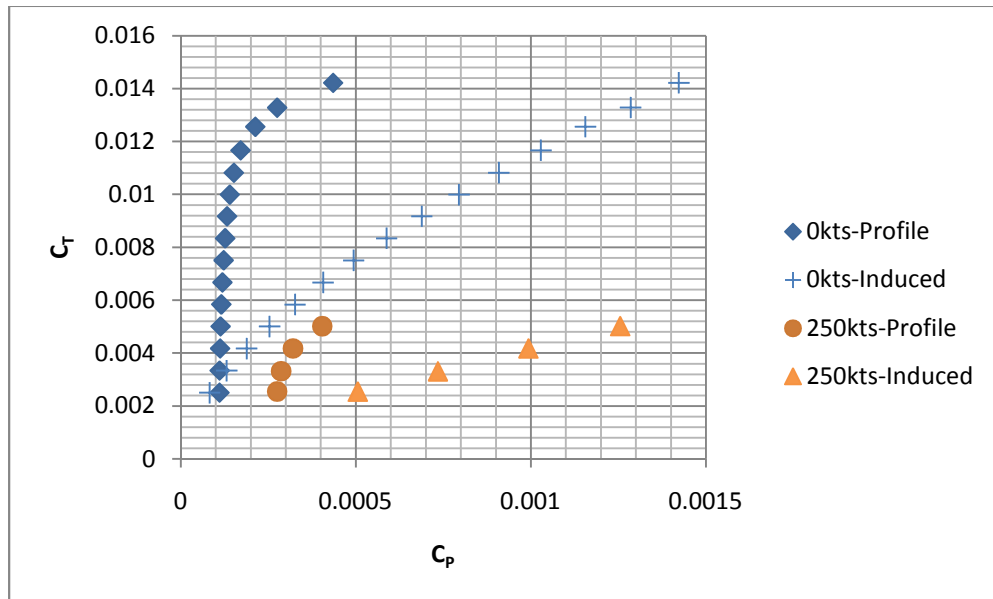


Figure 3.22- $C_T$  vs  $C_{P\_ind}$  and  $C_{P\_pro}$  as a Function of  $V_f$  ( $\alpha_m = 20^\circ$ )

The data shows that speed causes a large increase to both profile and induced power required. Profile power for 250 knots at a  $C_T$  of .005 increases 208% relative to 0 knots at the same  $C_T$ . Similarly, induced power 250 knots and  $C_T$  of .005 increases 400% relative to a speed of 0 knots at the same  $C_T$ . It should be noted that at a  $C_T$  of .005 ( $V_f = 0$ kts), induced power accounts for 69% of total power while profile accounts for the remaining 31%. When the speed is increased to 250 knots at the same  $C_T$ , induced power accounts for 75% of total power required with profile power only contributing the 25%. The rise in induced powers contribution to total power is caused by the increased inflow velocity through the disc ( $V_{ax}$ ) creating high inflow angles. As seen in Equations 15-26, higher inflow angles at a given thrust create increased inplane drag which in turn drives up torque and subsequent power required. The rate at which inflow angle increases with speed is primarily a function of forward mast tilt ( $\alpha_m$ ). Thus, the division of rotor power presented here (profile versus induced) is biased to the given mast angle.

The increased inplane drag seen at high speed further drives the growth of rotor H-force. H-force at a  $C_T$  of .005 has a value of .00155 ( $V_f = 250\text{kts}$ ) compared to a value of 0.0 ( $V_f = 0\text{kts}$ ). Figure 3.23 illustrates the relationship of rotor H-force to speed.

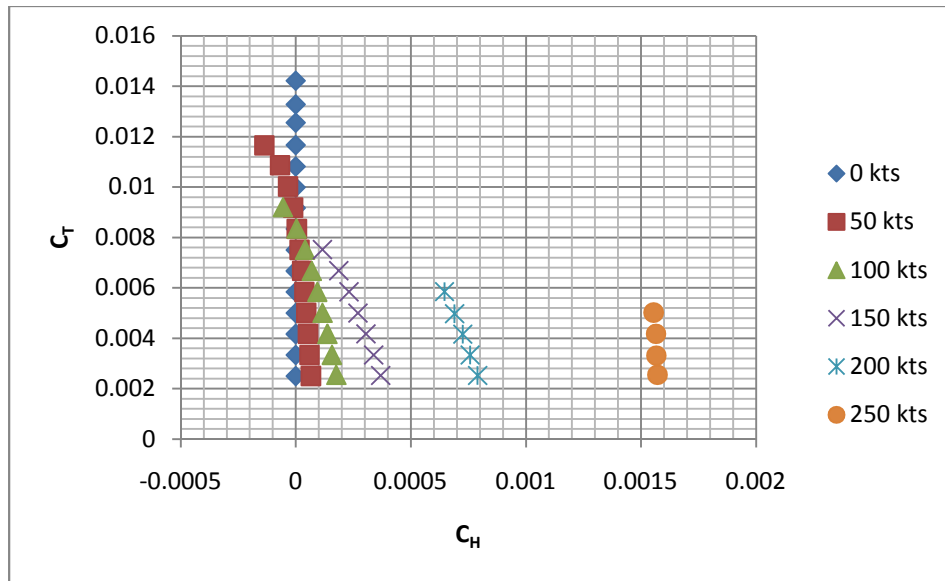


Figure 3.23- $C_T$  vs  $C_H$  as a Function of  $V_f$  ( $\alpha_m = 20\text{deg}$ )

The proportional growth of aft facing (aircraft axes) H-force with speed at a given thrust level can be attributed to the high drag region of the advancing tip. The concentration of previously noted Mach effects in this region yields drag coefficients that grow rapidly as speed increases. The significance of H-force growth is seen in compound design where the aircraft axes components of H-force create additional drag and wing offload considerations. It should be noted that a slight reduction in H-force is seen as thrust increases; the magnitude of which decreases with speed.

The behavior of the peak value of the torsional moment of the blade for the baseline rotor mirrors that of H-force with respect to speed increase. As Figure 3.24 illustrates, Torsional moment peak values are essentially zero for speeds below 100 knots.

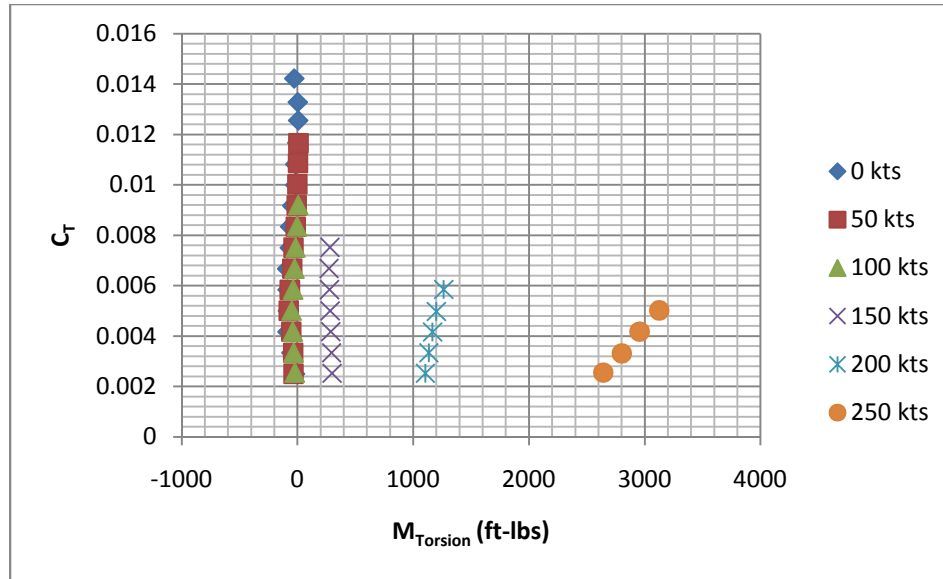


Figure 3.24- $C_T$  vs  $M_{Torsion}$  as a Function of  $V_f$  ( $\alpha_m = 20\text{deg}$ )

As speed increases, peak torsional moment values grow drastically. Peak torsional values occur at an azimuth position corresponding to the advancing blade. Consequently, the Mach effects present at the advancing tip drive torsional moment growth with speed. Peak torsional moments grow proportionally with thrust as well, albeit at a much slower rate than that of speed. Peak torsional moment growth is noteworthy due to its relevance as a primary driver of pitch link load sizing. Furthermore, the peak torsional moments will inevitably define blade torsion requirements in order to mitigate against dynamic blade twist (not modeled in the computational tool).

The final analyzed rotor performance metric whose dependence on speed should be noted is the required control input. Specifically, increasingly higher amounts of collective ( $\theta_0$ ) and longitudinal cyclic ( $B_1$ ) are required to trim the rotor to zero flapping at a given thrust as speed increases. Figure 3.25 and Figure 3.26 illustrate these two relationships.

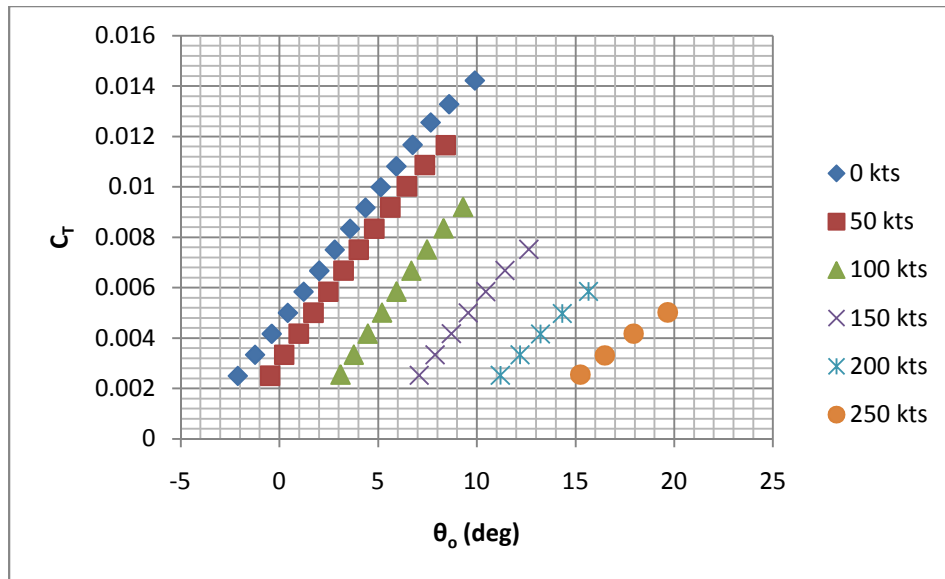


Figure 3.25- $C_T$  vs  $\theta_o$  as a Function of  $V_f$  ( $\alpha_m = 20\text{deg}$ )

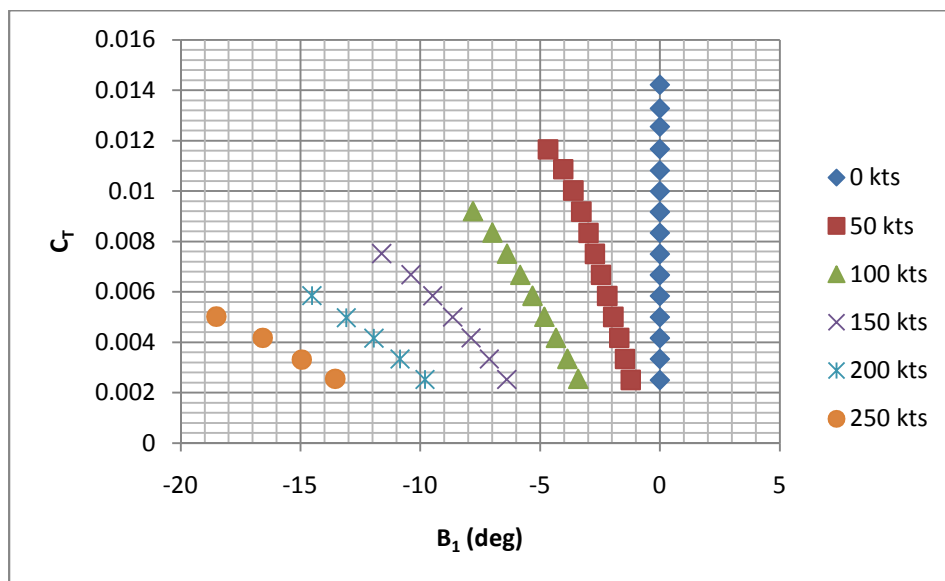


Figure 3.26- $C_T$  vs  $B_1$  as a Function of  $V_f$  ( $\alpha_m = 20\text{deg}$ )

Collective must be continually increased with speed at a given thrust in order to deliver the necessary angle of attack and corresponding lift coefficients. At a  $C_T$  of .005,  $\theta_o$  grows from 0.42 degrees ( $V_f = 0\text{kts}$ ) to 19.66 degrees ( $V_f = 250\text{kts}$ ). Longitudinal cyclic ( $B_1$ ) must similarly

be increased with speed in order to balance the non-symmetric lift distribution and trim the rotor moments ( $M_{lat}$  and  $M_{long}$ ). At a  $C_T$  of .005, the total deflection of  $B_1$  grows from 0 degrees ( $V_f = 0$  kts) to 18.15 degrees ( $V_f = 250$  kts). Similarly, both quantities grow proportionally with thrust until stall is reached. The lift discrepancy created by reversed flow and Mach effects which limits effective rotor lifting area to specific disc segments, drives this relationship. The total magnitude of required control input is significant in that rotor hub sizing, control design, and oscillatory loading ramifications arise with higher deflections.

### 3.3 Baseline Rotor Study – Performance Effects due to Variation of Forward Mast Tilt

The influence of forward mast tilt ( $\alpha_m$ ) on edgewise rotor performance is driven by the increase in axial velocity ( $V_{ax}$ ) through the rotor disc. Local inflow angle ( $\phi$ ) grows proportionally as the mast is tilted into the free stream, as evidenced by Equation 2.13. Figure 3.27 illustrates the growth of inflow angle with respect to  $\alpha_m$  and flight speed ( $V_f$ ).

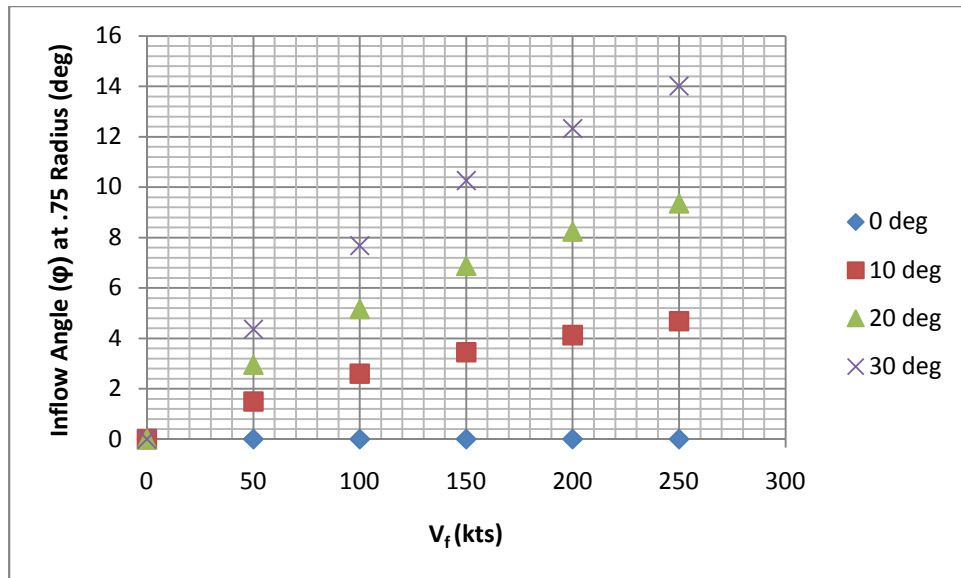


Figure 3.27-Advancing Blade Inflow Angle (.75 Radius) as a Function of  $V_f$  and  $\alpha_m$

For the 250 knot condition,  $\phi$  increase from 0 degrees ( $\alpha_m = 0$  deg) to 14 degrees ( $\alpha_m = 30$  deg) on the advancing blade at the 0.75 Radius.

As local inflow angles grow, power required follows suit. Figure 3.28 illustrates the relationship of total power coefficient to thrust coefficient at varying degrees of forward mast tilt at 200 knots.

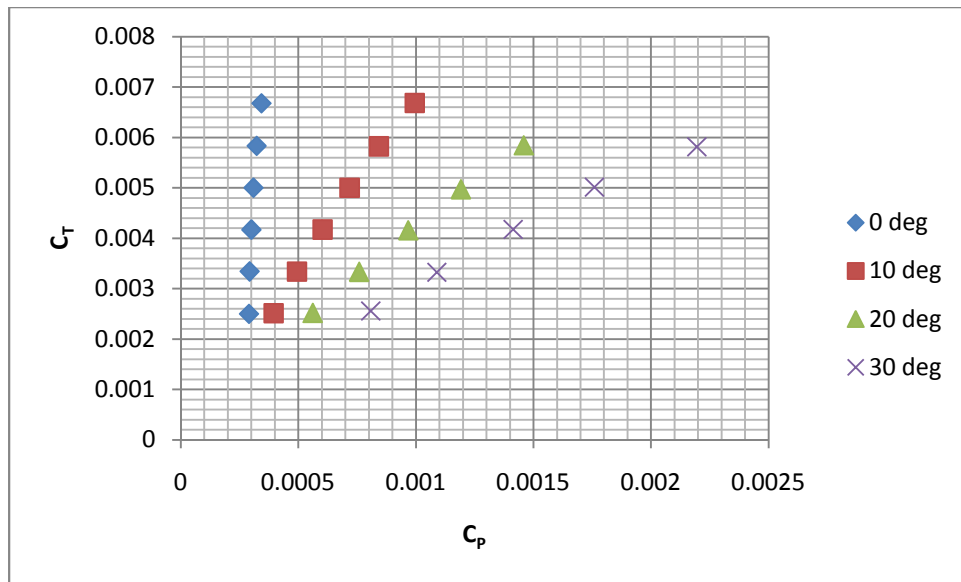


Figure 3.28- $C_T$  vs  $C_P$  as a Function of  $\alpha_m$  ( $V_f = 200$ kt)

For the given case at a  $C_T$  of .0058,  $C_P$  increases from a value of .0003 ( $\alpha_m = 0$  deg) to a value of .0022 ( $\alpha_m = 30$  deg). The large increase in power is further explained when the induced and profile power components are independently examined. Figure 3.29 illustrates the relationship of the induced and profile power coefficients with respect to thrust coefficient at mast angles of 0 and 30 degrees.

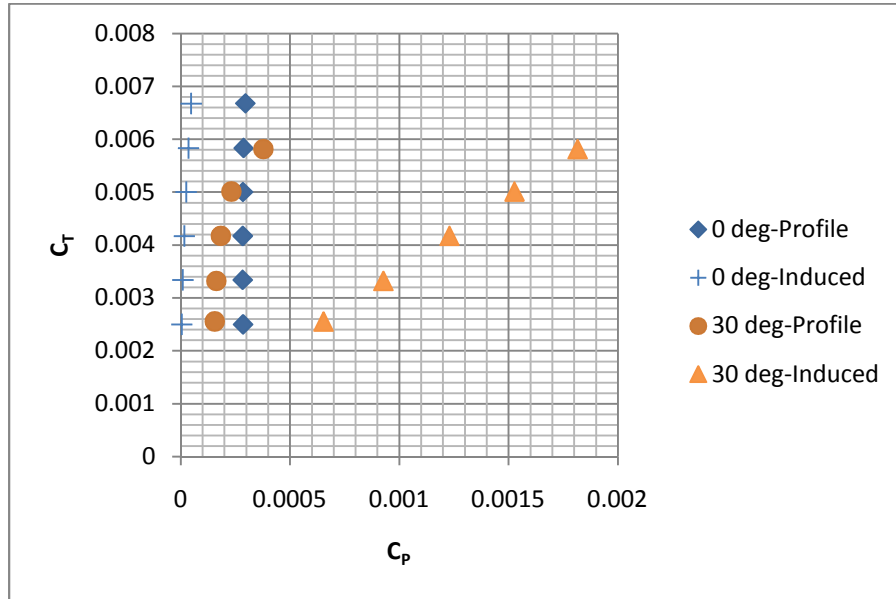


Figure 3.29- $C_T$  vs  $C_{P\_pro}$  and  $C_{P\_ind}$  as a Function of  $\alpha_m$  ( $V_f = 200kt$ )

As mast angle increases from 0 to 30 degrees at a given speed and thrust, induced power accounts for the vast majority of the total power increase. Profile, on the other hand experiences only minor increase due to the onset of rotor stall and actually decreases at low to intermediate values of  $C_T$  (caused by favorable inclination into freestream prior to rotor stall). To quantify, at a  $C_T$  of .0058,  $C_{P\_ind}$  increases from a value of 0.000035 ( $\alpha_m = 0$  deg) to a value of .00182 ( $\alpha_m = 30$  deg) while  $C_{P\_pro}$  increases from a value of 0.000287 to a value of .000379. The drastic increase in  $C_{P\_ind}$  is attributed to the proportional increase in local inflow angle ( $\phi$ ). Equation 2.17 demonstrates the dependence of rotor inplane drag and subsequent power on  $\phi$ .

Rotor H-force fails to show the expected trending with respect to forward mast tilt. For the 200 knot condition, rotor H-force grows then shrinks as the mast tilts from 0 to 30 degrees. As thrust increases, H-force tends to decrease for all mast angles except 0 degrees. The magnitude of the decrease in H-force with respect to thrust grows as mast angle increases. Figure 3.30 illustrates the relationship of H-force to forward mast tilt for the 200 knot flight condition.



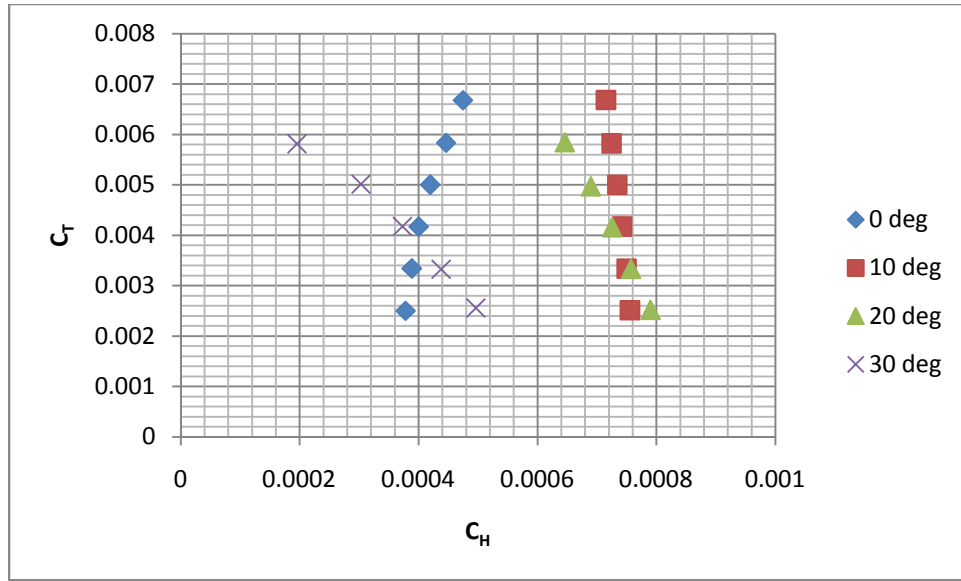


Figure 3.30- $C_T$  vs  $C_H$  as a Function of  $\alpha_m$  ( $V_f = 200\text{kt}$ )

The peak value of blade torsional moment decreases as the mast tilts forward from 0 to 30 degrees. Once again, peak torsional moment values are found in the disc region corresponding to  $\psi$  equal to 90 degrees (advancing blade tip). As the mast is tilted further forward, the advance ratio and subsequent local Mach number at the advancing tip lessen, allowing for peak torsional moment decrease. Conversely, as previously discussed, peak torsional moments grow proportionally with thrust. Peak torsional moment growth is noteworthy due to its relevance as a primary driver of oscillatory and pitch link load sizing. Furthermore, the peak torsional moments will inevitably define blade torsion requirements in order to mitigate against dynamic blade twist (not modeled in the computational tool). Figure 3.31 illustrates the relationship of peak torsional moment to forward mast tilt as a function of  $C_T$  for the 200 knot flight condition.

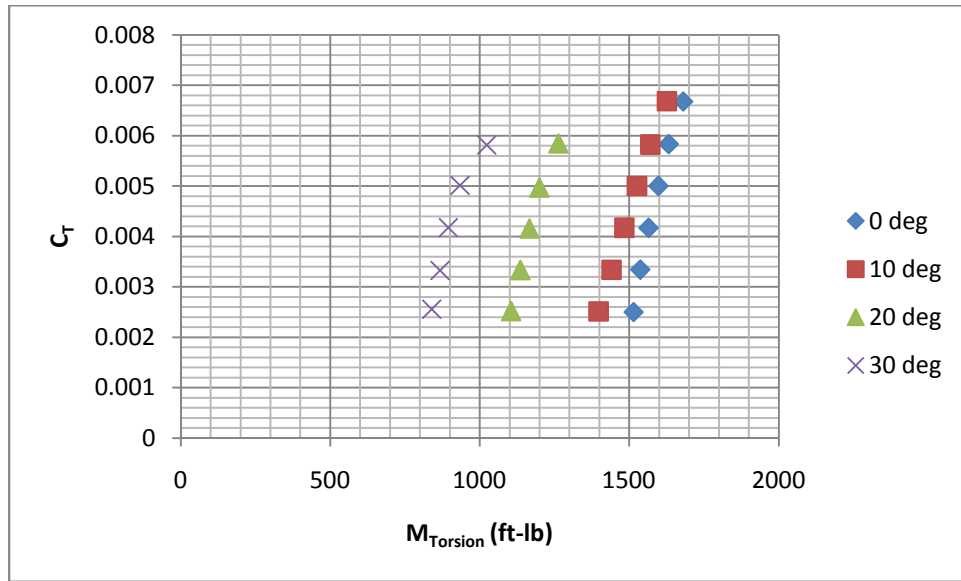


Figure 3.31-  $C_T$  vs  $M_{Torsion}$  as a Function of  $\alpha_m$  ( $V_f = 200\text{kt}$ )

The final rotor performance metric that was analyzed and whose dependence on forward mast tilt should be noted is that of required control inputs. Specifically, increasingly higher absolute values of collective ( $\theta_o$ ) and longitudinal cyclic ( $B_1$ ) are required to trim the rotor to zero flapping at a given thrust as speed increases. Figure 3.32 and Figure 3.33 illustrate these two relationships.

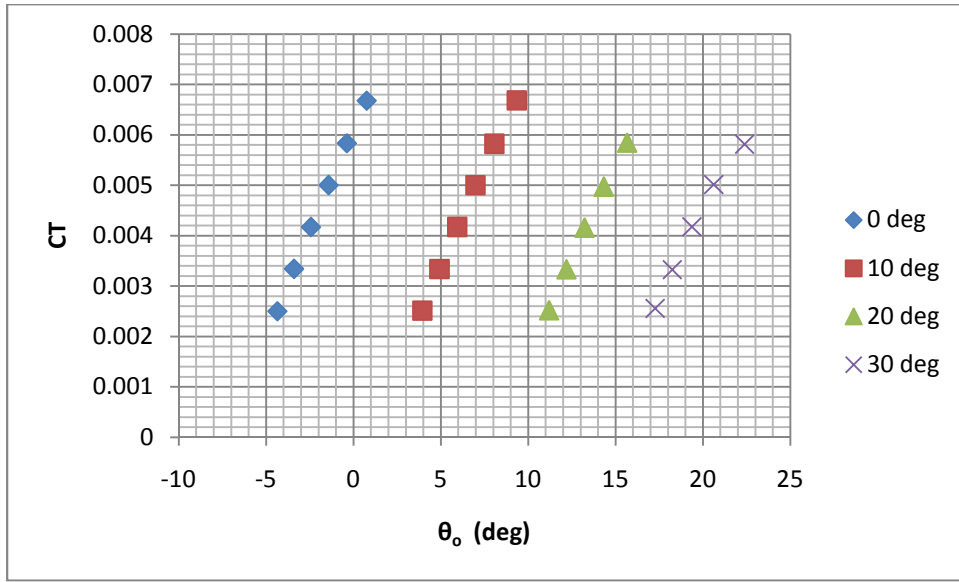


Figure 3.32-  $C_T$  vs  $\theta_o$  as a Function of  $\alpha_m$  ( $V_f=200\text{kt}$ )

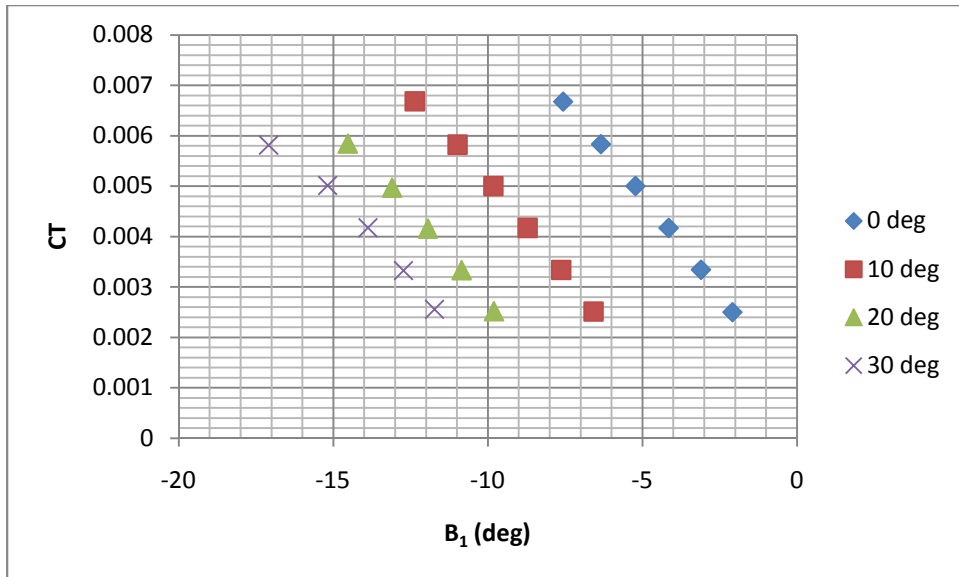


Figure 3.33-  $C_T$  vs  $B_1$  as a Function of  $\alpha_m$  ( $V_f=200\text{kt}$ )

At a  $C_T$  of .005,  $\theta_o$  grows from -1.41 degrees ( $\alpha_m = 0$  deg) to 20.62 degrees ( $\alpha_m = 30$  deg). Longitudinal cyclic ( $B_1$ ) must similarly be increased with forward mast tilt in order to trim balance the non-symmetric lift distribution and trim the rotor moments ( $M_{lat}$  and  $M_{long}$ ). At a  $C_T$

of .005, the total deflection of  $B_1$  grows from 6 degrees ( $\alpha_m = 0$  deg) to 15.18 degrees ( $\alpha_m = 30$  deg). Similarly, both quantities grow proportionally with thrust until stall is reached. Collective ( $\theta_0$ ) and longitudinal cyclic ( $B_1$ ) must be increased continually with forward mast tilt at a given thrust in order to overcome increasing inflow angle ( $\phi$ ) and deliver the necessary angle of attack as well as corresponding lift coefficients. The total magnitude of required control input is significant in that rotor hub sizing, control design, and oscillatory loading ramifications arise with higher deflections.

### 3.4 Baseline Rotor Study – Parameter Variation Study

The second part of the baseline rotor study involves the perturbation of multiple design variables at the high speed, high inflow flight condition, the goal of which is to ascertain potential design optimization trends for high speed, high inflow designs. The study occurs at the extreme operational condition of  $V_f=250$  knots and  $\alpha_m=30$  degrees. Number of blades and radius are varied while maintaining thrust equivalent solidity. Tip speed and thrust equivalent solidity are also varied. Ideally, the designer should strive to lower total power, H-force, control inputs, and peak blade torsional moments. The plotted results of each parameter variation can be found in Appendix B.

Table 3.4 illustrates the percent variations of multiple performance metrics for the perturbed cases relative to the baseline rotor.

Table 3.4-Parameter Variation Performance Deltas Compared to Baseline Rotor  
( $V_f=250\text{knots}$   $\alpha_m=30\text{deg}$   $C_T=.005$ )

	$C_p$	$C_H$	$\theta_o$	$B_1$	$M_{\text{Torsion}}$
-1 Blade	3.58%	-13.47%	0.04%	0.16%	81.85%
+1 Blade	-3.55%	17.97%	-0.61%	-1.30%	-39.40%
+10% solidity	-0.93%	6.26%	-2.66%	-4.02%	18.77%
-10% Solidity	-0.82%	-5.64%	2.50%	3.72%	-18.01%
+10% Radius	0.96%	-6.68%	0.55%	0.82%	29.25%
-10% Radius	-2.64%	7.01%	-0.49%	-0.75%	-28.65%
+10% Vtip	2.88%	-14.41%	-10.66%	-11.37%	30.70%
-10% Vtip	-6.10%	30.73%	10.96%	11.23%	-30.40%

The results indicate that increasing the number of rotor blades results in a reduction in total power ( $C_p$ ), collective ( $\theta_o$ ), longitudinal cyclic ( $B_1$ ), and peak blade torsional moment ( $M_{\text{Torsion}}$ ) while rotor H-force ( $C_H$ ) increases sharply. Additional blades allow the rotor to distribute thrust loading in more preferable regions of the rotor disc. Consequently, the blade requires less pitch in the high velocity regions (advancing blade tip) and spends less time in the reversed flow region. Additional blades also maintain solidity while requiring each blade to have reduced chord. Equations 2.15-2.26 show that lower chord results in reduced torque and peak blade torsional moments.

Reducing thrust equivalent solidity results in lower total power ( $C_p$ ), H-force ( $C_H$ ), and peak blade torsional moment ( $M_{\text{Torsion}}$ ), while collective ( $\theta_o$ ), and longitudinal cyclic ( $B_1$ ) increase. Less blade area relative to the total disc area requires additional pitch from the blades in order to maintain thrust. Fortunately, higher drag associated with increased blade pitch is overcome by the reduction in drag caused by reduced blade chord. The result is lower power required. Furthermore, peak blade torsional moments are a second order function of blade chord. It is not surprising then that a reduction in blade chord drastically diminishes peak blade torsional moments.

Reducing radius while maintaining equivalent solidity yields lower power ( $CP$ ), collective ( $\theta_o$ ), longitudinal cyclic ( $B_1$ ), and peak blade torsional moment ( $M_{Torsion}$ ) while causing an increase in rotor H-force ( $C_H$ ). Lower radius requires additional chord in order to maintain equivalent solidity. The power and moment penalties seen previously for increasing chord are outweighed by the influence of lower radius.

Reducing rotor tip speed allows for marked reduction in power ( $CP$ ), and peak blade torsional moment ( $M_{Torsion}$ ). Unfortunately, the penalty for such desirable reductions is a heavy increase in rotor H-force ( $C_H$ ), collective ( $\theta_o$ ), and longitudinal cyclic ( $B_1$ ). An additional consequence is that lower tip speed markedly reduces the maximum achievable thrust of the rotor prior to stall.

Actual design modification aims to maximize the aforementioned desirable trends while maintaining a physically realizable product. To clarify, one cannot infinitely decrease solidity or number of blades. Eventually, the principle of diminishing returns will dominate; most noticeably seen in the earlier onset of stall and reduction in achievable thrust. Further structural limitations will govern the maximal reductions in geometric blade area but are not discussed in this study. Additionally, the reductions in solidity or radius are desirable in high speed forward flight but will penalize hover performance.

## CHAPTER 4

### CONCLUSION

Based on the results presented, the aforementioned objectives have been met and the following conclusions can be stated:

1. The computational tool is validated for analysis of rotor performance at varying speeds and mast inclinations. The computational tool correctly reproduces the total power coefficient versus thrust coefficient trends with respect to mast angle at high speed seen in Reference 4. Results accuracy is within acceptable ranges given methodology assumptions and hub modeling differences. Error reduces with increased mast angle which inspires confidence in deducing mast angle performance trends in forthcoming experiments. Additionally, control input required trends are analogous between the computational tool and empirical data after being corrected for rigging discrepancies. As a result, computational tool modeling accuracy is validated and further experimentation can commence with confidence. Model modification through removal of aforementioned assumptions can further improve accuracy.
2. The results of the baseline rotor study with respect to speed variation demonstrate the inherent rotorcraft considerations with respect to maintaining forward flight efficiency at high speed. Compressibility (i.e. Mach effects), velocity dissymmetry, and rotor stall combine to create measureable reductions in thrust available while driving up power, H-force, torsional moments, and required control inputs.

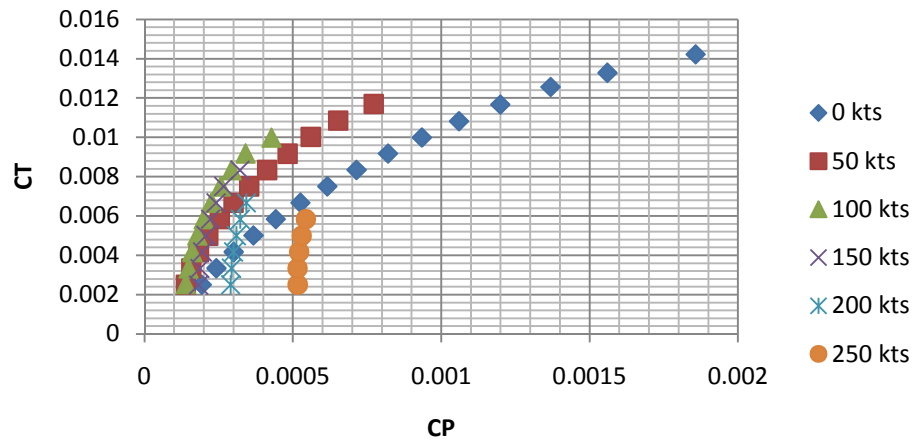
3. The results of the baseline rotor study with respect to forward mast tilt demonstrate the considerations inherent to optimizing the position of the rotor thrust vector in forward flight. Increasing levels of velocity inflow through the disc create measureable reductions in thrust available while driving up power and required control inputs. Increased forward mast tilt does allow for significant reduction of peak blade torsional moments and has mixed effect on rotor H-force.
4. Variation of design parameters at the high speed, high inflow flight conditions yields useful design trends. Reduction of rotor radius, thrust equivalent solidity, and tip speed all aid in reducing total power and peak blade torsional moments. The penalty for such reductions is a larger amount of control input required as well as a marked reduction in maximum achievable thrust prior to stall. Additionally, structural considerations and design hover requirements may further limit available design liberalism. Increasing the number of blades provides the most optimal approach to lowering blade torsional moments but substantially increases hub complexity.
5. Low disc loading edgewise rotorcraft designs utilizing forward mast tilt as a method for achieving high speed is plausible. Configurations utilizing variable mast tilt will require some type of lift compounding in order to counter the loss of thrust and high power/torsional moments seen at high speeds. Through understanding of the high speed, high inflow regime, proper design steps can be employed such that compound configurations may efficiently operate.



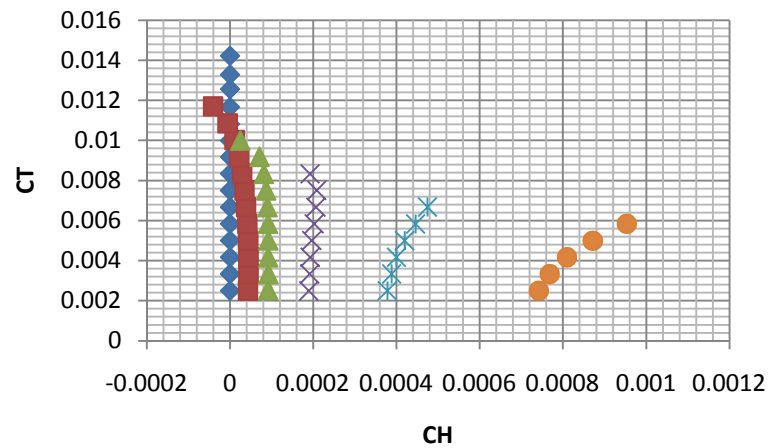
## APPENDIX A

### BASELINE ROTOR ANALYSIS STUDY DATA

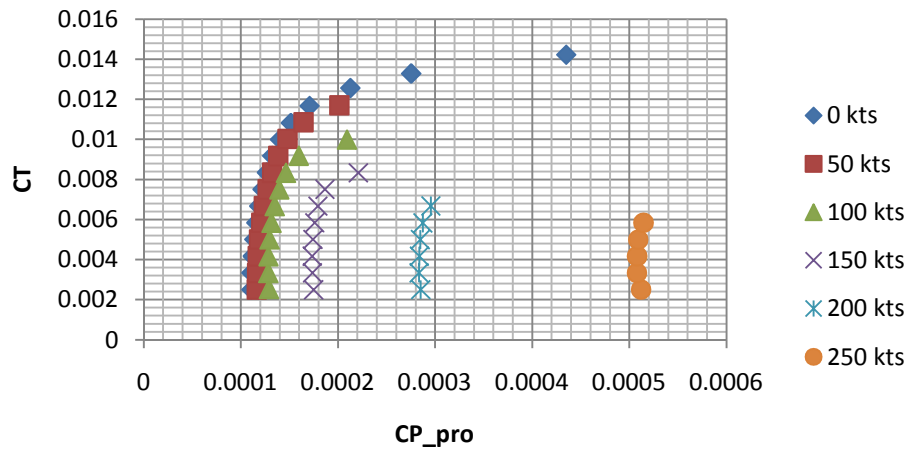
### Mast Angle = 0 deg



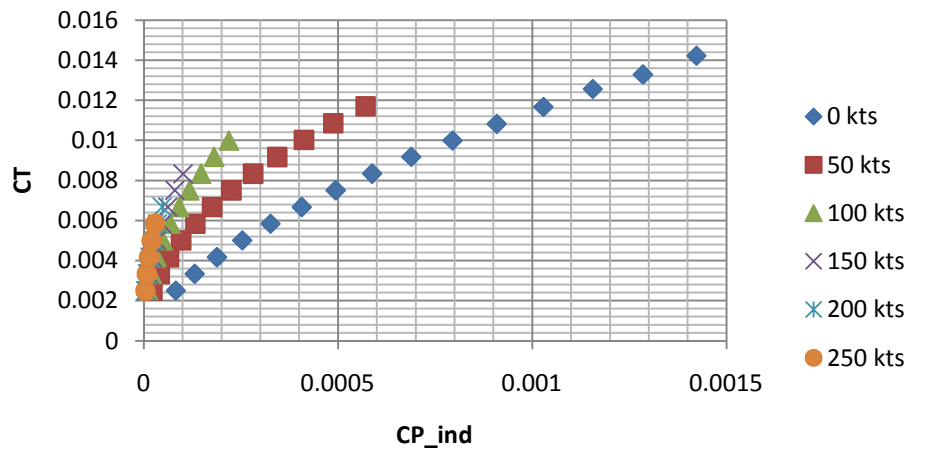
### Mast Angle = 0 deg



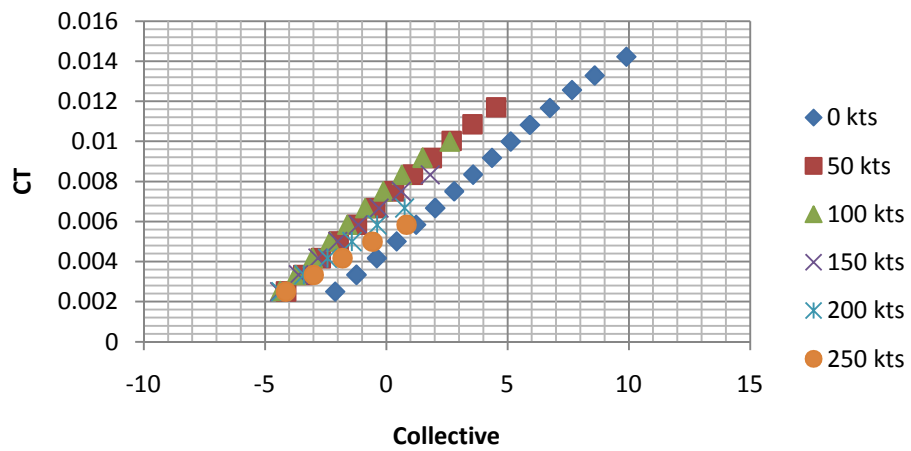
### Mast Angle = 0 deg



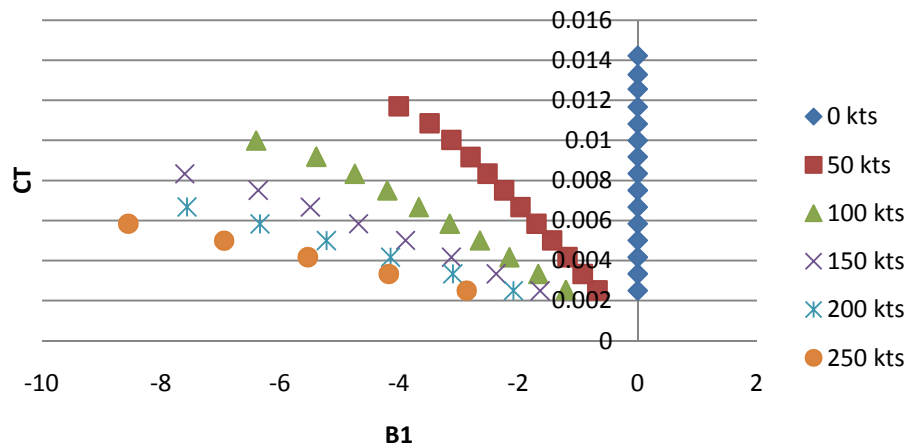
### Mast Angle = 0 deg

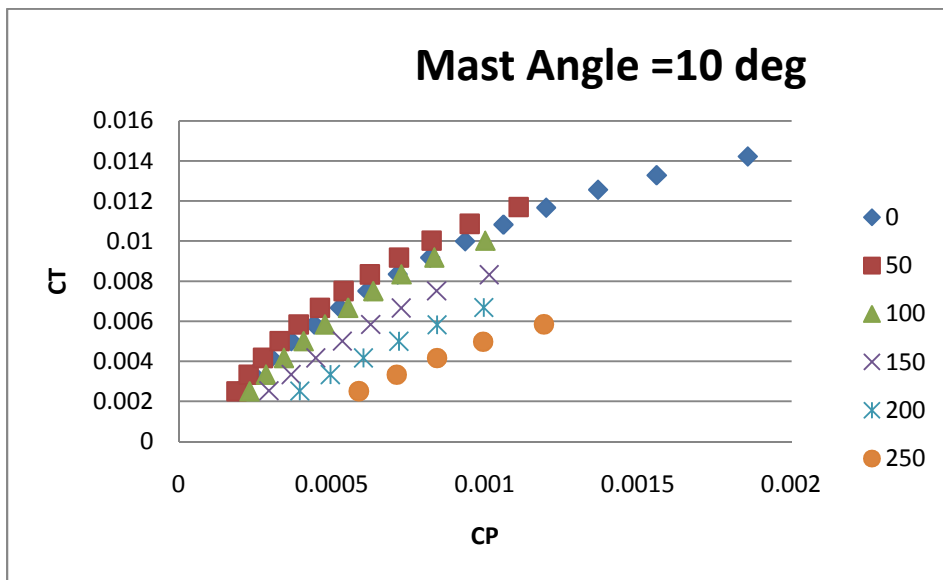
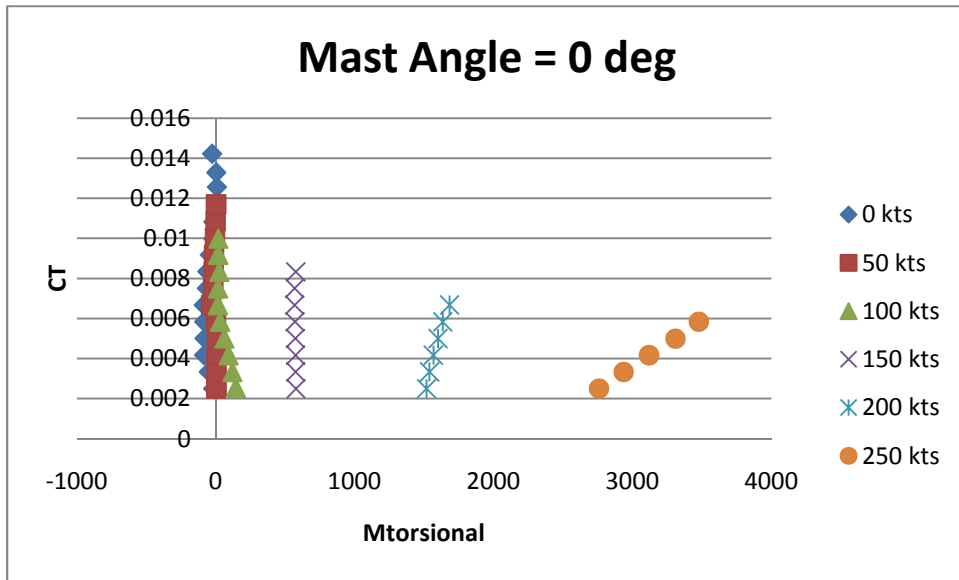


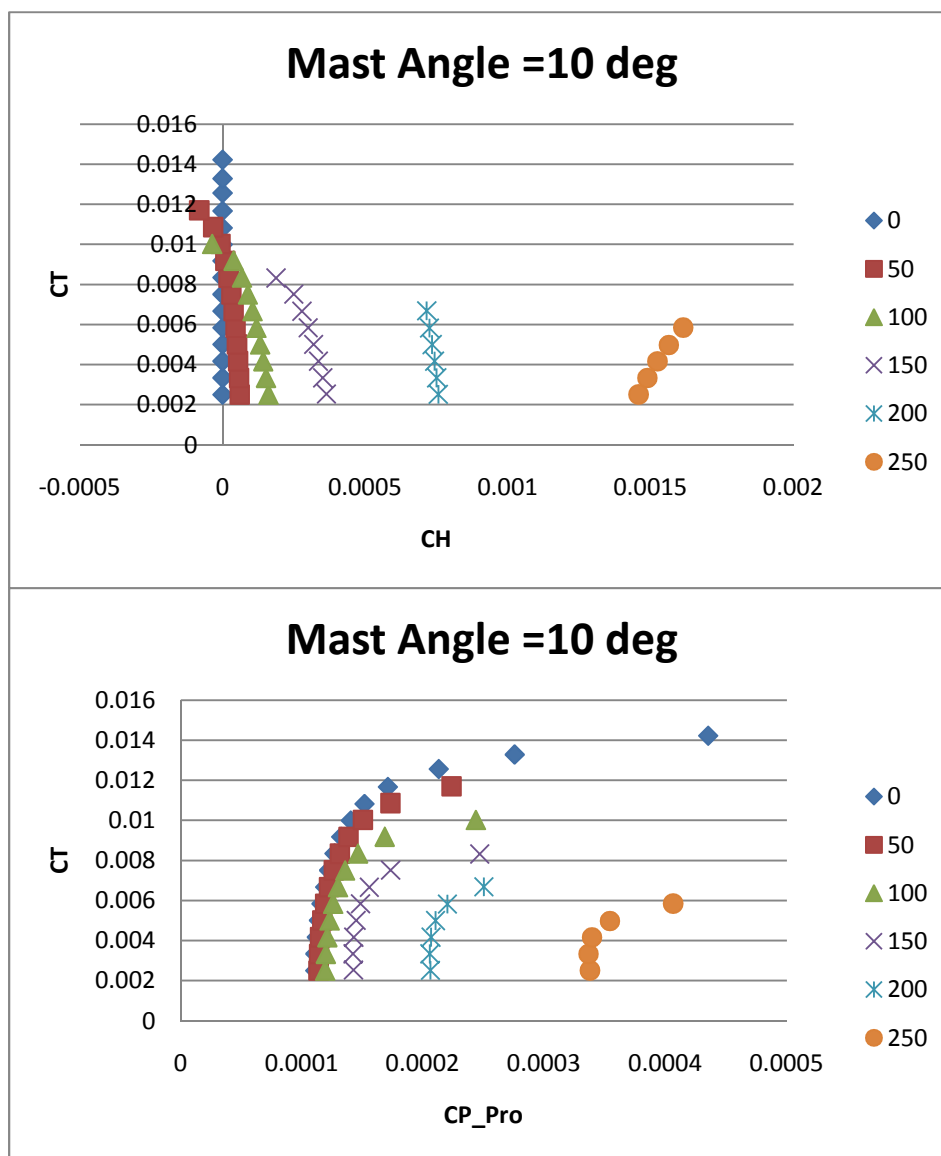
### Mast Angle = 0 deg

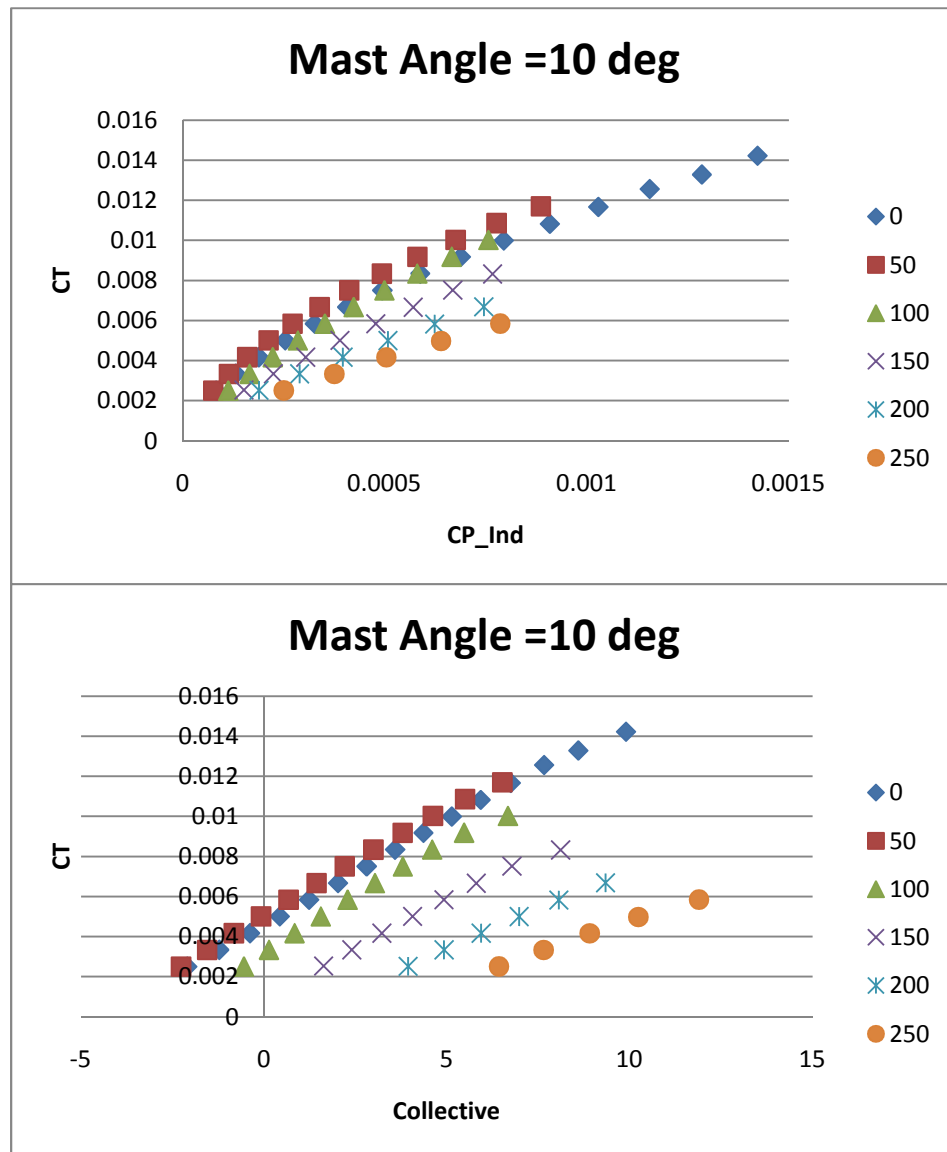


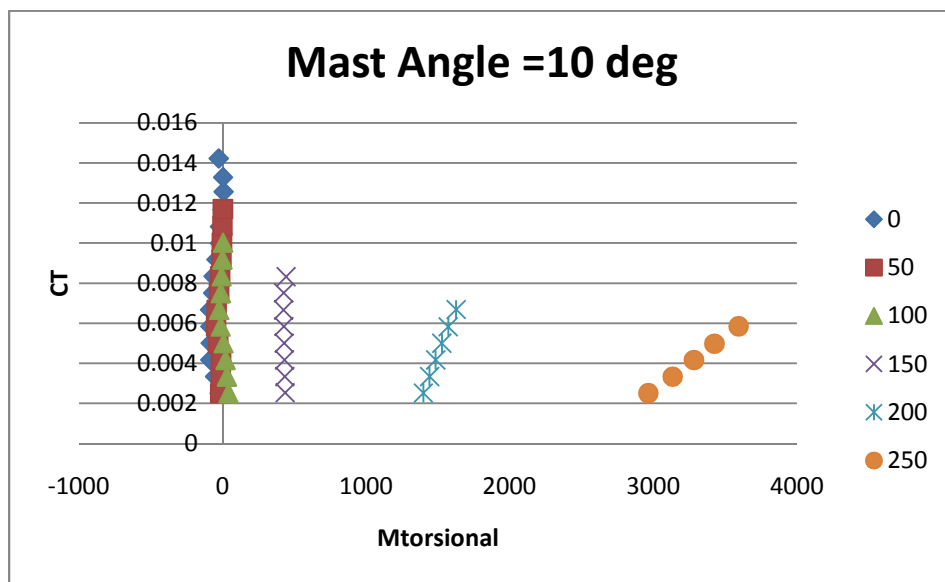
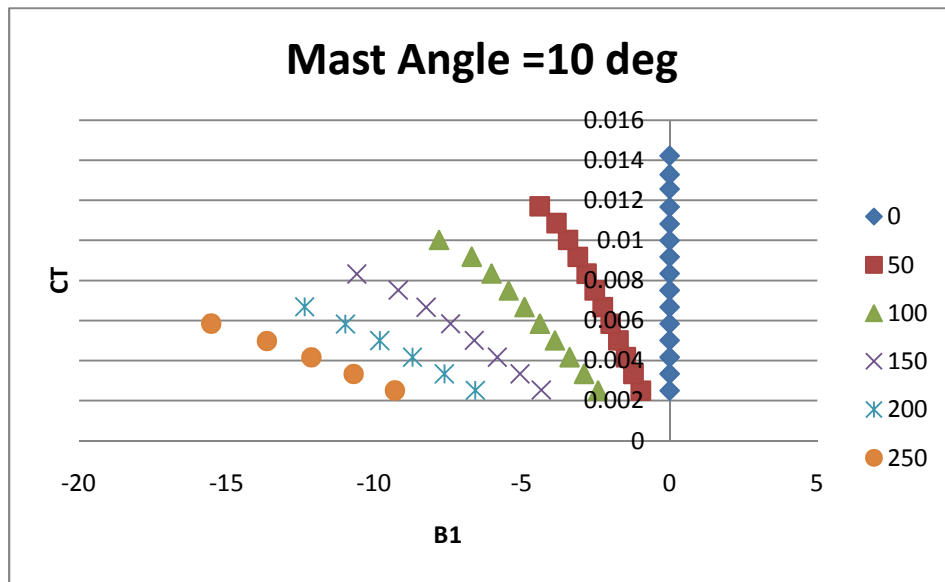
### Mast Angle = 0 deg





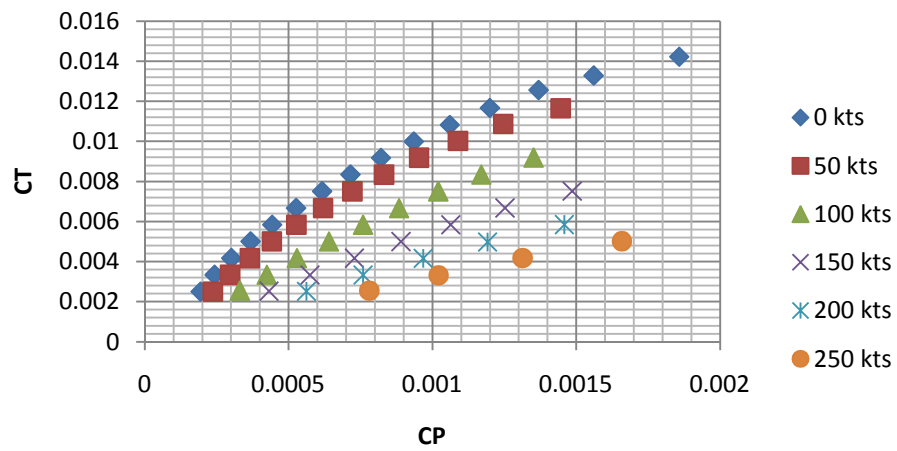




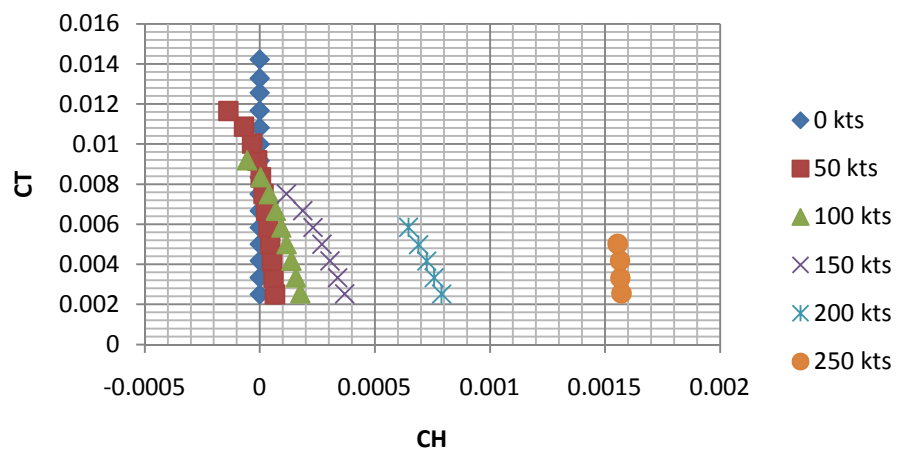




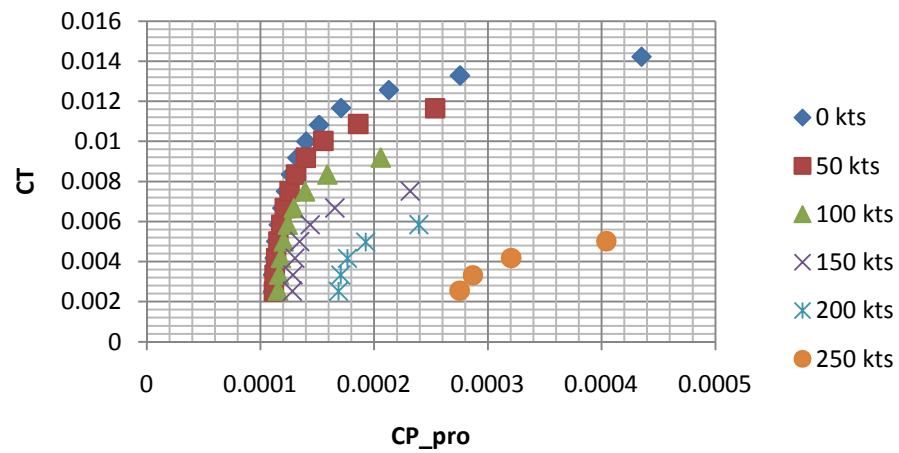
### Mast Angle = 20 deg



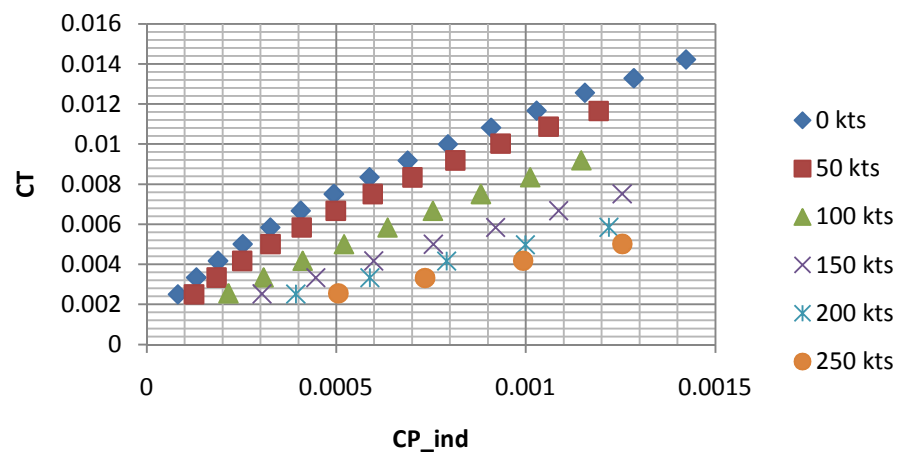
### Mast Angle = 20 deg



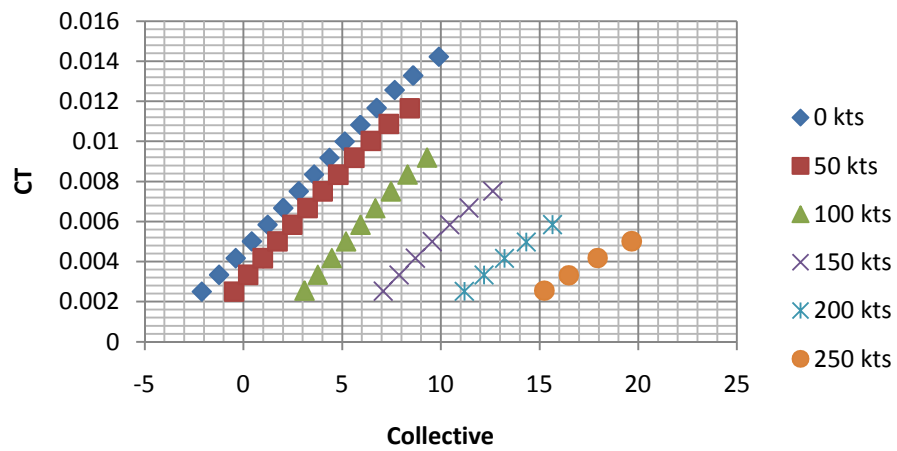
### Mast Angle = 20 deg



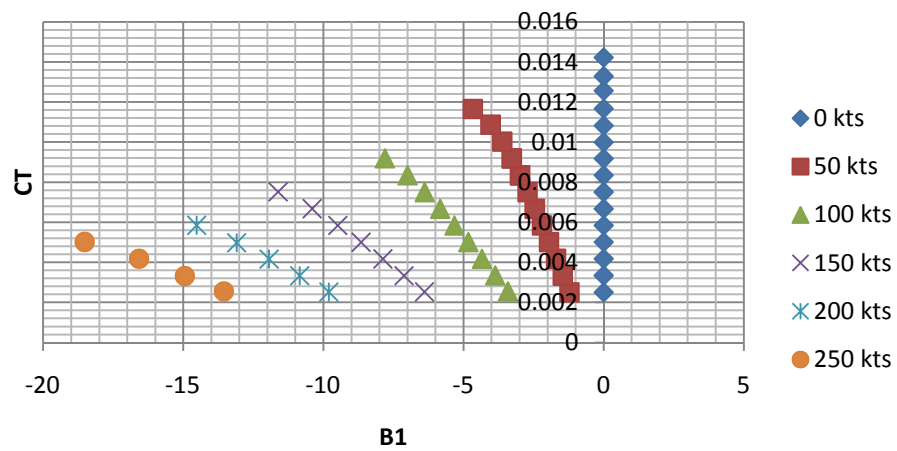
### Mast Angle = 20 deg

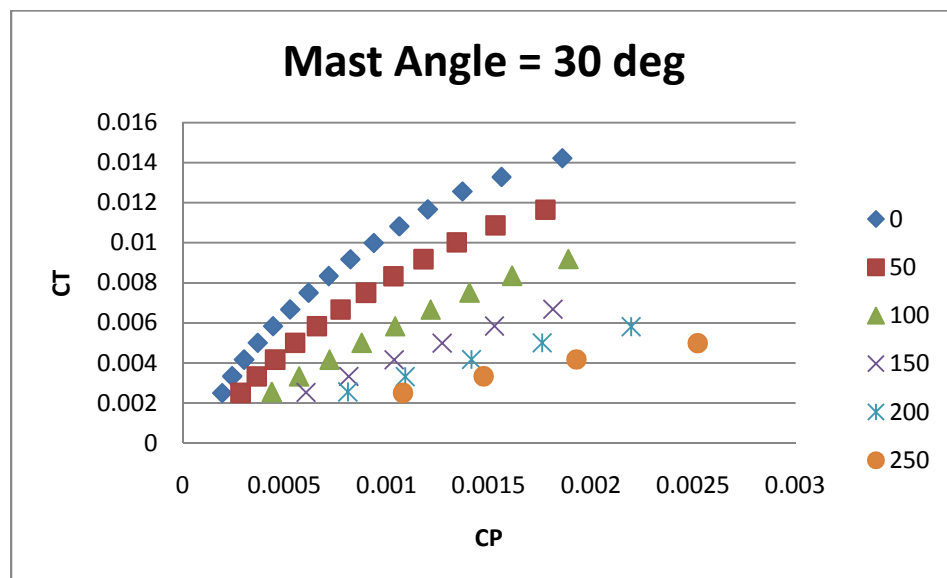
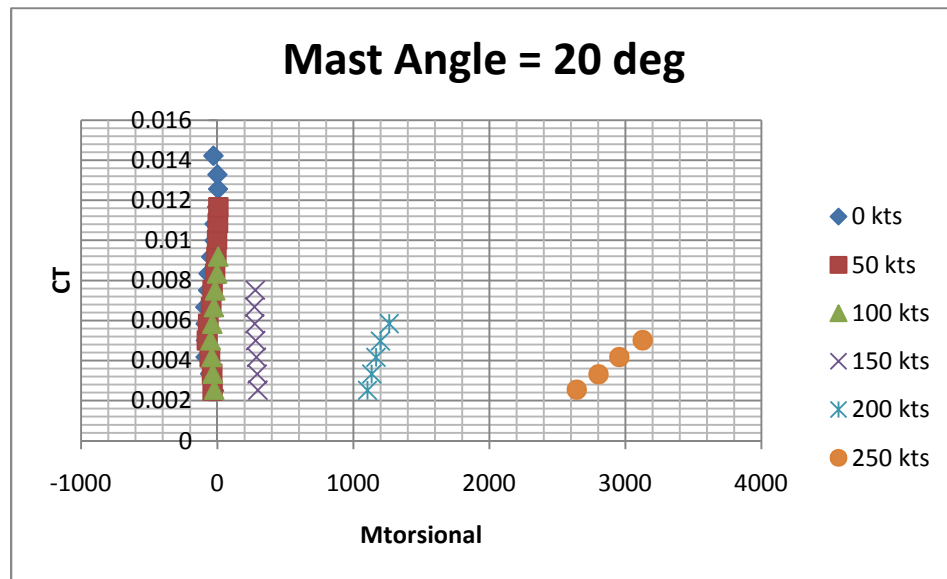


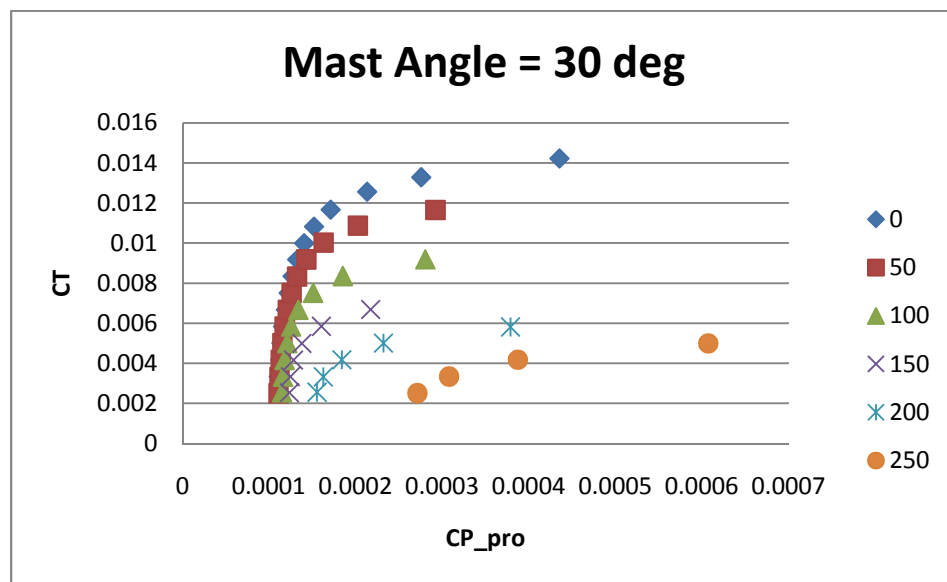
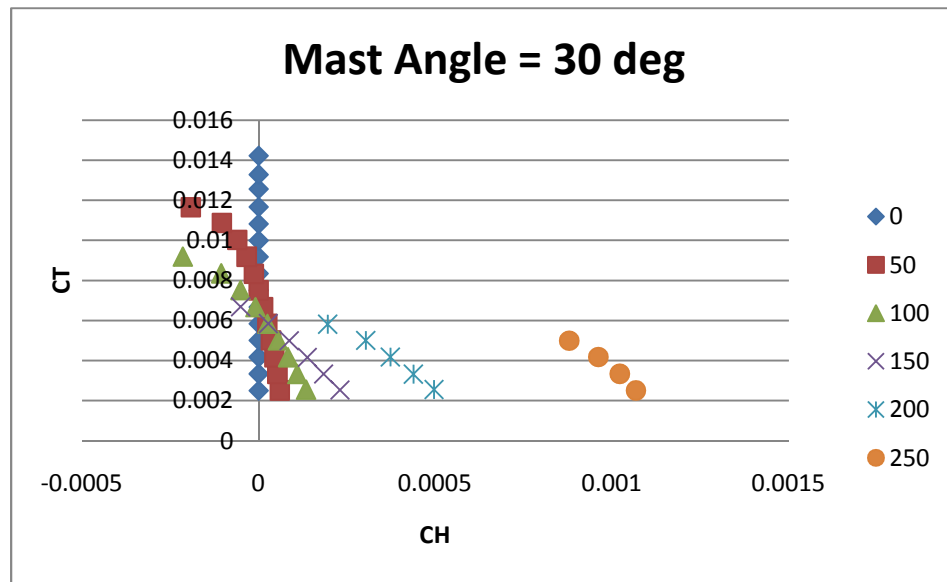
### Mast Angle = 20 deg

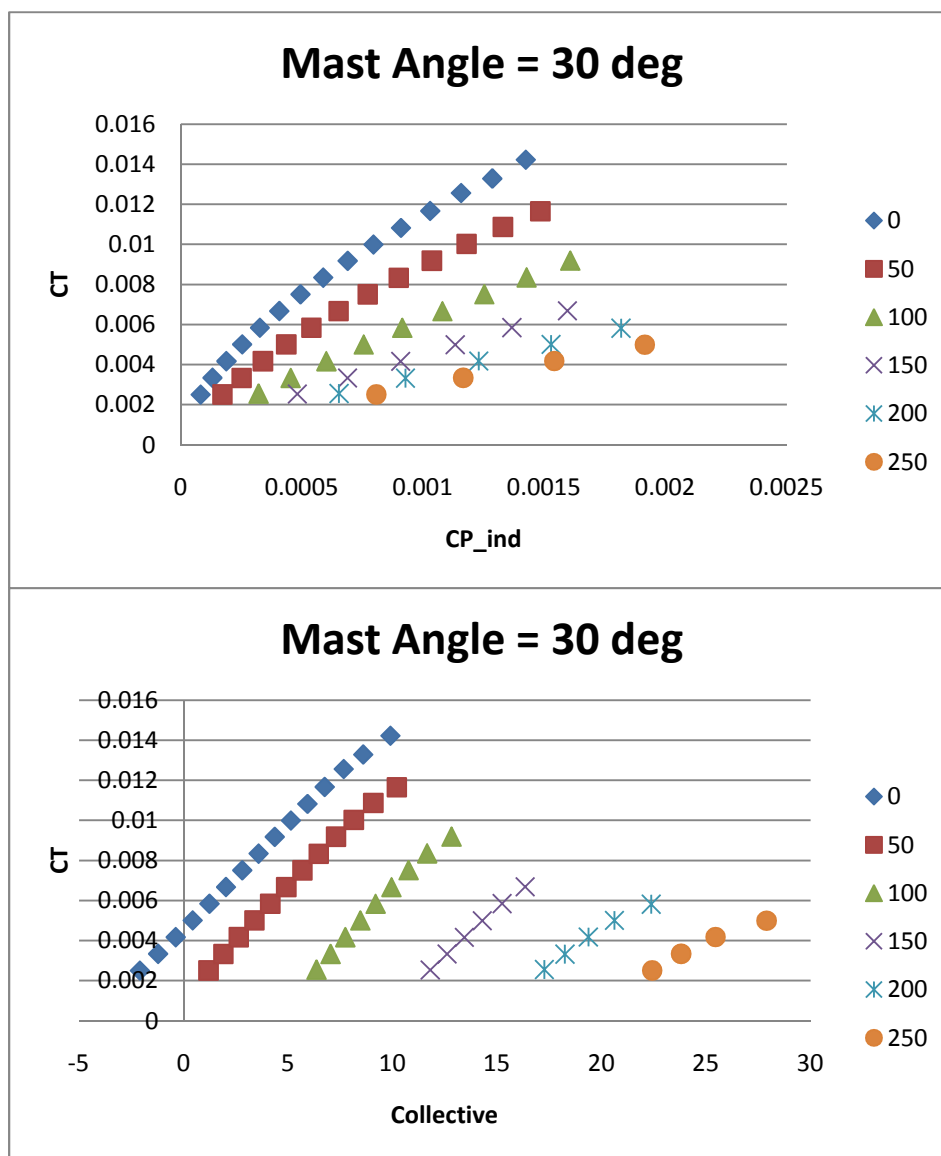


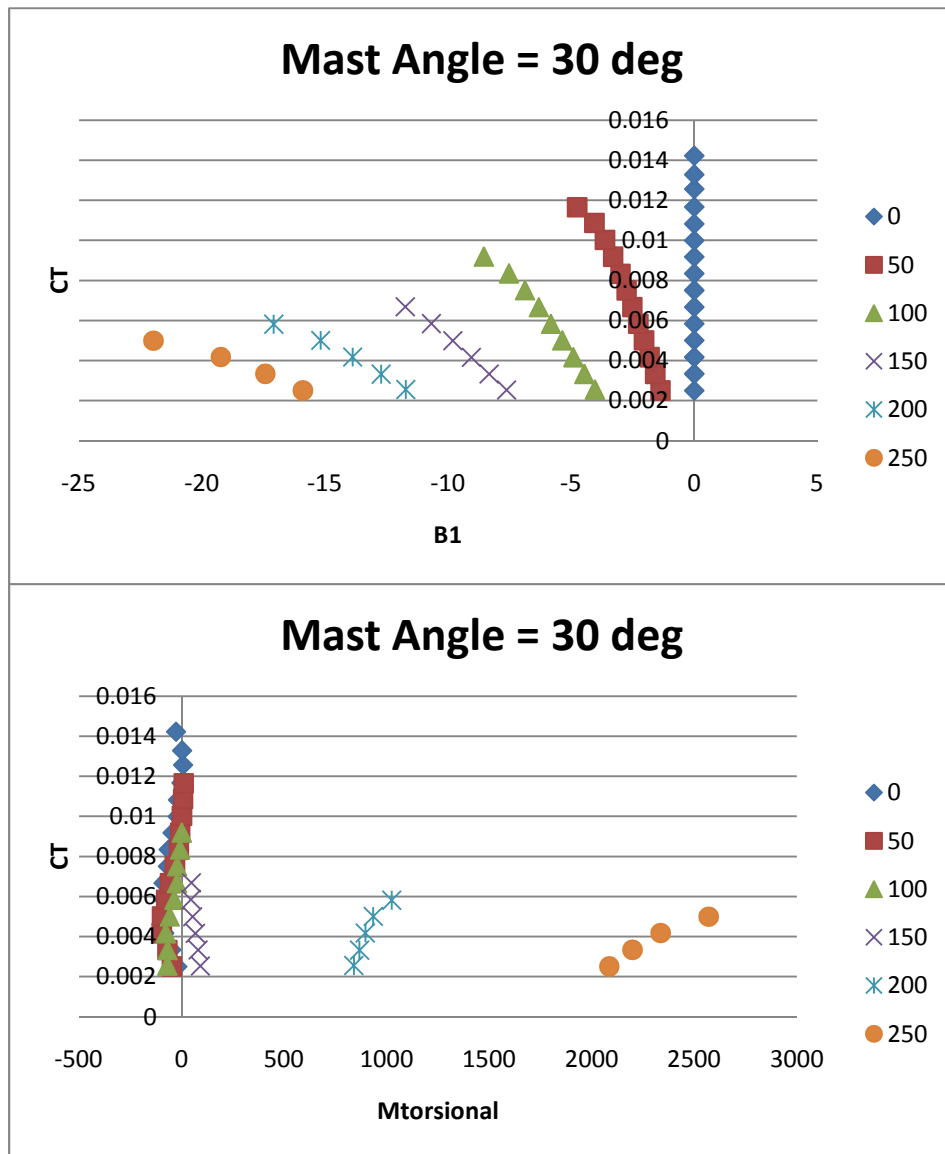
### Mast Angle = 20 deg

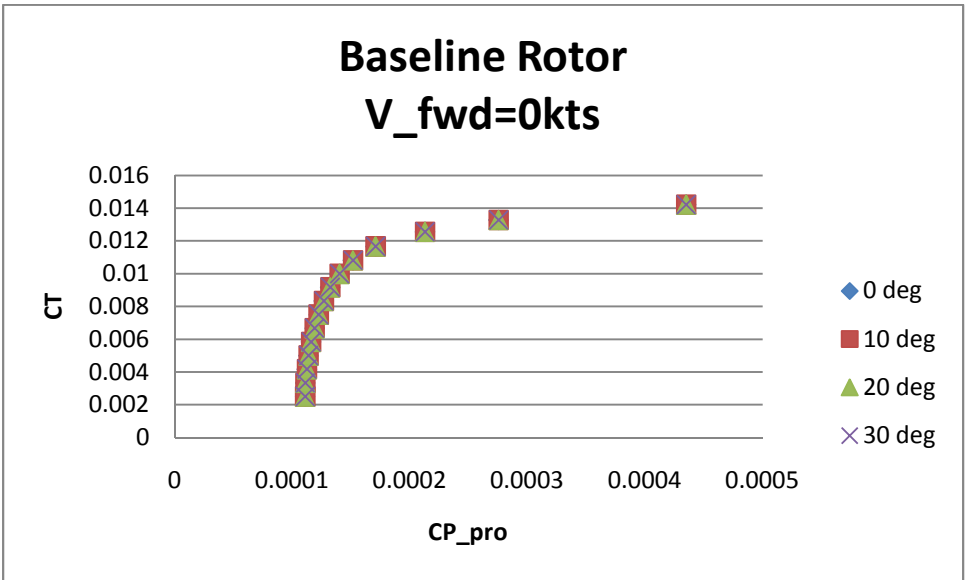
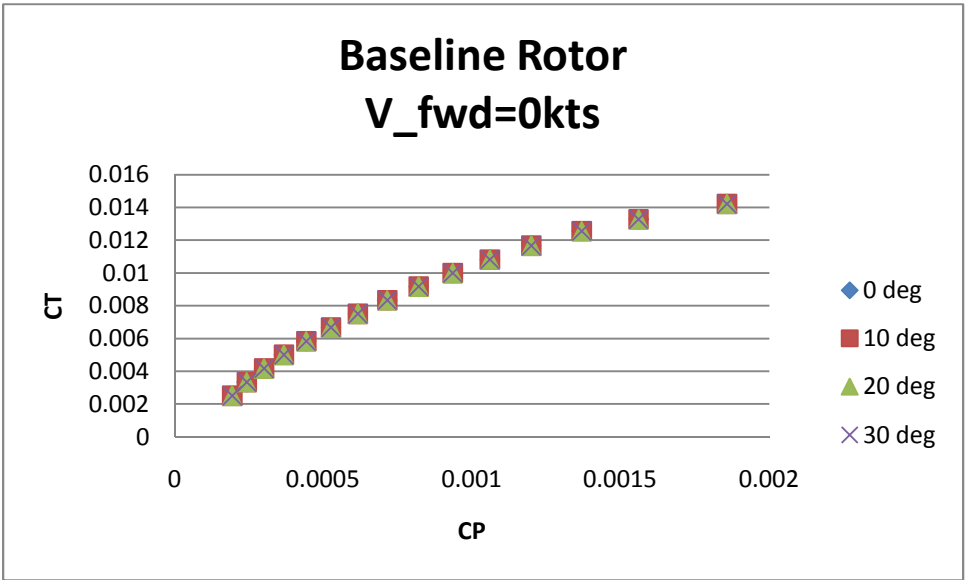




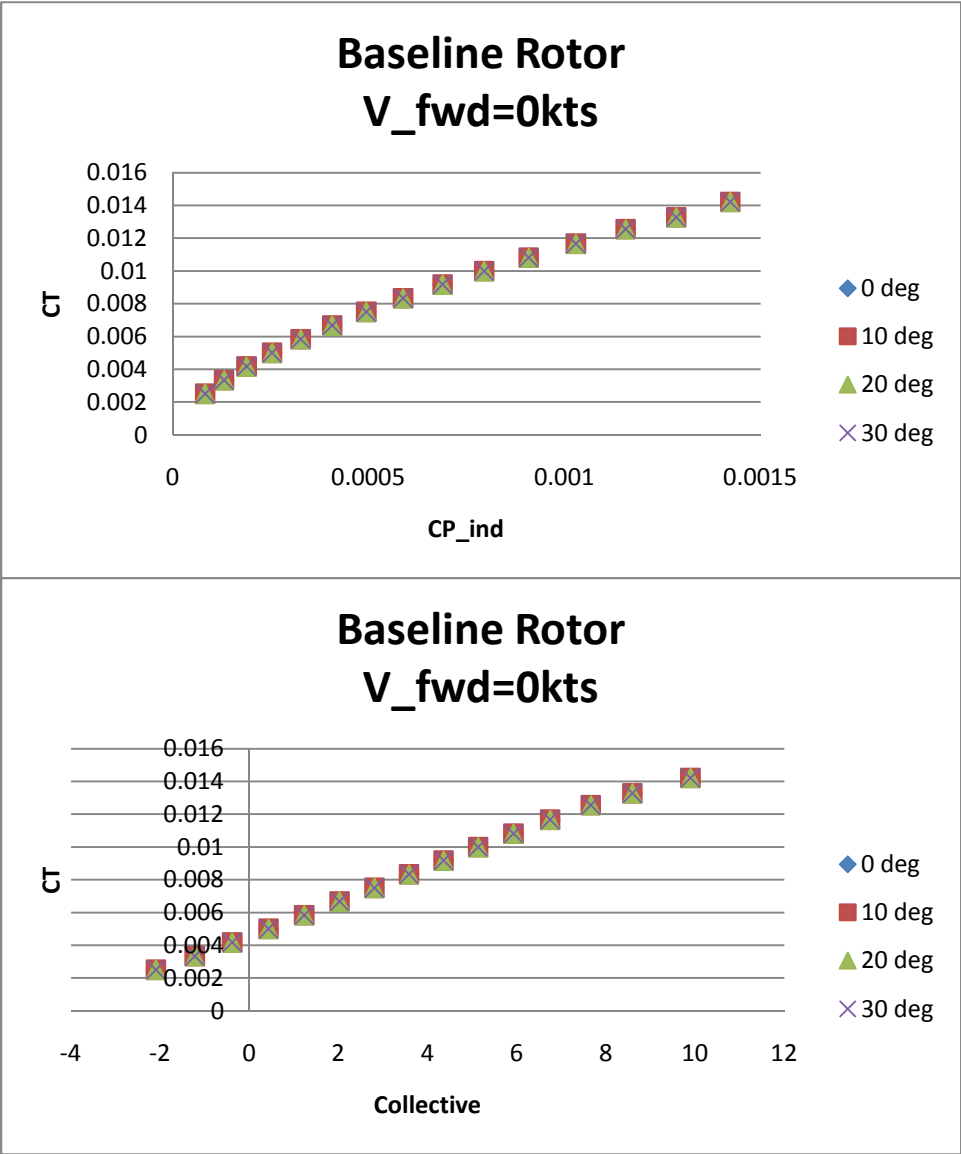


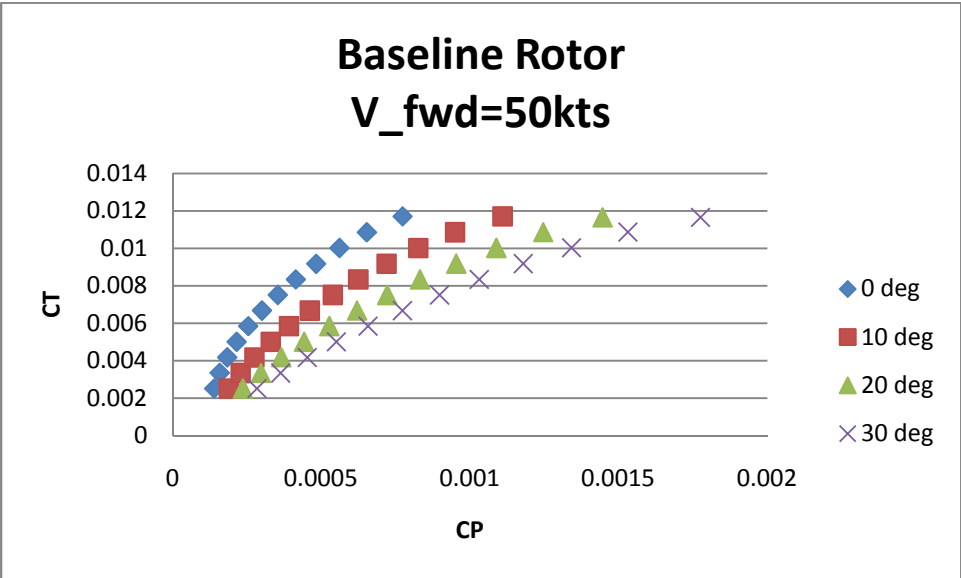
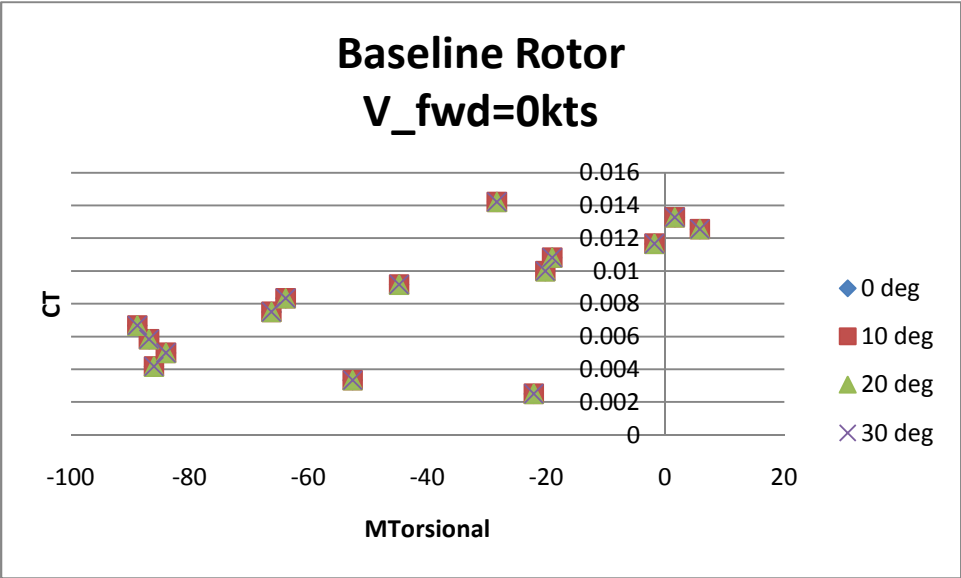


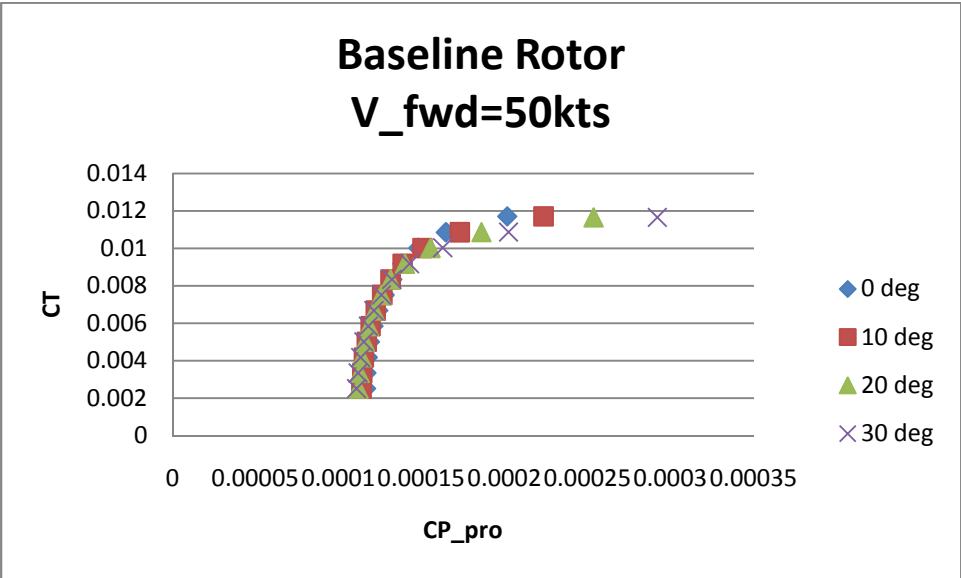
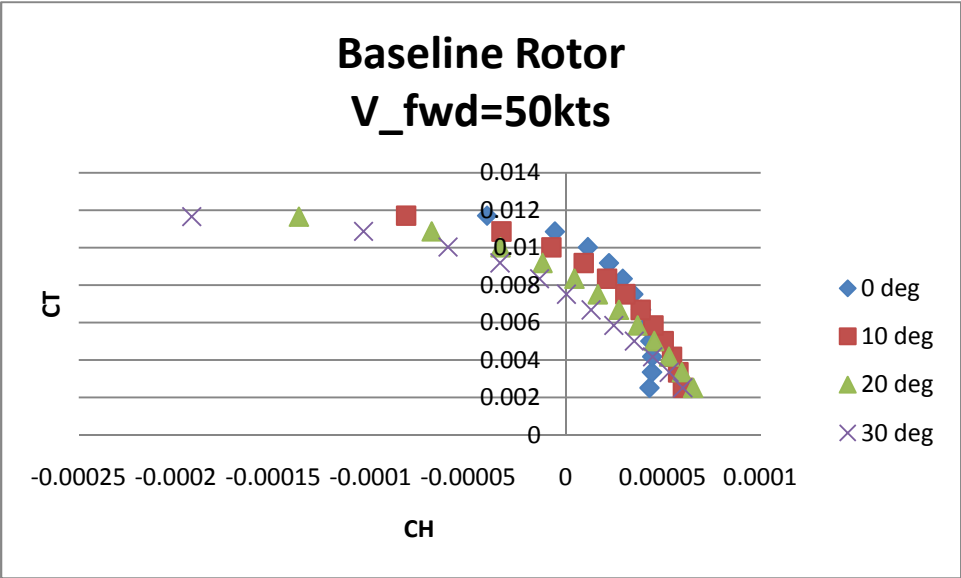


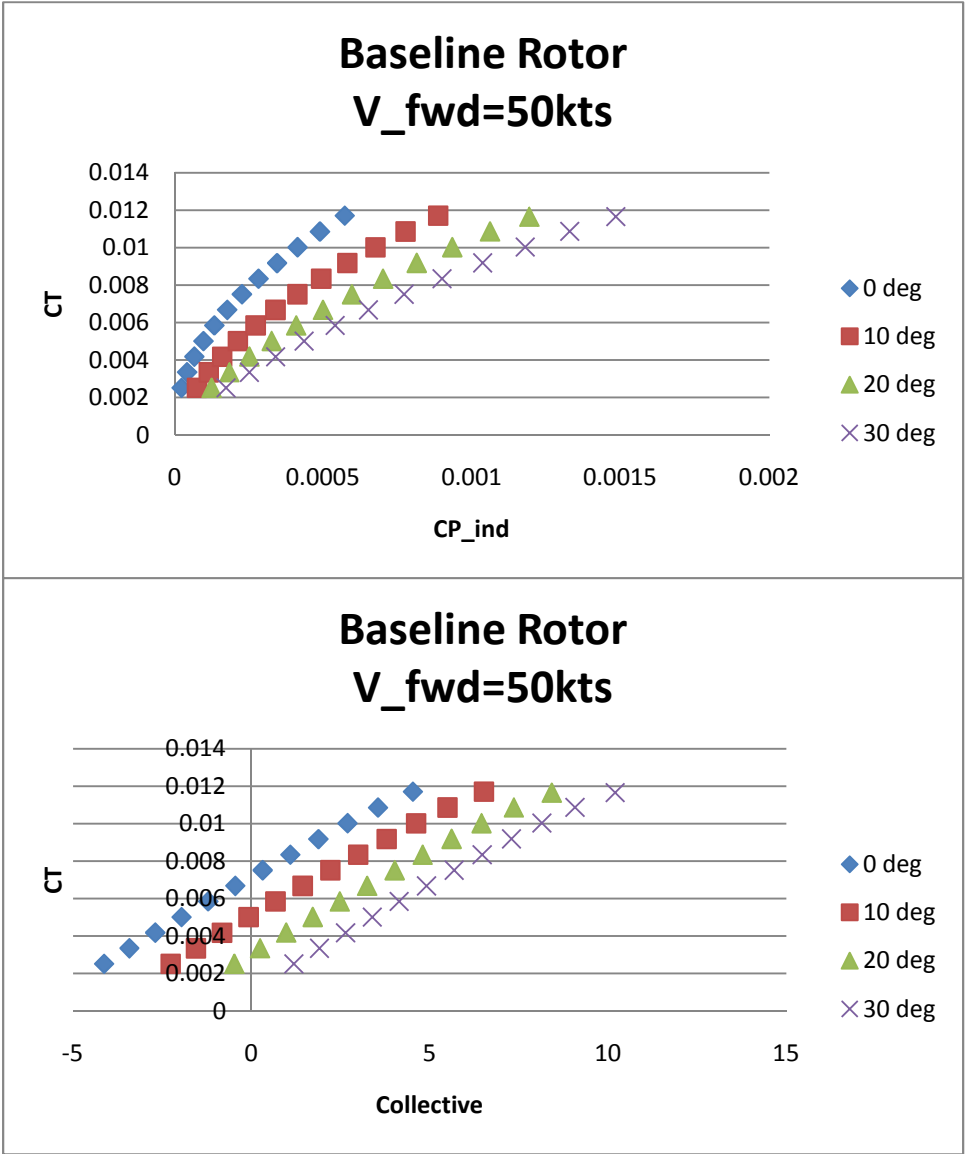


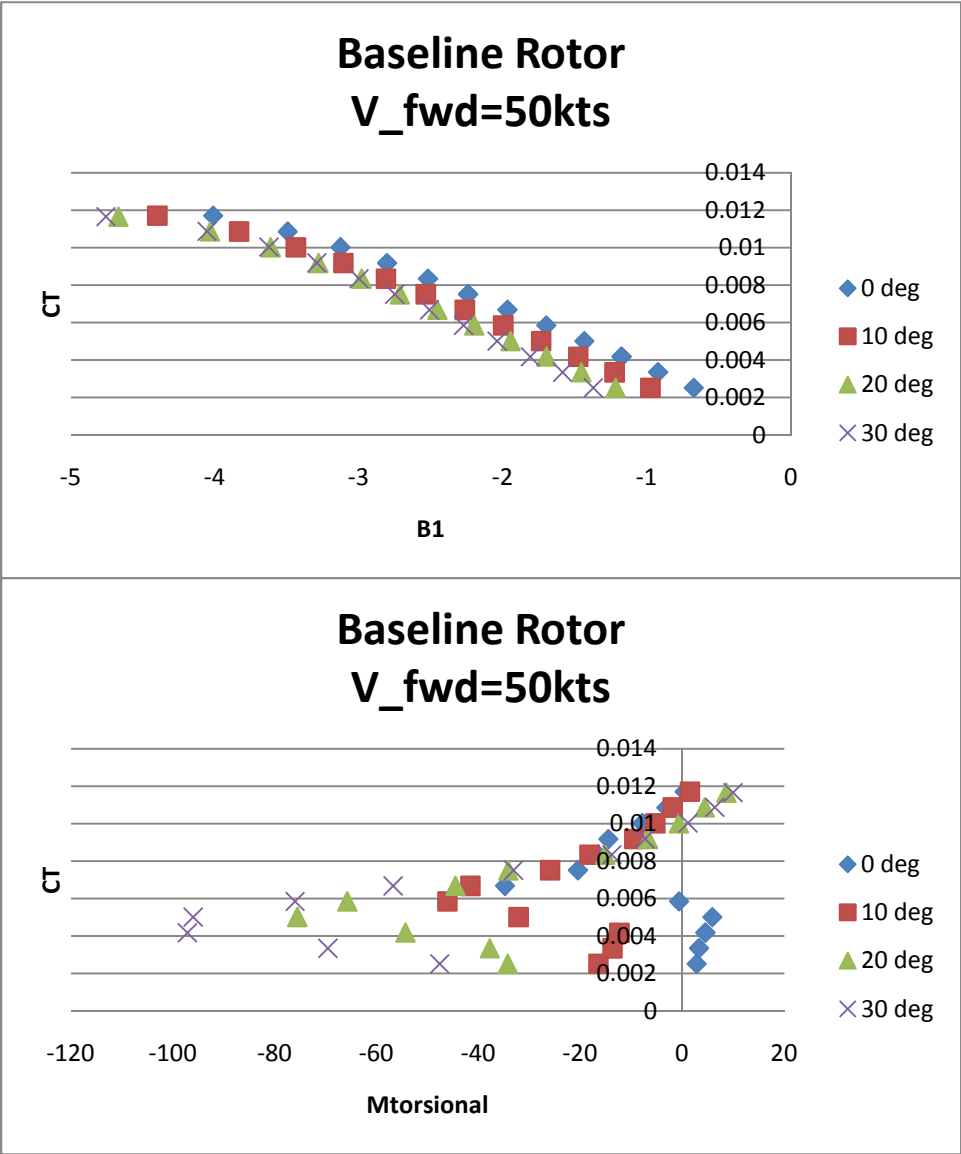


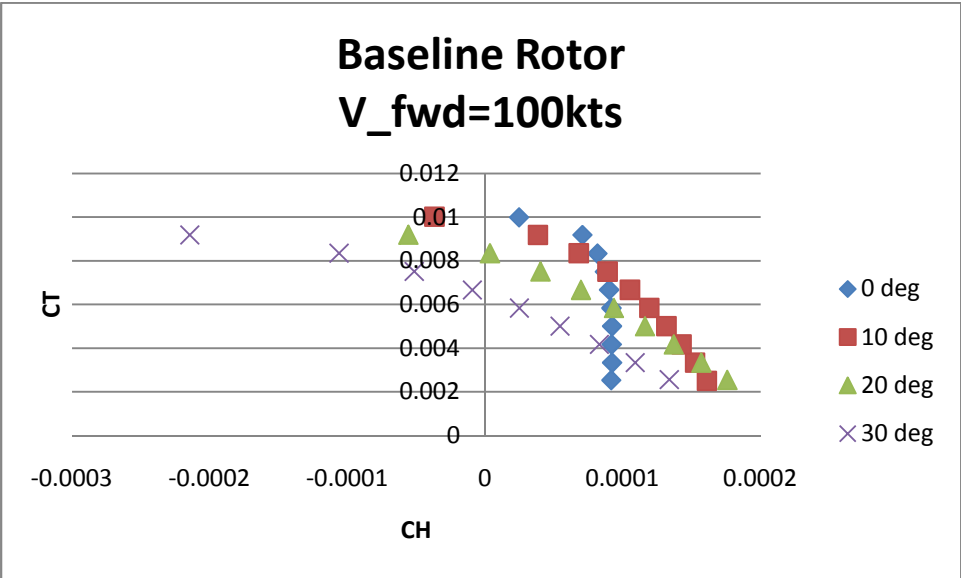
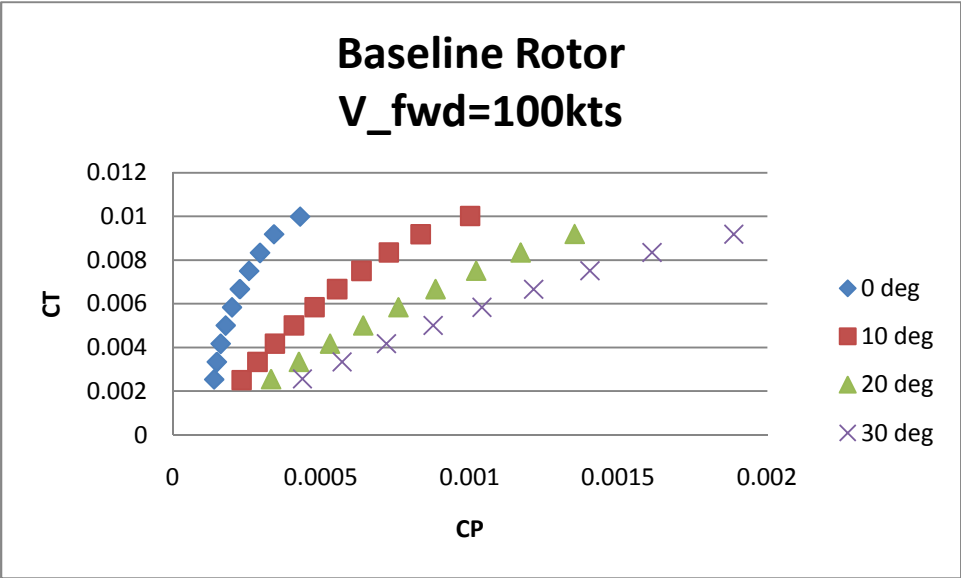


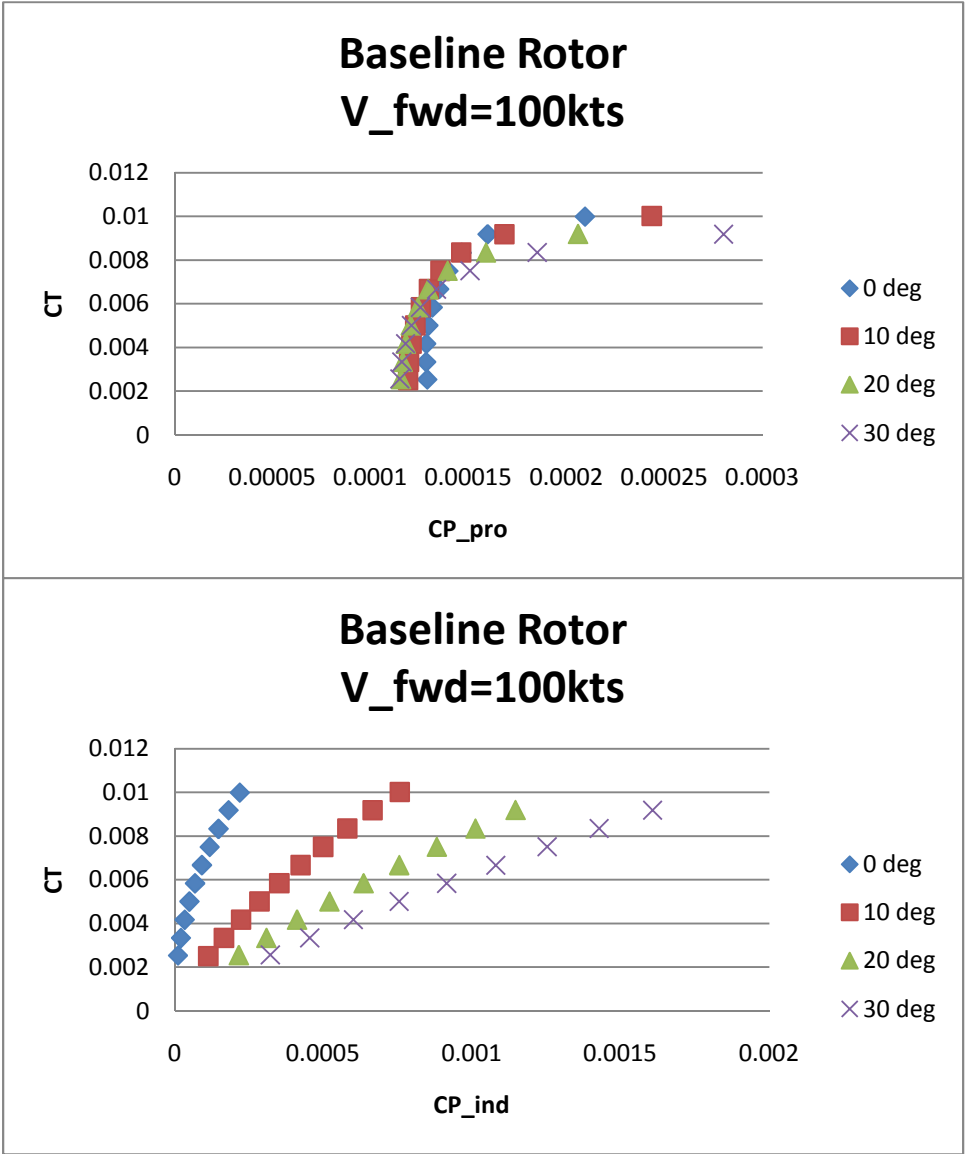


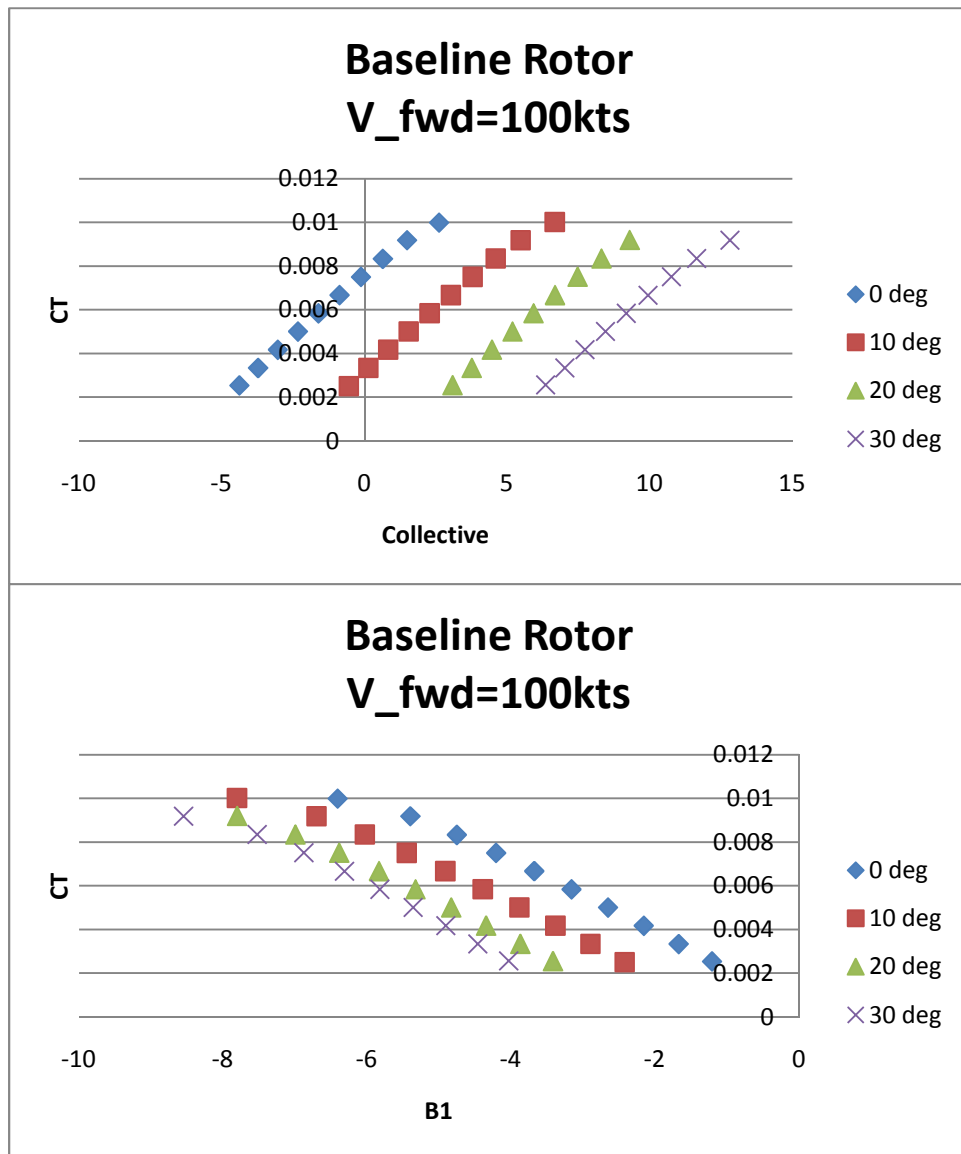




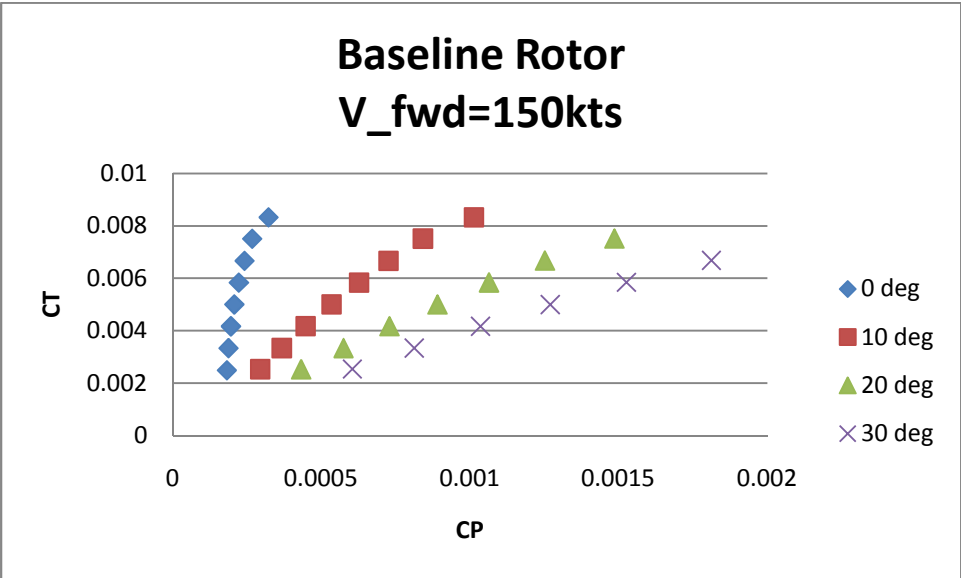
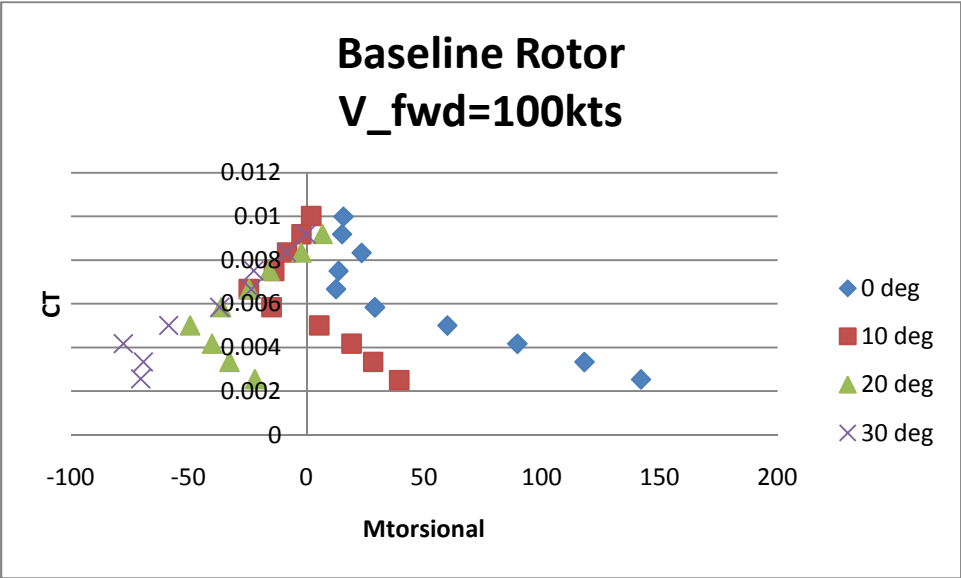


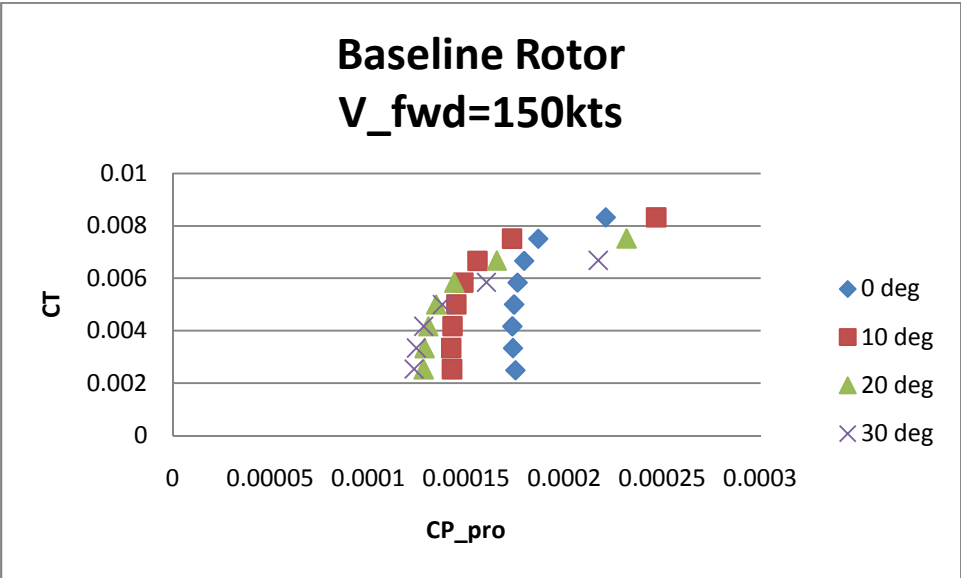
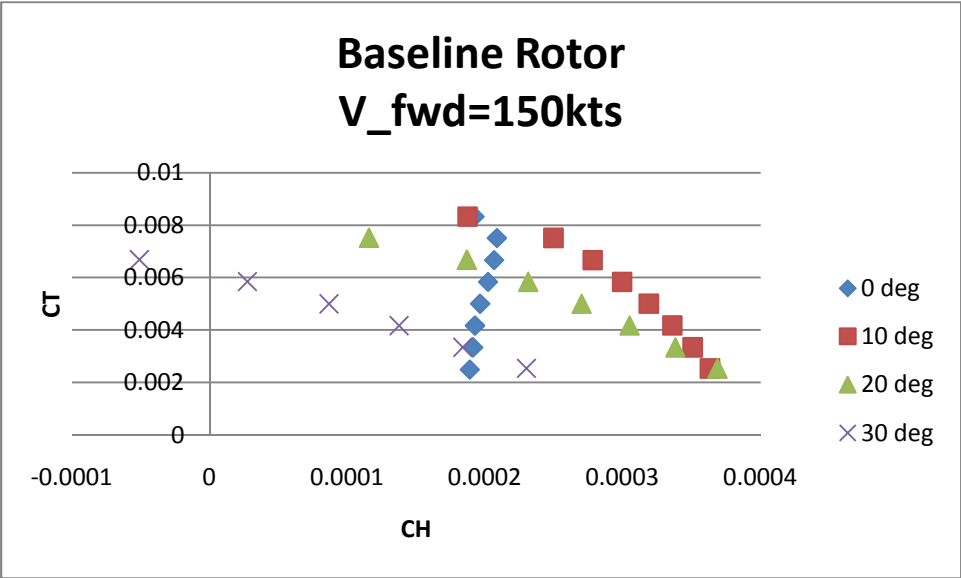


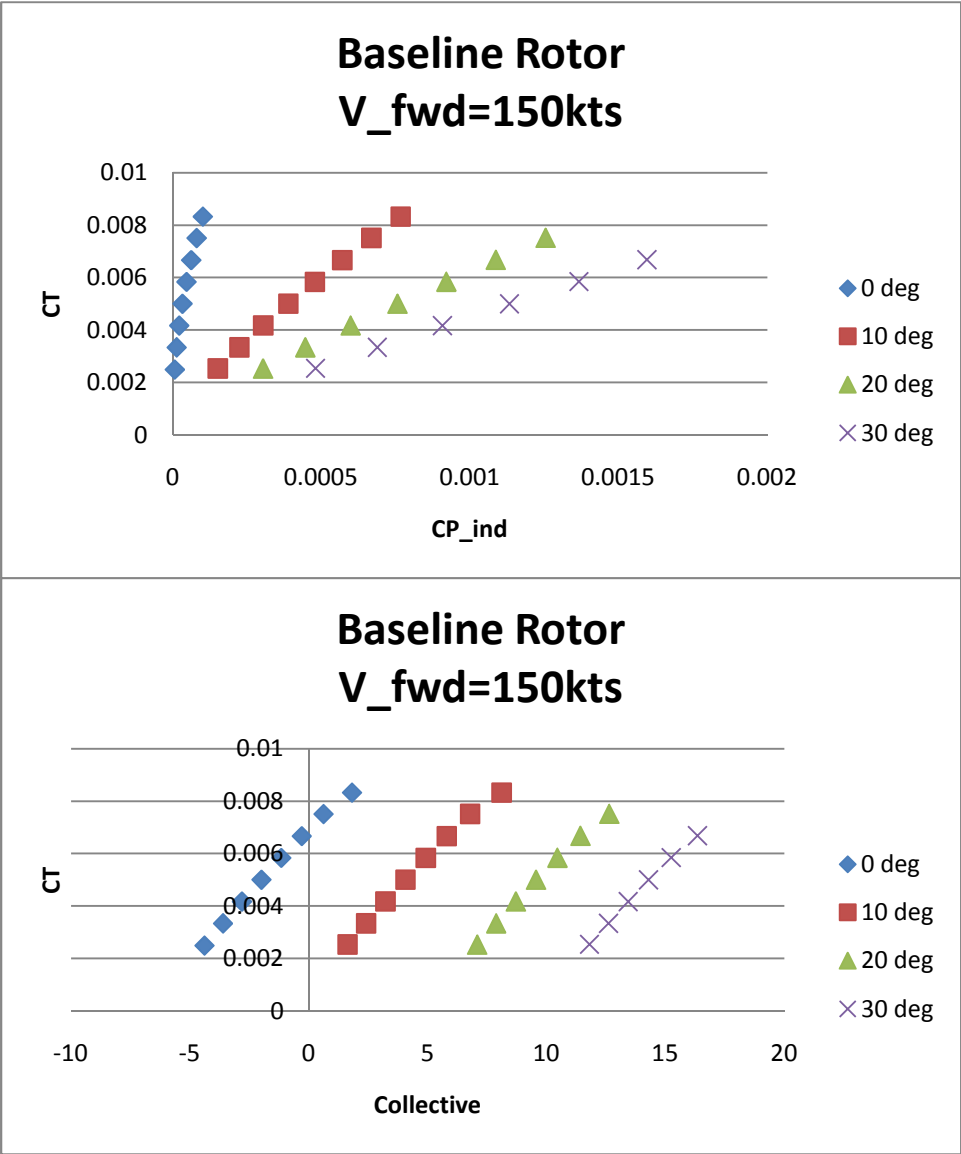


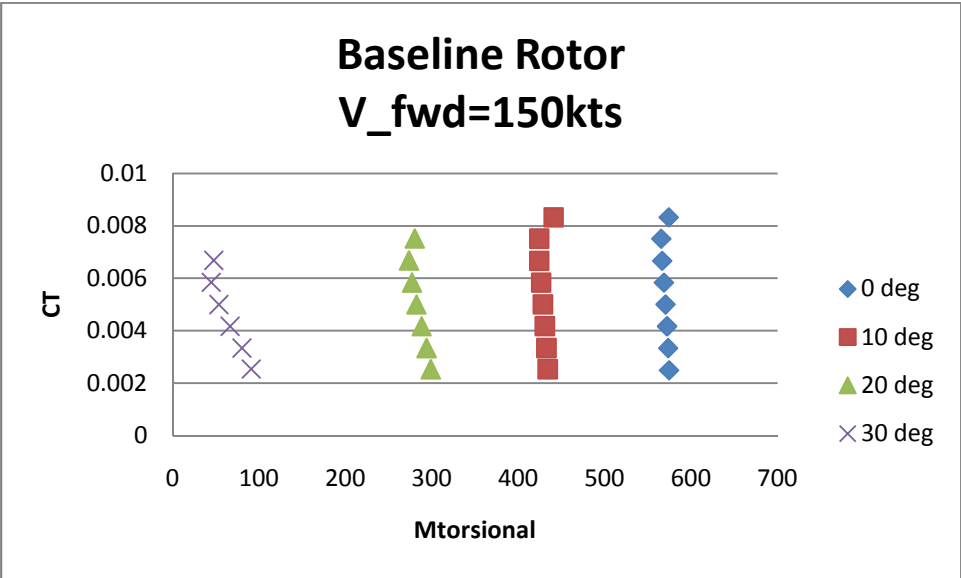
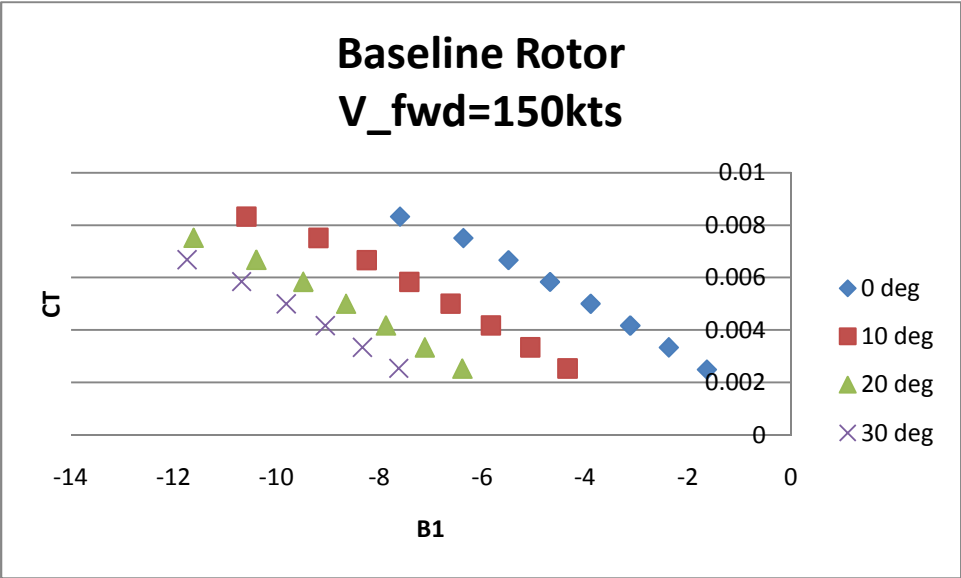


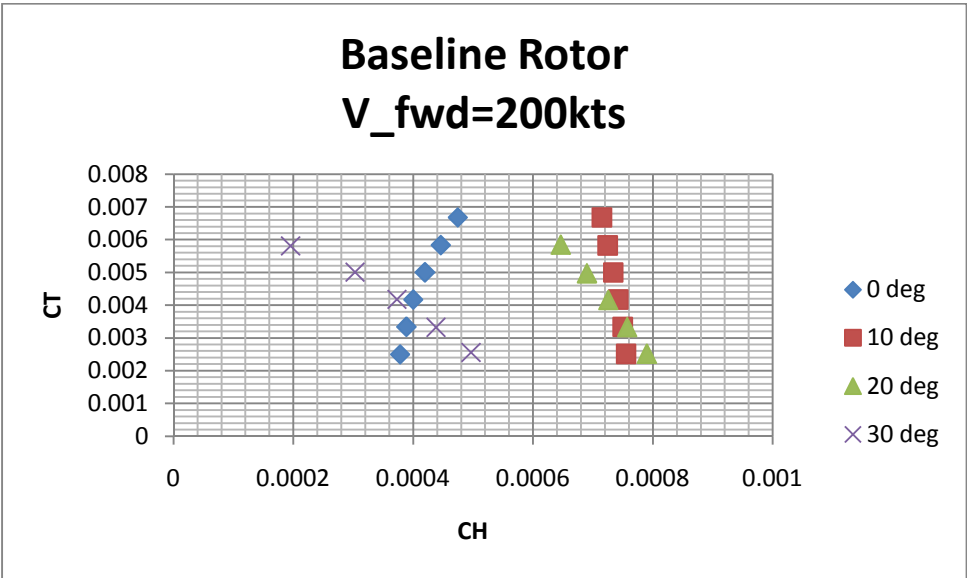
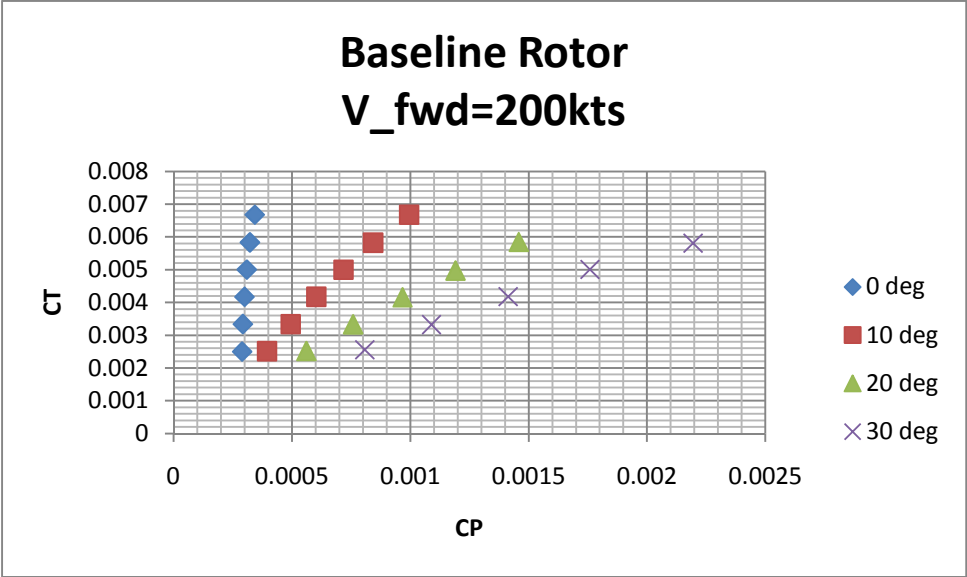


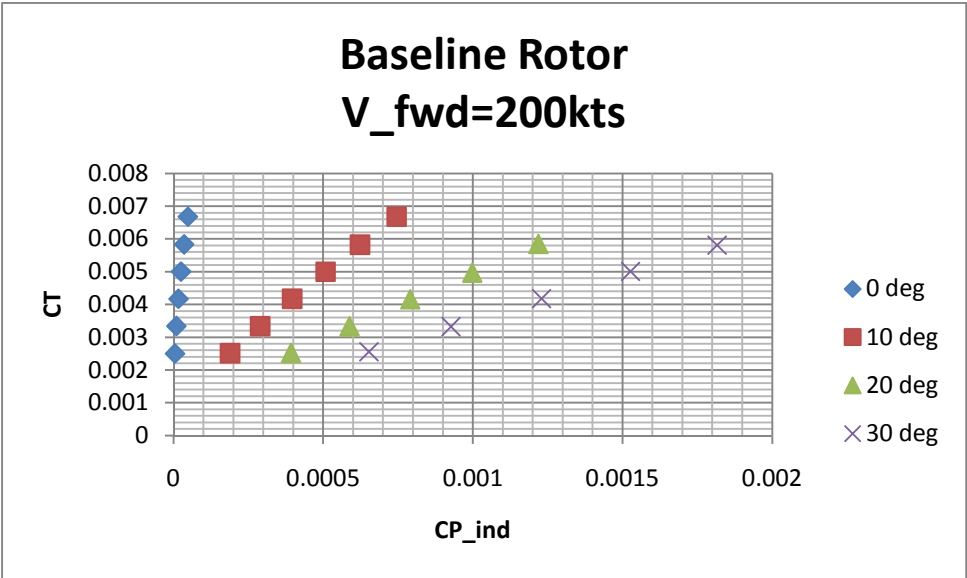
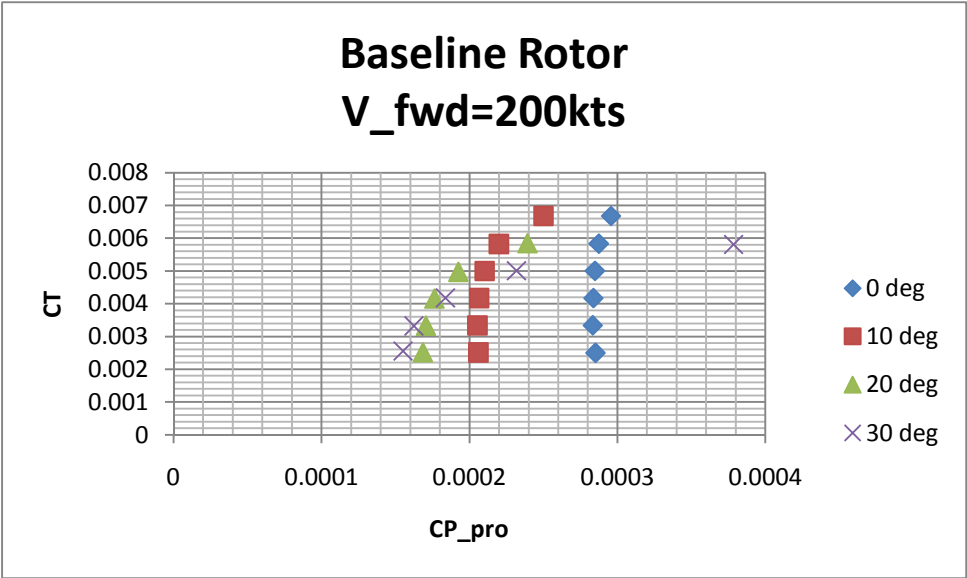


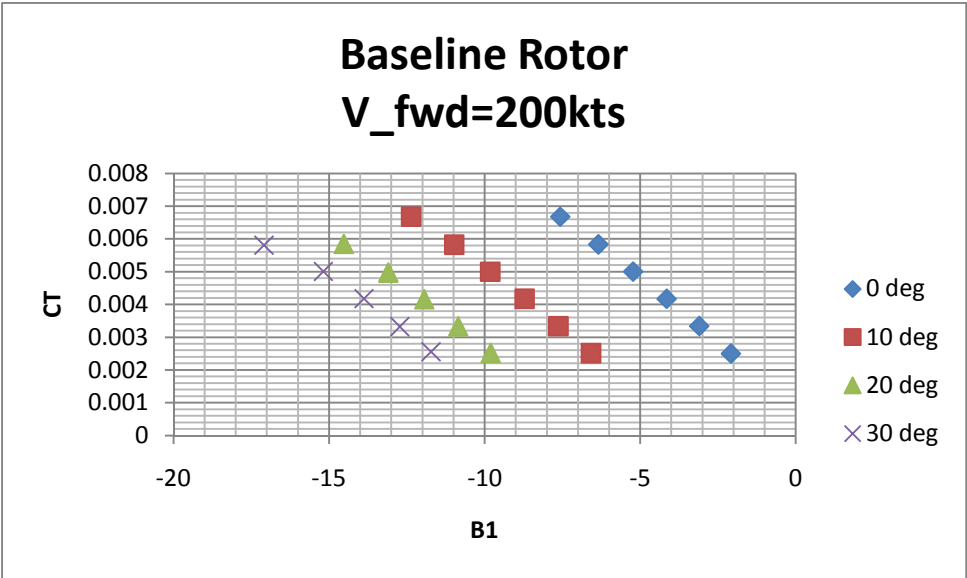
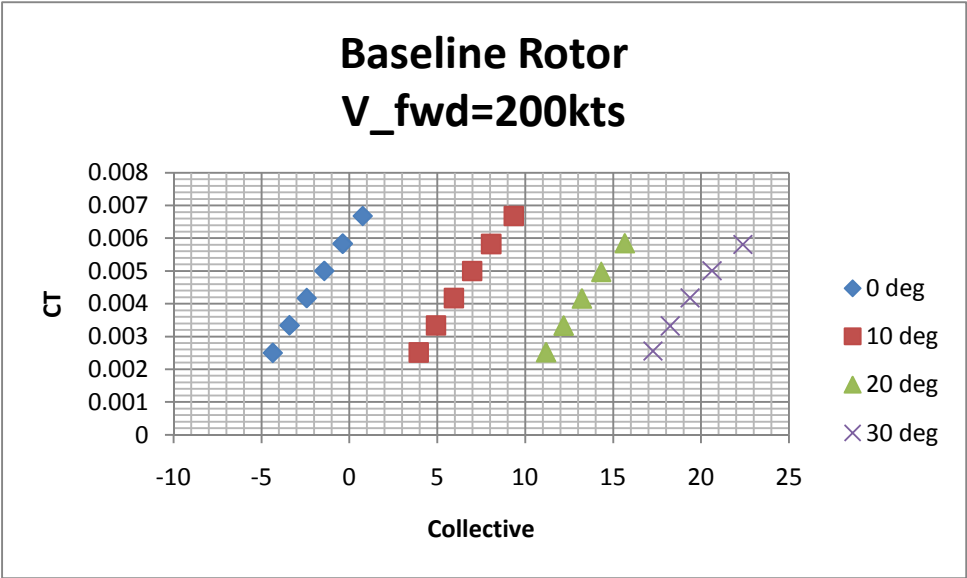


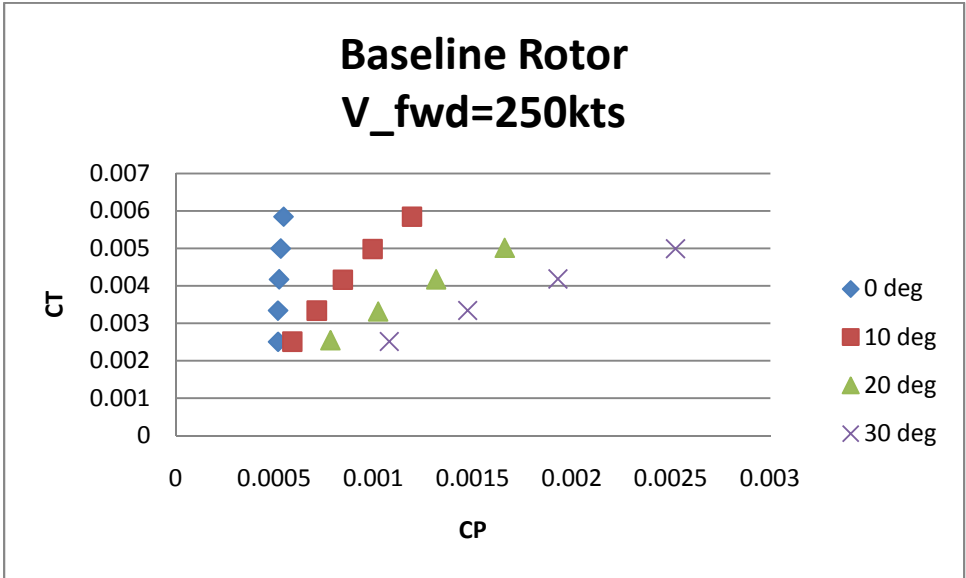
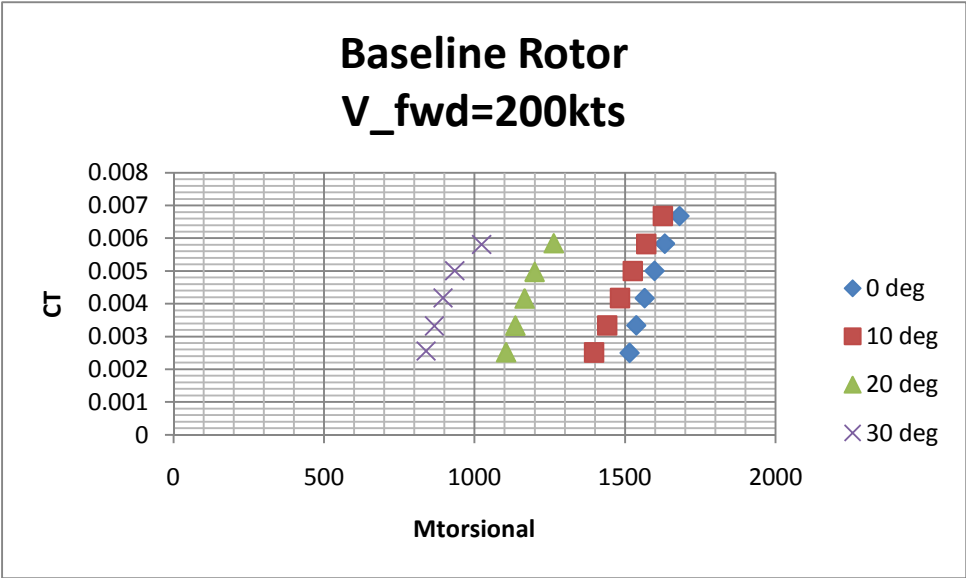




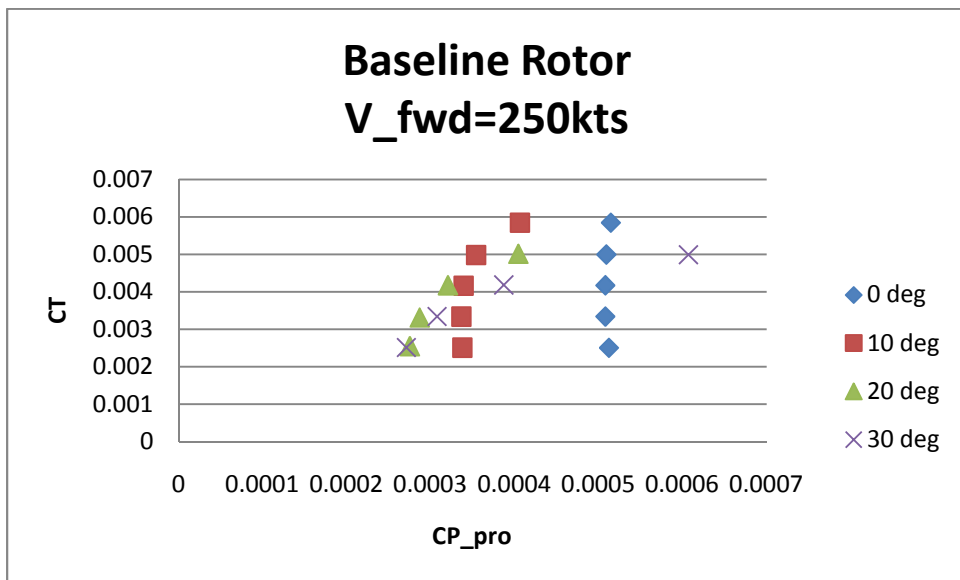
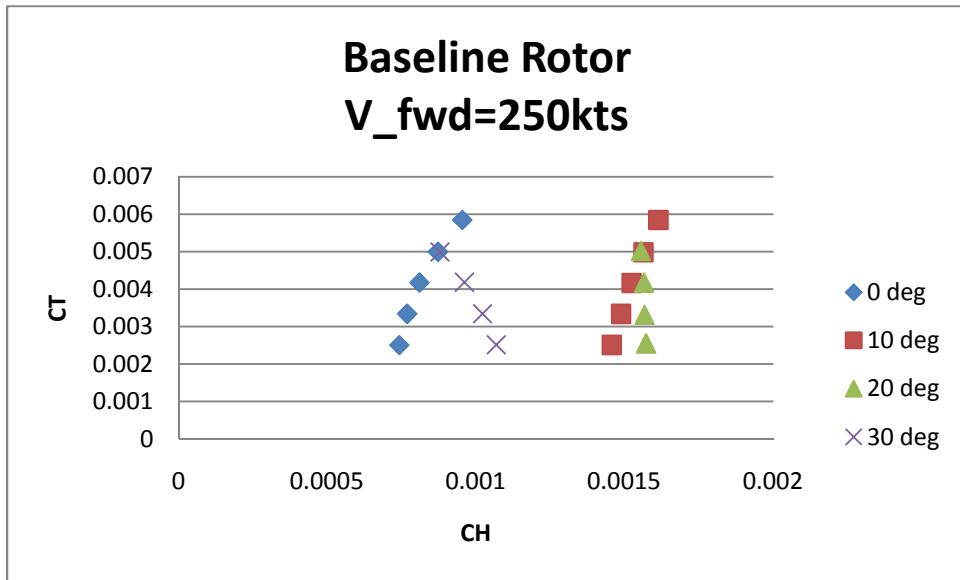


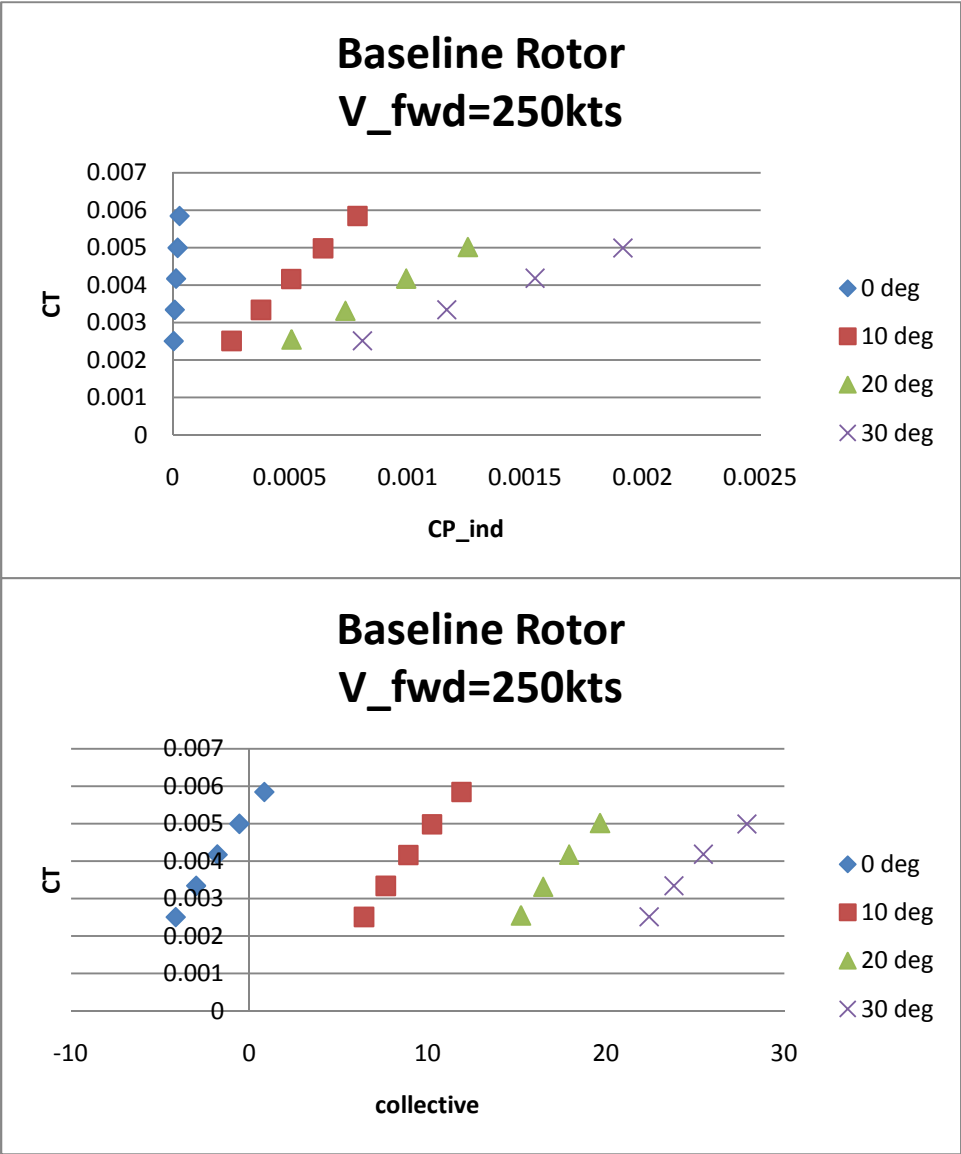


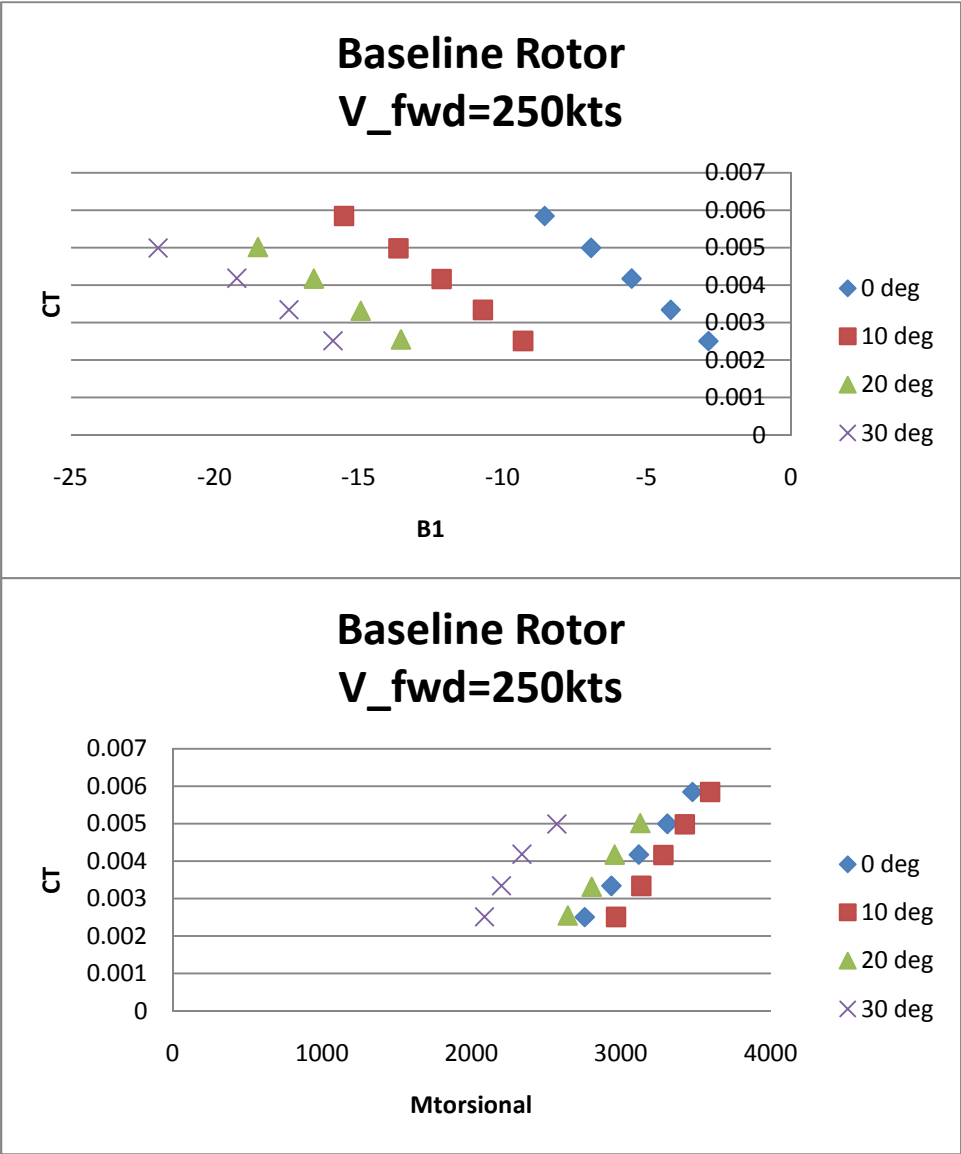






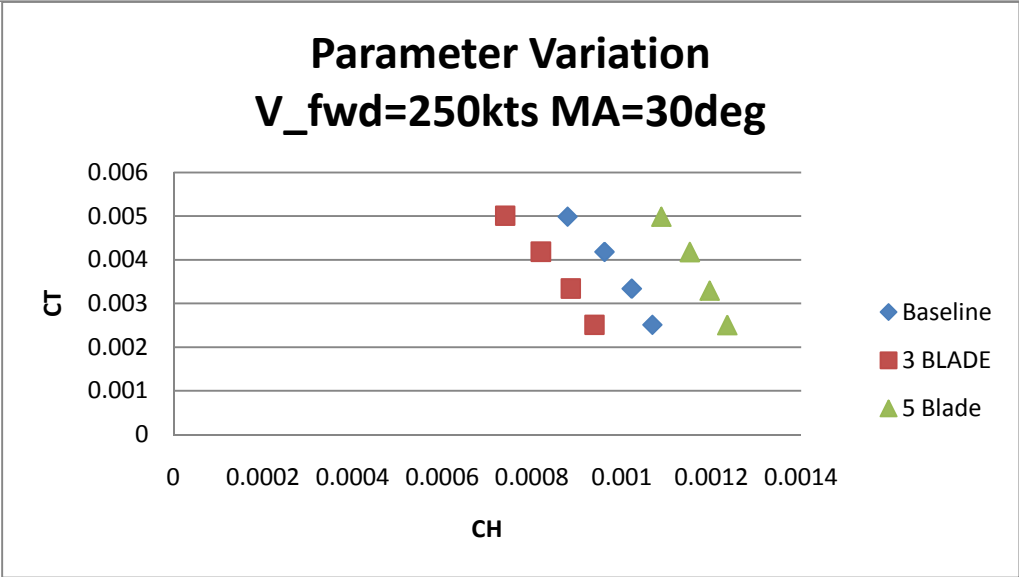
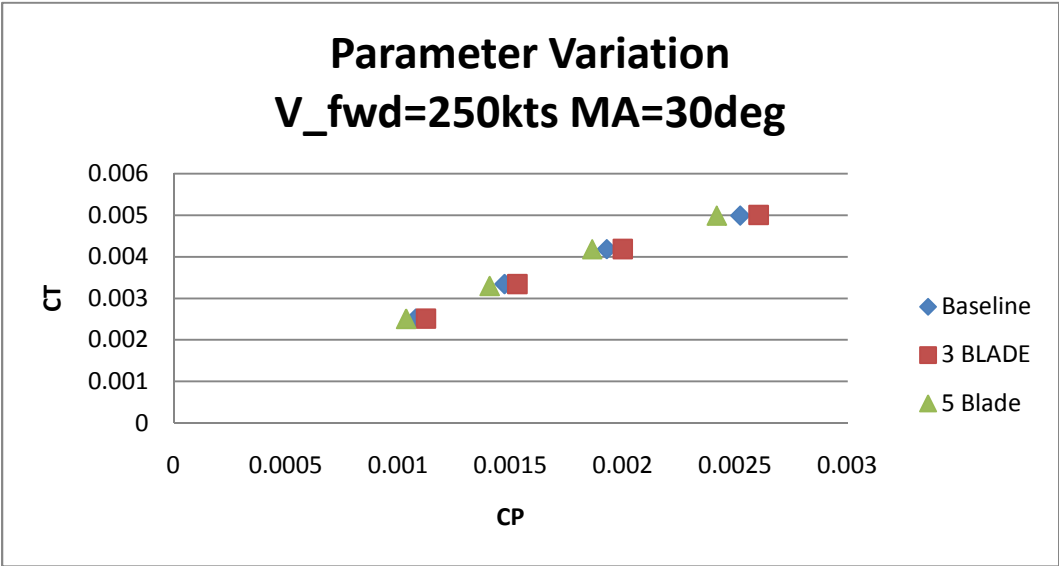


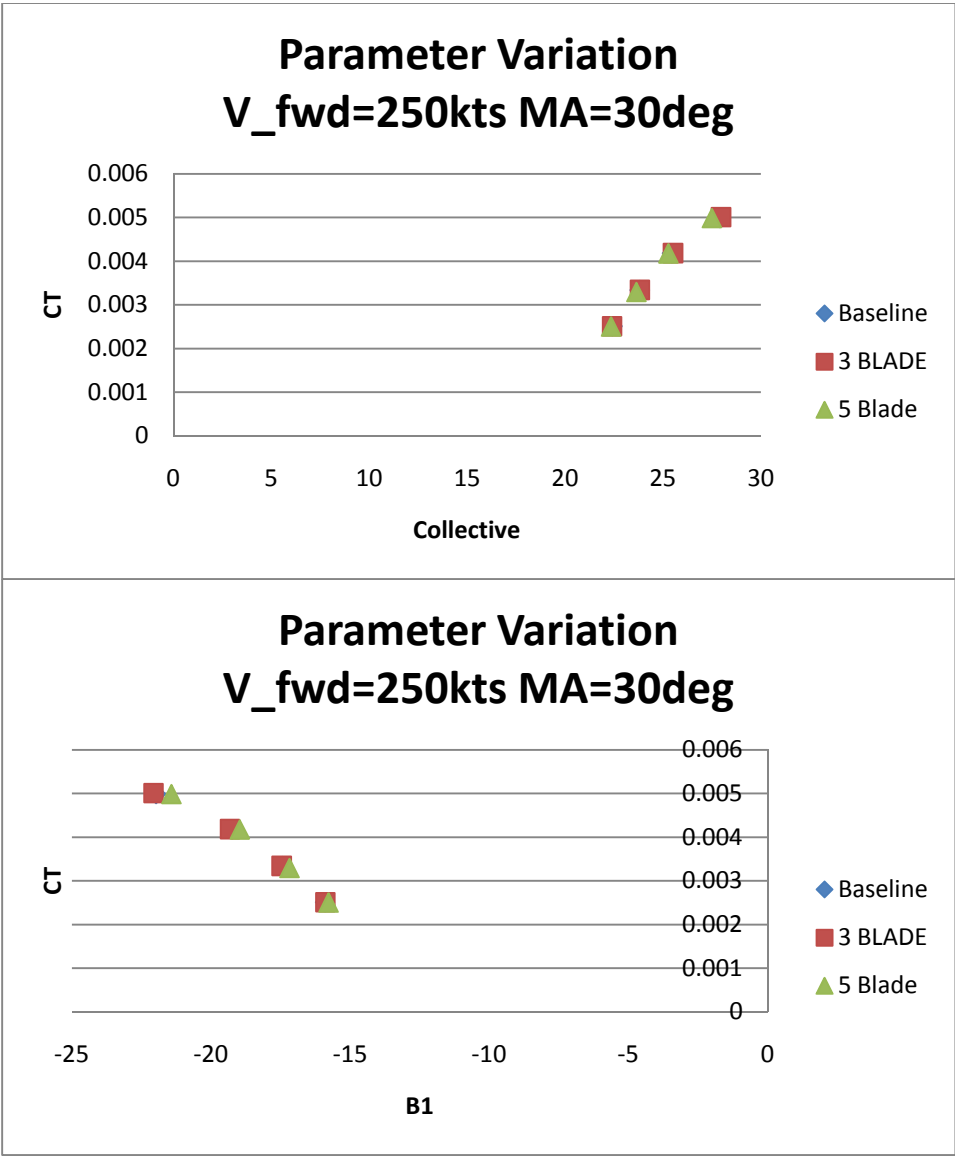


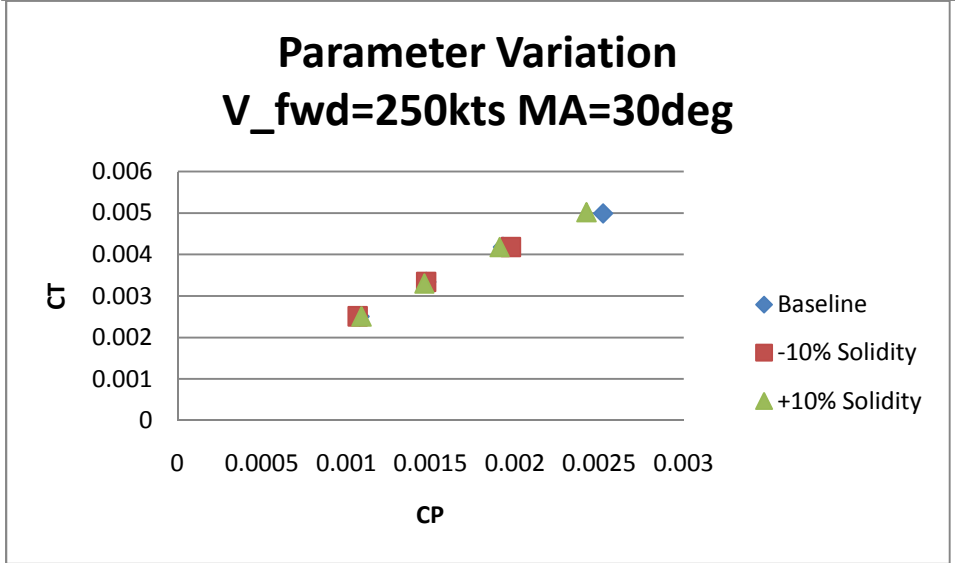
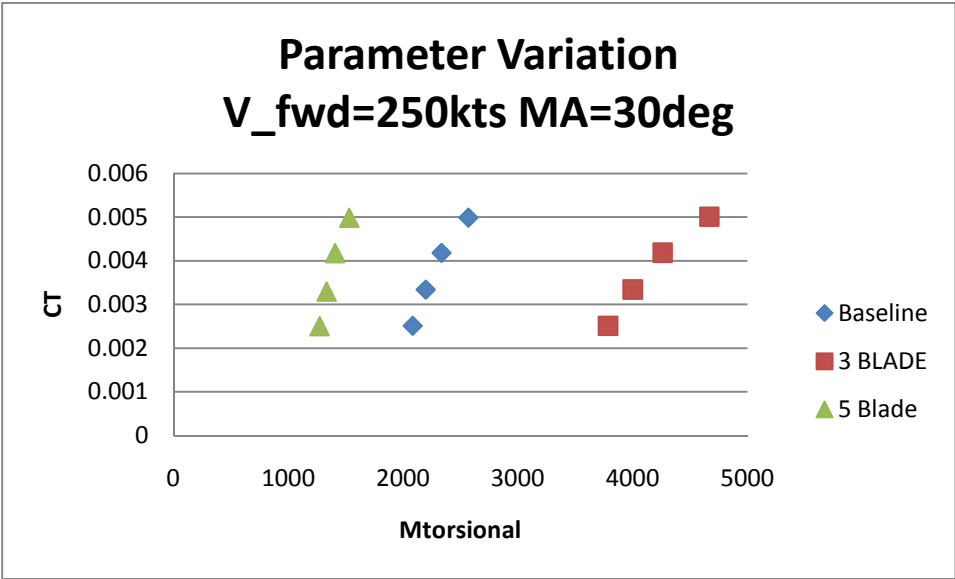


## APPENDIX B

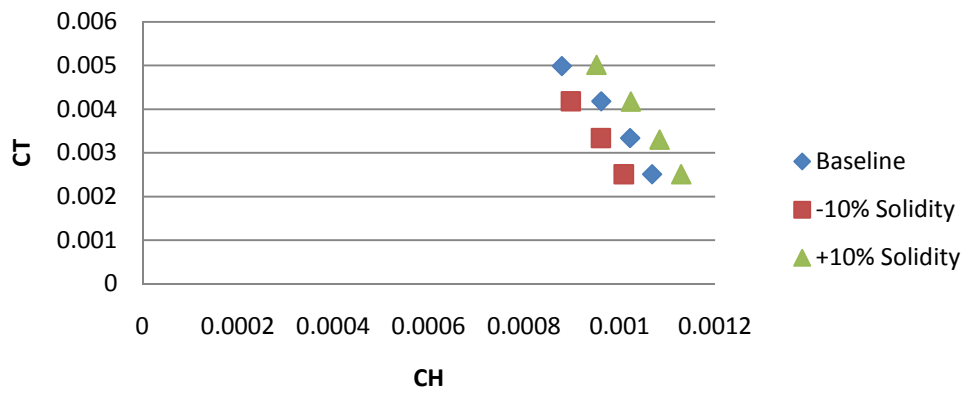
### ROTOR PARAMETER VARIATION STUDY DATA



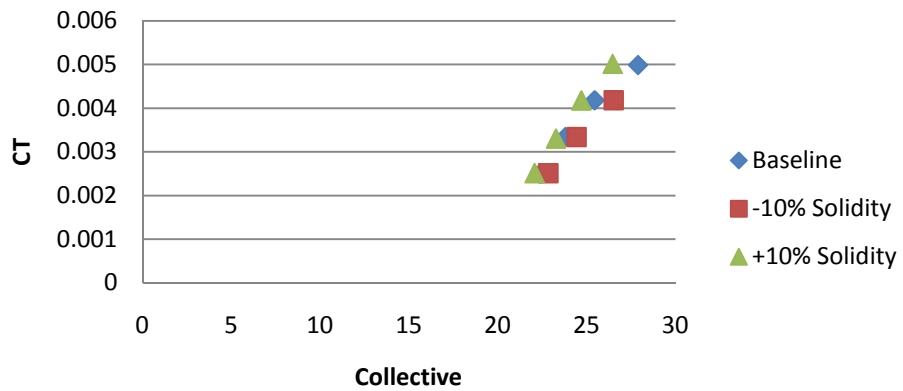




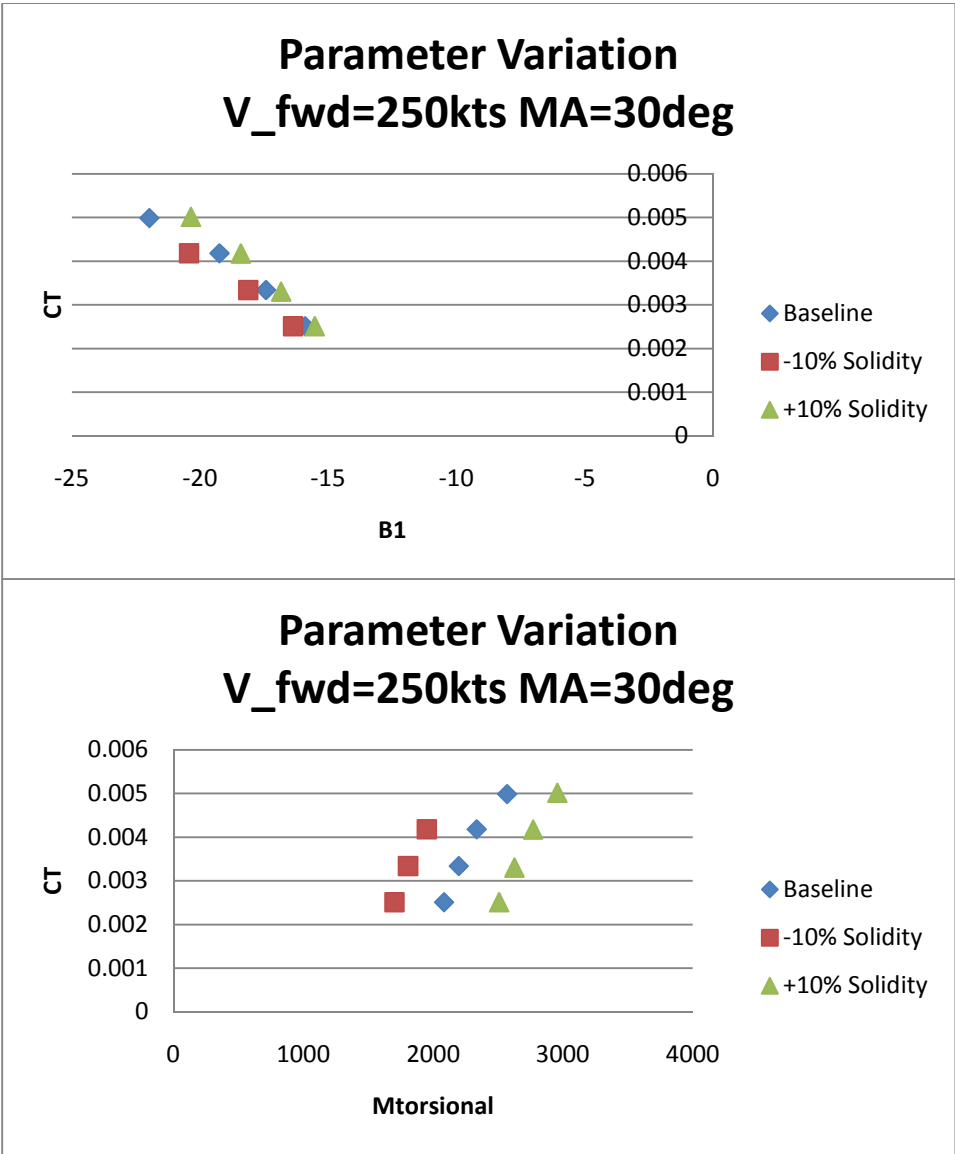
### Parameter Variation V\_fwd=250kts MA=30deg



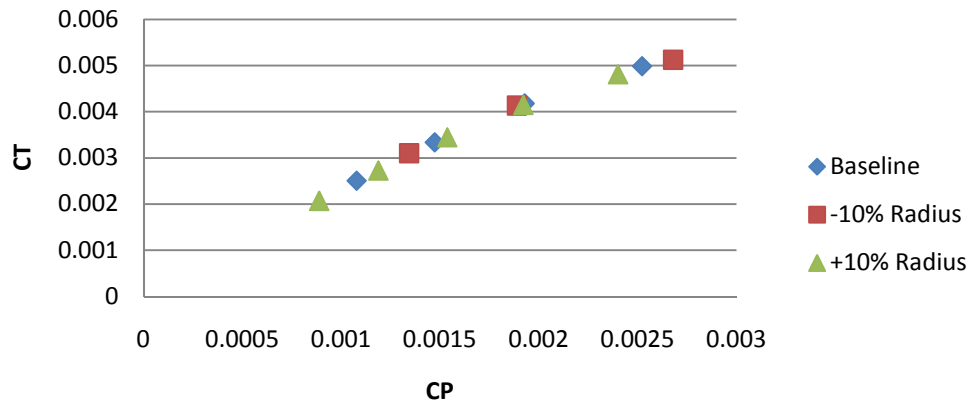
### Parameter Variation V\_fwd=250kts MA=30deg



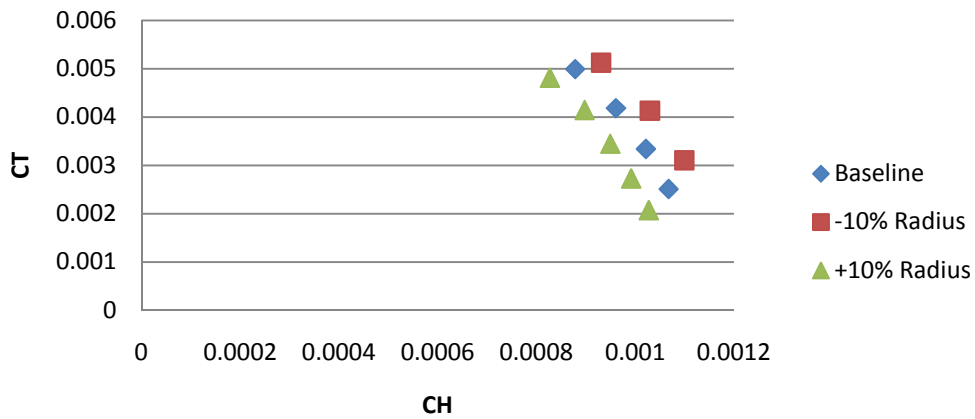


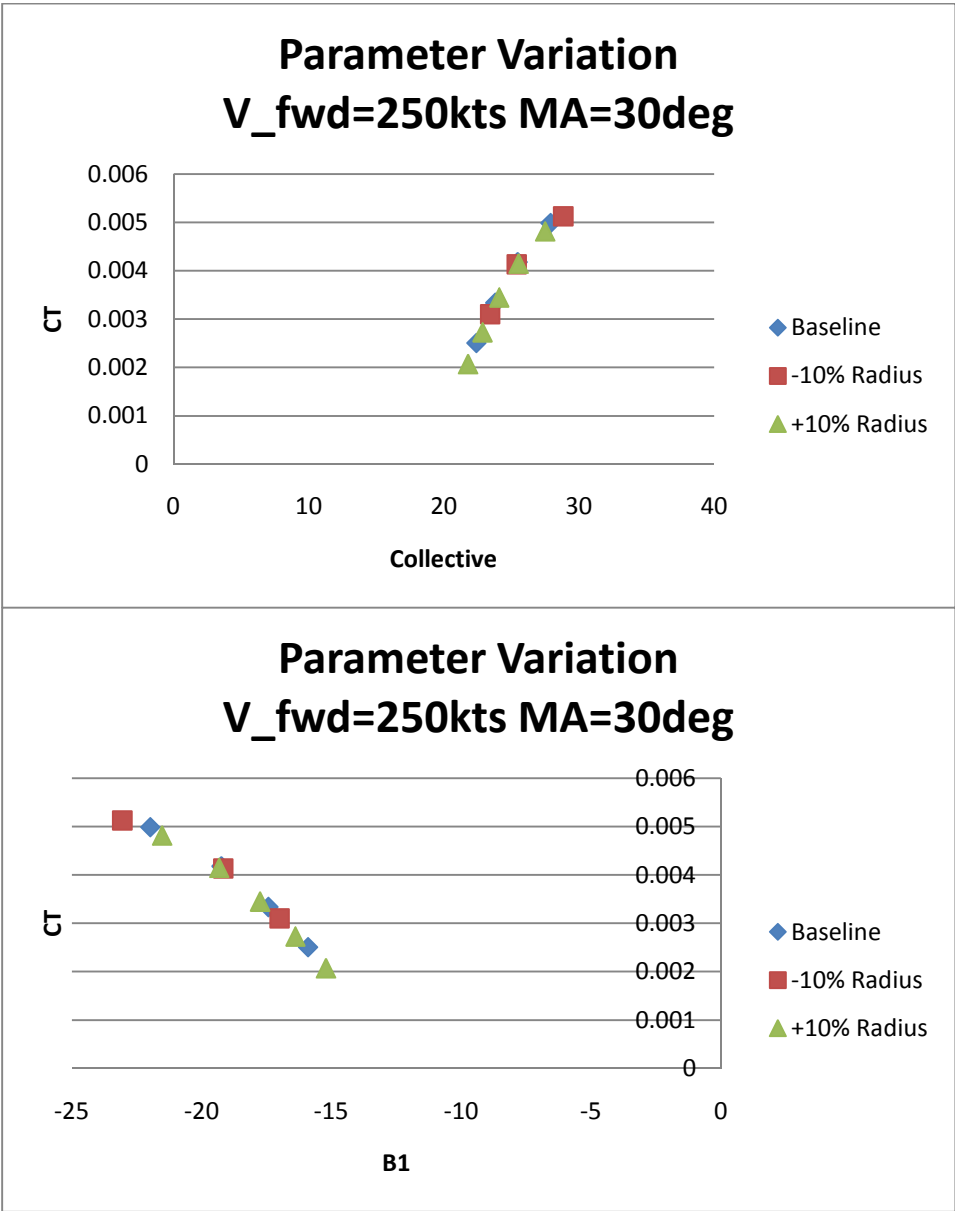


### Parameter Variation V\_fwd=250kts MA=30deg

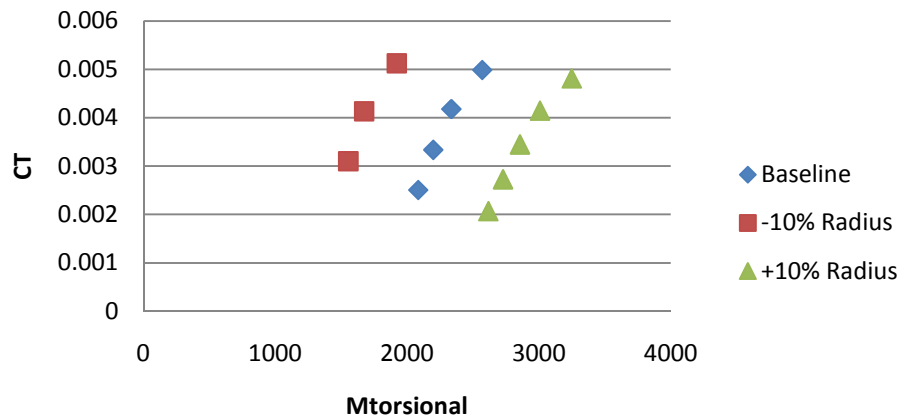


### Parameter Variation V\_fwd=250kts MA=30deg

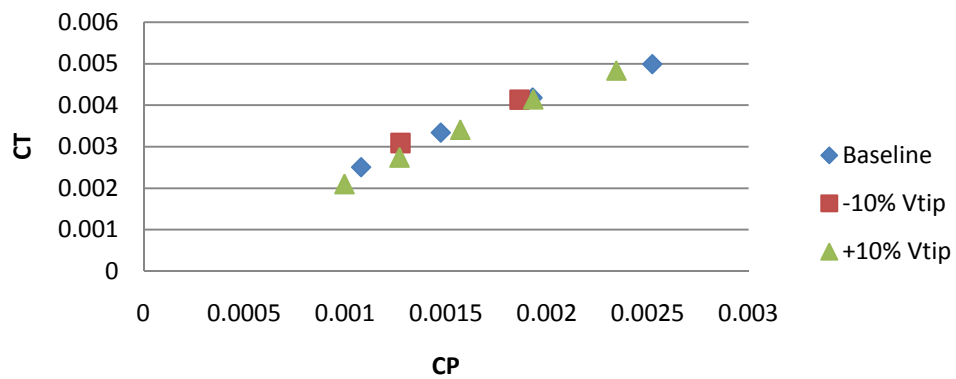




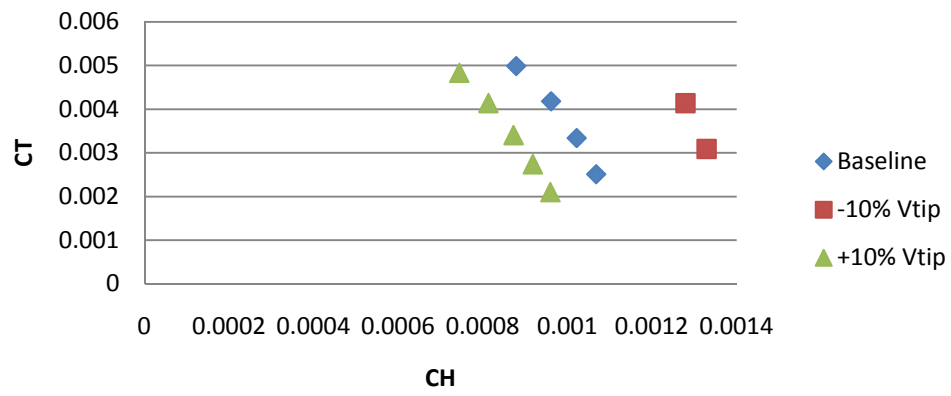
### Parameter Variation V\_fwd=250kts MA=30deg



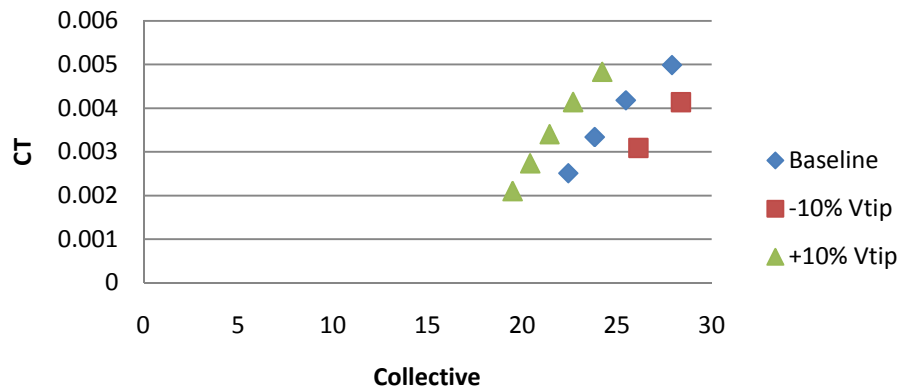
### Parameter Variation V\_fwd=250kts MA=30deg

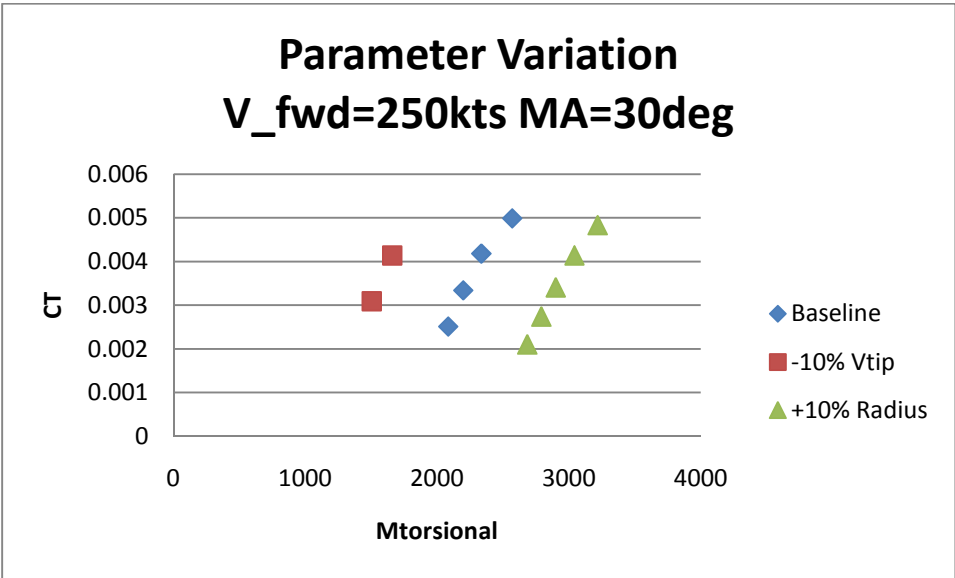
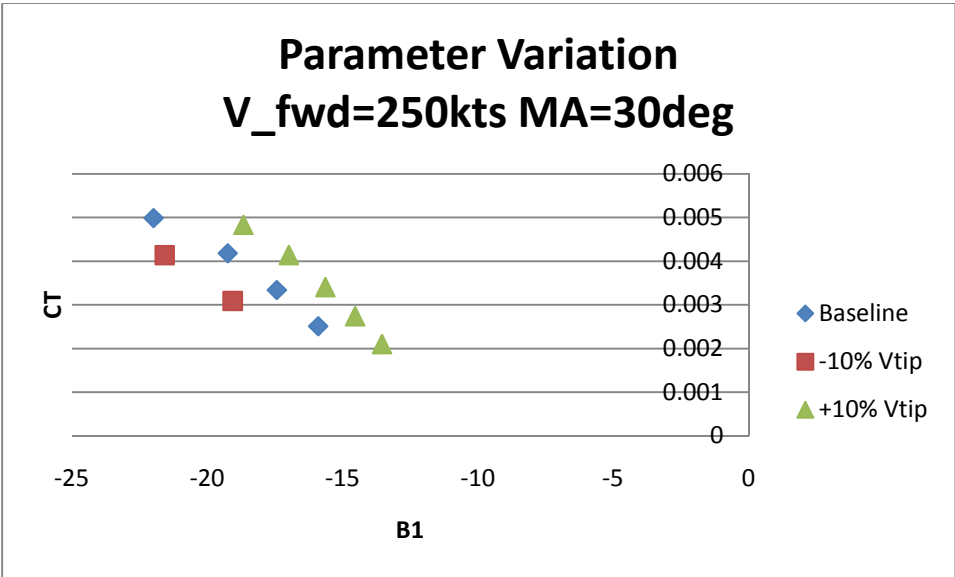


### Parameter Variation V\_fwd=250kts MA=30deg



### Parameter Variation V\_fwd=250kts MA=30deg





## APPENDIX C

### ROTOR ANALYSIS TOOL SOURCE CODE

## **IGPPM**

```
% Description: The IGPPM is the control program for an included rotor
% analysis suite. It allows for detailed sizing, trade-study, and
% performance analysis of conceptual and known rotor
% geometries/configurations.

%%%%%%%%%%%%%%%%%%%%%%%%%%%%%%%%%%%%%%%%%%%%%%%%%%%%%%%%%%%%%%%%%%%%%%%%
%Initialize Program and Clear Stored Variables
clc
clear
close all
format compact
format long
%%%%%%%%%%%%%%%%%%%%%%%%%%%%%%%%%%%%%%%%%%%%%%%%%%%%%%%%%%%%%%%%%%%%%%%%
%INPUTS
%%%%%%%%%%%%%%%%%%%%%%%%%%%%%%%%%%%%%%%%%%%%%%%%%%%%%%%%%%%%%%%%%%%%%%%%
%Analysis
Analysis_switch=3      % 3-Thrust Sweep
Compressibility=1      %1-Compressible Analysis 0-Incompressible

%Integration Spacing
r_int=.1;
psi_int=15;

%Flight Condition
alt_press=0;           %ft
delT_C=0;              %C
Tamb_F=0;              %F
Vclimb=0               %fps;
Vfwd=220               %kts;

%Rotor
R_bld=24;               %ft Historical Data Teetering Rotor validation case
R_bld=14;               %ft
R_bld=28               %ft Historical Data Articulated Rotor validation case
num_blds=4;            %n/d %2Historical Teetering
Vtip=640               %fps
pitch_link_arm=16.5;   %in
root_cutout=0.3;       %n/d
tiploss=1

%Blade Geometry
cl_alpha=.1;           %1/deg
airfoil=[1 1 1 1 1 1 1 1 1 1]; %1=Naca0012

chord_override=0;       %n/d
chord_bld=15;           %in

if chord_override==0
%chord=[11 11 11 11 11 16.5 16.5 16.5 16.5 16.5 16.5 16.5] %in
%chord=[16.044 16.044 16.044 16.044 16.044 16.044 16.044 16.044 16.044 16.044 16.044] %Historical
Data Articulated Rotor validation case
%chord=[21.0 21.0 21.0 21.0 21.0 21.0 21.0 21.0 21.0 21.0 21.0] %Historical Data Teetering Rotor
validation case
%chord=[11 11 11 11 12.78 12.78 12.78 12.78 12.78 12.78 12.78] %-10% SOLIDITY
chord=[11 11 11 11 14.25 14.25 14.25 14.25 14.25 14.25 14.25] %BASELINE
%chord=[11 11 11 11 15.72 15.72 15.72 15.72 15.72 15.72 15.72] %+10% SOLIDITY
%chord=[11 11 11 11 17.5 17.5 17.5 17.5 17.5 16.0 13.5] %2 tapered tip
%chord=[11 11 11 11 11.30 11.30 11.30 11.30 11.30 11.30 11.30] %5 Blades
%chord=[11 11 11 11 19.16 19.16 19.16 19.16 19.16 19.16 19.16] %3 Blades
%chord=[11 11 11 11 15.37 15.37 15.37 15.37 15.37 15.37 15.37] %15.4 ft
%BASELINE +10% RADIUS
%chord=[11 11 11 11 12.78 12.78 12.78 12.78 12.78 12.78 12.78] %12.6ft
%BASELINE -10% RADIUS

else
for i=1:r_int+1
chord(i)=chord_bld;
end
end
twist=[19.25 17.55 15.85 14.15 12.45 10.75 9.05 7.35 5.65 3.95 2.25] %0deg collective rigging
(BASELINE)
```



```

%twist=[29.25 27.55 25.85 24.15 22.45 20.75 19.05 17.35 15.65 13.95 12.25]    %Active Collective
Device
%twist=[8.0 7.2 6.4 5.6 4.8 4.0 3.2 2.4 1.6 0.8 0.0]    %Historical Data Articulated Rotor
validation case
%twist=[10.9 9.81 8.72 7.63 6.54 5.45 4.36 3.27 2.18 1.09 0.0]    %Historical Data Teetering Rotor
validation case
%twist=[12.75 11.05 9.35 7.65 5.95 4.25 2.55 0.85 -0.85 -2.55 -4.25]
%twist=[28 26.3 24.6 22.9 21.2 19.5 17.8 16.1 14.4 12.7 11]    %17 deg
%twist=[26 24.5 23 21.5 20 18.5 17 15.5 14 12.5 11]    %15 deg
%twist=[30 28.1 26.2 24.3 22.4 20.5 18.6 16.7 14.8 12.9 11]    %19 deg
%twist=[22 20.3 18.6 16.9 15.2 13.5 11.8 10.1 8.4 6.7 5.0]    %deg

```

```

%Configuration
GW=14000;    %lb
num_rot=2;    %n/d
fe=11;    %ft^2
residual_thrust=0;    %lb
download=.04 ;    %pct_Thrust

```

```

%Wing
alpha_wing=0;    %deg
e=.85;    %n/d
b_wing=31.5;    %ft
c_wing=4.48;    %ft

```

```

%Initial Control Conditions
alpha_mast=25 ;    %deg
theta_o=10;    %deg
theta_long=0;    %deg
theta_lat=0;    %deg
als=0;    %deg
bls=0;    %deg
ao=0;    %deg

```

```

%%%%%%%%%%%%%%%%%%%%%%%%%%%%%%%%%%%%%%%%%%%%%%%%%%%%%%%%%%%%%%%%%%%%%%%%

```

```

%Conversions and General Calculations

```

```

%Radial Indexing

```

```

r_nondim_count=0;
for i=1:(1/r_int)+1
    r_nondim(i)=r_nondim_count;
    norm_fac(i)=r_nondim_count^2;
    chord_fac(i)=chord(i)/12*norm_fac(i);
    r_nondim_count=r_nondim(i)+r_int;
end

```

```

for i=1:1/r_int
    mean_chord_fac(i)=(chord_fac(i+1)+chord_fac(i))/2;
    mean_norm_fac(i)=(norm_fac(i+1)+norm_fac(i))/2;
end

```

```

chord_ThrustEquiv=sum(mean_chord_fac(:))/sum(mean_norm_fac(:))
solidity_ThrustEquiv=num_blds*chord_ThrustEquiv/(pi*R_bld)
solidity=num_blds*mean(chord)/12/(pi*R_bld)    %mean geometric

```

```

Vfwd_fps=Vfwd*1.688;
d2r=pi/180;
r2d=180/pi;
control=[theta_o theta_long theta_lat alpha_wing];
control_initial=control;
[rho,a_amb]=atmosphere(alt_press,Tamb_F,delt_C);
%%%%%%%%%%%%%%%%%%%%%%%%%%%%%%%%%%%%%%%%%%%%%%%%%%%%%%%%%%%%%%%%%%%%%%%%
%Analysis Selection
if (Analysis_switch==1)

```

```

%%%%%%%%%%%%%%%%%%%%%%%%%%%%%%%%%%%%%%%%%%%%%%%%%%%%%%%%%%%%%%%%%%%%%%%%
%TC-mu SWEEP
%%%%%%%%%%%%%%%%%%%%%%%%%%%%%%%%%%%%%%%%%%%%%%%%%%%%%%%%%%%%%%%%%%%%%%%%
    theta_o_initial=theta_o;
    theta_long_initial=theta_long;
    theta_lat_initial=theta_lat;
    for i=1:6
        Vfwd=0+50*(i-1);

```

```

        if Vfwd<=100
            Vtip=640
            theta_o=5;
        else
            Vtip=640
            if alpha_mast~=0
                theta_o=17*alpha_mast/25;
                theta_long=-10*alpha_mast/25;
            else
                theta_o=5*alpha_mast/25
            end
        end

        Vfwd_fps=Vfwd*1.688;

        [T,control,Q,T_history,Q_history,control_history,Hforce_history]=tcmu_sweep(tiploss,Compressibility,G
        W,cl_alpha,airfoil,Vclimb,Vfwd,R_bld,alpha_mast,num_blds,num_rot,Vtip,pitch_link_arm,twist,root_cutou
        t,theta_o,theta_long,theta_lat,chord,r_int,psi_int,rho,a_amb,als,bls,ao);
        mu(i)=Vfwd_fps*cosd(alpha_mast)/Vtip;
        theta_o_sweep(i)=control(1,1)
        theta_long_sweep(i)=control(1,2)
        theta_lat_sweep(i)=control(1,3)
        omega=Vtip/R_bld;
        Power_MR_sweep(i)=Q*omega/550;
        Thrust(i)=T;
        CT=T/(rho*Vtip^2*(pi*R_bld^2));
        cl_bld=6*CT/solidity_ThrustEquiv;
        tc(i)=cl_bld/3
        solidity_ThrustEquiv
        theta_o=theta_o_initial;
        theta_lat=theta_lat_initial;
        theta_long=theta_long_initial;
        %       T_history(i,:)=T_history'
        %       Q_history(i,:)=Q_history'
        %       Hforce_history(i,:)=Hforce_history'
        %       control_history(i,:)=control_history'
    end

    %%%%%%%%%%%%%%%%%%%%%%%%%%%%%%%%%%%%%%%%%%%%%%%%%%%%%%%%%%%%%%%%%%%%%%%%%%%%%%%
    %Thrust SWEEP
    %%%%%%%%%%%%%%%%%%%%%%%%%%%%%%%%%%%%%%%%%%%%%%%%%%%%%%%%%%%%%%%%%%%%%%%%%%%%%%%
    elseif (Analysis_switch==3)
        for j=1:1
            alpha_mast=30+10*(j-1)
        for i=1:1
            Vfwd=250+50*(i-1); %170 Historical Articulated 160.5 Historical Teetering
            if Vfwd<=150
                Vtip=640 %640 BASELINE %627.03 Historical Articulated %677.57 Historical Teetering
                theta_o=-1*alpha_mast/25-.5+10;
            else
                Vtip=640 %640 BASELINE %627.03 Historical Articulated %677.57 Historical Teetering
                if alpha_mast~=0
                    theta_o=17*alpha_mast/25;
                    theta_long=-10*alpha_mast/25;
                else
                    theta_o=-1*alpha_mast/25-.5;
                end
            end
        end

        if Vfwd<=80
            fe=20
        else
            fe=11
        end

        Vfwd_fps=Vfwd*1.688;

        [count,T_hist,CT_hist,tc_hist,H_hist,CH_hist,Q_hist,Power_MR_hist,CP_hist,D_pro_bld_hist,Power_pro_hi
        st,CPpro_hist,D_ind_bld_hist,Power_ind_hist,CPind_hist,control_hist,PLL_bld_max_hist,PLL_bld_min_hist
        ]=Thrust_sweep2(tiploss,Compressibility,download,b_wing,c_wing,e,alpha_wing,airfoil,GW,fe,residual_th
        rust,cl_alpha,Vclimb,Vfwd_fps,R_bld,alpha_mast,num_blds,num_rot,Vtip,pitch_link_arm,twist,root_cutout
        ,theta_o,theta_long,theta_lat,chord,r_int,psi_int,rho,a_amb,als,bls,ao,solidity_ThrustEquiv)
        omega=Vtip/R_bld
        mu=Vfwd_fps*cosd(alpha_mast)/Vtip;
        TestCase1={Vfwd/alpha_mast;mu/R_bld;Vtip;solidity_ThrustEquiv;root_cutout};
    end

```

```

TestCase1_label={'Vfwd';'alpha_mast';'mu';'R_bld';'Vtip';'Solidity_ThrustEquiv';'root_cutout'};
TestCase2={'twist';'chord'};
Data_label={'T';'CT';'tc';'H';'CH';'Q';'Power_MR';'CP';'Profile Power';'CPpro';'Induced
Power';'CPind';'collective';'long_cyclic';'lat_cyclic';'PLL_bld_max';'PLL_bld_min'};
xlswrite('ThrustSweep.xls',TestCase1_label,j,['A',num2str(1+28*(i-1))])
xlswrite('ThrustSweep.xls',TestCase2,j,['B',num2str(1+28*(i-1))])
xlswrite('ThrustSweep.xls',Data_label,j,['A',num2str(8+28*(i-1))])
xlswrite('ThrustSweep.xls',Data_label,j,['A',num2str(10+28*(i-1))])
xlswrite('ThrustSweep.xls',T_hist,j,['B',num2str(10+28*(i-1))])
xlswrite('ThrustSweep.xls',CT_hist,j,['B',num2str(11+28*(i-1))])
xlswrite('ThrustSweep.xls',tc_hist,j,['B',num2str(12+28*(i-1))])
xlswrite('ThrustSweep.xls',H_hist,j,['B',num2str(13+28*(i-1))])
xlswrite('ThrustSweep.xls',CH_hist,j,['B',num2str(14+28*(i-1))])
xlswrite('ThrustSweep.xls',Q_hist,j,['B',num2str(15+28*(i-1))])
xlswrite('ThrustSweep.xls',Power_MR_hist,j,['B',num2str(16+28*(i-1))])
xlswrite('ThrustSweep.xls',CP_hist,j,['B',num2str(17+28*(i-1))])
xlswrite('ThrustSweep.xls',Power_pro_hist,j,['B',num2str(18+28*(i-1))])
xlswrite('ThrustSweep.xls',CPpro_hist,j,['B',num2str(19+28*(i-1))])
xlswrite('ThrustSweep.xls',Power_ind_hist,j,['B',num2str(20+28*(i-1))])
xlswrite('ThrustSweep.xls',CPind_hist,j,['B',num2str(21+28*(i-1))])
xlswrite('ThrustSweep.xls',control_hist(:,1),j,['B',num2str(22+28*(i-1))])
xlswrite('ThrustSweep.xls',control_hist(:,2),j,['B',num2str(23+28*(i-1))])
xlswrite('ThrustSweep.xls',control_hist(:,3),j,['B',num2str(24+28*(i-1))])
xlswrite('ThrustSweep.xls',PLL_bld_max_hist,j,['B',num2str(25+28*(i-1))])
xlswrite('ThrustSweep.xls',PLL_bld_min_hist,j,['B',num2str(26+28*(i-1))])

end
end

end

%%%%%%%%%%%%%%%%%%%%%%%%%%%%%%%%%%%%%%%%%%%%%%%%%%%%%%%%%%%%%%%%%%%%%%%%%%%%%%
% 'Summary'
control
control_total=sum(abs(control))
T
Hforce
Power_MR=Q*omega/550
offload
Q
CT=T/(rho*Vtip^2*(pi*R_bld^2))
cl_bld=6*CT/solidity_ThrustEquiv
tc=cl_bld/3
PLL_bld
PLL_bld_max=max(PLL_bld)
PLL_bld_min=min(PLL_bld)
PLL_bld_mean=mean(PLL_bld)
PLL_bld_oscillatory=PLL_bld_max-PLL_bld_mean

z=num_blds
psi_count=(z-1)*360/num_blds;
for i=1:(360/psi_int)+1
    psi_bld(i)=psi_count+psi_int*(i-1);
    if(psi_bld(i)>=360)
        psi_bld(i)=psi_bld(i)-360;
    end
end
end
PLL_bld(i)=PLL_bld(1);

```

## **ISTM**

```
function
[count,T_hist,CT_hist,tc_hist,H_hist,CH_hist,Q_hist,Power_MR_hist,CP_hist,D_pro_bld_hist,Power_pro_hist,CPpro_hist,D_ind_bld_hist,Power_ind_hist,CPind_hist,control_hist,PLL_bld_max_hist,PLL_bld_min_hist]=Thrust_sweep2(tiploss,Compressibility,download,b_wing,c_wing,e,alpha_wing,airfoil,GW,fe,residual_thrust,cl_alpha,Vclimb,Vfwd_fps,R_bld,alpha_mast,num_blds,num_rot,Vtip,pitch_link_arm,twist,root_cutout,theta_o,theta_long,theta_lat,chord,r_int,psi_int,rho,a_amb,als,bls,ao,solidity_ThrustEquiv)
theta_o
theta_lat
theta_long
num_controls=3;
perturb=.01;
iteration_count=0;
iteration_count_max=10;
GW_int=1000;
GW_count=0;
GW_o=3000
count=1;
exit_condition=0;
error_max=50;

%null initial values
T_hist=0;
CT_hist=0;
tc_hist=0;
H_hist=0;
CH_hist=0;
Q_hist=0;
Power_MR_hist=0;
CP_hist=0;
D_pro_bld_hist=0;
Power_pro_hist=0;
CPpro_hist=0;
D_ind_bld_hist=0;
Power_ind_hist=0;
CPind_hist=0;
control_hist=[0 0 0];
PLL_bld_max_hist=0;
PLL_bld_min_hist=0;

%Conversions
omega=Vtip/R_bld;
Vfwd=Vfwd_fps/1.688;
d2r=pi/180;
r2d=180/pi;
alpha_mast_rad=alpha_mast*d2r;

%Initialize values
Jacob_fwd=zeros(num_controls);
Jacob_rev=zeros(num_controls);
Jacob_cent=zeros(num_controls);

while iteration_count<iteration_count_max
    iteration_count=0;
    exit_condition=0;
    GW=GW_o+GW_int*GW_count
    T_start=GW/num_rot;

    [T,M_long,M_lat,Q,Qpro,Qind,Hforce,Yforce,L,D_pro_bld,D_ind_bld,D_inplane,PLL_bld,beta]=BladeElement(
    tiploss,Compressibility,airfoil,T_start,GW,cl_alpha,Vclimb,Vfwd,R_bld,alpha_mast,num_blds,num_rot,Vtip,
    pitch_link_arm,twist,root_cutout,theta_o,theta_long,theta_lat,chord,r_int,psi_int,rho,a_amb,als,bls
    ,ao);
    Fz=GW/num_rot-T;

    control=[theta_o theta_long theta_lat];
    control_fwd=control;
    control_rev=control;
    trim_val=[Fz; M_lat; M_long];

    error=sum(abs(trim_val));

    while exit_condition==0
        for i=1:num_controls
%Build Forward Difference
```

```

        control_fwd(1,i)=control_fwd(1,i)+perturb;

[T,M_long,M_lat,Q,Qpro,Qind,Hforce,Yforce,L,D_pro_bld,D_ind_bld,D_inplane,PLL_bld,beta]=BladeElement(
tiploss,Compressibility,airfoil,T_start,GW,cl_alpha,Vclimb,Vfwd,R_bld,alpha_mast,num_blds,num_rot,Vtip,
pitch_link_arm,twist,root_cutout,control_fwd(1,1),control_fwd(1,2),control_fwd(1,3),chord,r_int,psi
_int,rho,a_amb,als,bls,ao);
    Fz_fwd=GW/num_rot-T;
    M_lat_fwd=M_lat;
    M_long_fwd=M_long;
    trim_val_fwd=[Fz_fwd; M_lat_fwd; M_long_fwd];
    Jacob_fwd(:,i)=trim_val_fwd-trim_val;
    control_fwd(1,i)=control(1,i);
%Build Reverse Difference
    control_rev(1,i)=control_rev(1,i)-perturb;

[T,M_long,M_lat,Q,Qpro,Qind,Hforce,Yforce,L,D_pro_bld,D_ind_bld,D_inplane,PLL_bld,beta]=BladeElement(
tiploss,Compressibility,airfoil,T_start,GW,cl_alpha,Vclimb,Vfwd,R_bld,alpha_mast,num_blds,num_rot,Vti
p,pitch_link_arm,twist,root_cutout,control_rev(1,1),control_rev(1,2),control_rev(1,3),chord,r_int,psi
_int,rho,a_amb,als,bls,ao);
    Fz_rev=GW/num_rot-T;
    M_lat_rev=M_lat;
    M_long_rev=M_long;
    trim_val_rev=[Fz_rev; M_lat_rev; M_long_rev];
    Jacob_rev(:,i)=trim_val_rev-trim_val;
    control_rev(1,i)=control(1,i);

%Build Central Difference
    Jacob_cent(:,i)=(Jacob_fwd(:,i)-Jacob_rev(:,i))/(2*perturb);
end

%Invert and solve
if det(Jacob_cent)==0
    exit_condition=1;
end
del_control_inp=inv(Jacob_cent)*(-1*trim_val);
theta_o=del_control_inp(1,1)+theta_o;
theta_long=del_control_inp(2,1)+theta_long;
theta_lat=del_control_inp(3,1)+theta_lat;

control=[theta_o theta_long theta_lat];
control_fwd=control;
control_rev=control;

[T,M_long,M_lat,Q,Qpro,Qind,Hforce,Yforce,L,D_pro_bld,D_ind_bld,D_inplane,PLL_bld,beta]=BladeElement(
tiploss,Compressibility,airfoil,T_start,GW,cl_alpha,Vclimb,Vfwd,R_bld,alpha_mast,num_blds,num_rot,Vti
p,pitch_link_arm,twist,root_cutout,control(1,1),control(1,2),control(1,3),chord,r_int,psi_int,rho,a_a
mb,als,bls,ao);%0,0,0,chord,r_int,psi_int,rho,a_amb,als,bls,ao);%
    T_start=T;
    Fz=GW/num_rot-T;
    Fx=0;

iteration_count=iteration_count+1
trim_val=[Fz; M_lat; M_long];
error=sum(abs(trim_val));

if iteration_count>=iteration_count_max
    exit_condition=1;
end
if error<=error_max
    exit_condition=1;
end
if isnan(error)
    exit_condition=1;
    iteration_count=iteration_count_max+1;
end
end
control=[control(1,1) theta_long theta_lat];
T_hist2(count)=T;
CT_hist2(count)=T/(pi*R_bld^2*rho*Vtip^2);
tc_hist2(count)=2*CT_hist2(count)/solidity_ThrustEquiv;
H_hist2(count)=Hforce;
CH_hist2(count)=Hforce/(pi*R_bld^2*rho*Vtip^2);
Q_hist2(count)=Q;

```

```

Power_MR_hist2(count)=Q*omega/550;
CP_hist2(count)=(Q*omega)/(pi*R_bld^2*rho*Vtip^3);
D_pro_bld_hist2(count)=D_pro_bld;
Power_pro_hist2(count)=Qpro*omega/550;
CPpro_hist2(count)=(Qpro*omega)/(pi*R_bld^2*rho*Vtip^3);
D_ind_bld_hist2(count)=D_ind_bld;
Power_ind_hist2(count)=Qind*omega/550;
CPind_hist2(count)=(Qind*omega)/(pi*R_bld^2*rho*Vtip^3);
control_hist2(count,:)=control;
PLL_bld_min2(count)=min(PLL_bld);
PLL_bld_max2(count)=max(PLL_bld);

GW_count=GW_count+1;
count=count+1;
end

for i=1:count-2
    T_hist(i)=T_hist2(i);
    CT_hist(i)=CT_hist2(i);
    tc_hist(i)=tc_hist2(i);
    H_hist(i)=H_hist2(i);
    CH_hist(i)=CH_hist2(i);
    Q_hist(i)=Q_hist2(i);
    Power_MR_hist(i)=Power_MR_hist2(i);
    CP_hist(i)=CP_hist2(i);
    D_pro_bld_hist(i)=D_pro_bld_hist2(i);
    Power_pro_hist(i)=Power_pro_hist2(i);
    CPpro_hist(i)=CPpro_hist2(i);
    D_ind_bld_hist(i)=D_ind_bld_hist2(i);
    Power_ind_hist(i)=Power_ind_hist2(i);
    CPind_hist(i)=CPind_hist2(i);
    control_hist(i,:)=control_hist2(i,:);
    PLL_bld_max_hist(i)=PLL_bld_max2(i);
    PLL_bld_min_hist(i)=PLL_bld_min2(i);
end

```

## BEAMM

```
function
[T,M_long,M_lat,Q,Qpro,Qind,Hforce,Yforce,L,D_pro_bld,D_ind_bld,D_inplane,PLL_bld,beta]=BladeElement(
tiploss,Compressibility,airfoil,T_start,GW,cl_alpha,Vclimb,Vfwd,R_bld,alpha_mast,num_blds,num_rot,Vtip
p,pitch_link_arm,twist,root_cutout,theta_o,theta_long,theta_lat,chord,r_int,psi_int,rho,a_amb,als,bls
,ao)

%%%%%%%%%%%%%%%%%%%%%%%%%%%%%%%%%%%%%%%%%%%%%%%%%%%%%%%%%%%%%%%%%%%%%%%%
%BLADE ELEMENT
%%%%%%%%%%%%%%%%%%%%%%%%%%%%%%%%%%%%%%%%%%%%%%%%%%%%%%%%%%%%%%%%%%%%%%%%

% Created By:   Cory Hitte
% Date:         06/05/2011

% Description:  Blade element rotor model created using equations from
%              Stepniewski & Keys as well as Prouty.  Model has been
%              further modified to utilize compressible airfoil tables,
%              first order flapping, and does not use the Small Angle
%              Assumption (allows for high inflow rotor analysis).  This
%              model assumes uniform inflow for forward flight and applies
%              a radial inflow distribution in hover.

%Inputs:
% airfoil - airfoil table
% T_start - initial thrust value
% GW - configuration GW
% cl_alpha - standard 0012 lift curve slope for hover induced velocity calc
% Vclimb
% Vfwd
% R_bld
% alpha_mast
% num_blds
% num_rot
% Vtip
% pitch_link_arm
% twist
% root_cutout
% theta_o
% theta_long
% theta_lat
% chord
% r_int
% psi_int
% rho
% a_amb
% als
% bls
% ao

% Outputs:
% T
% M_long
% M_lat
% Q
% Hforce
% L
% D_pro_bld
% D_ind_bld
% D_inplane
% PLL_bld
% beta
%%%%%%%%%%%%%%%%%%%%%%%%%%%%%%%%%%%%%%%%%%%%%%%%%%%%%%%%%%%%%%%%%%%%%%%%
%Radial Indexing
r_nondim_count=0;
for i=1:(1/r_int)+1
    r_nondim(i)=r_nondim_count;
    r_nondim_count=r_nondim(i)+r_int;
end
%%%%%%%%%%%%%%%%%%%%%%%%%%%%%%%%%%%%%%%%%%%%%%%%%%%%%%%%%%%%%%%%%%%%%%%%
%Conversions
d2r=pi/180;
r2d=180/pi;
Vfwd_fps=Vfwd*1.688;
```

```

alpha_mast_rad=alpha_mast*d2r;
cl_alpha_rad=cl_alpha*r2d;
%%%%%%%%%%%%%%%%%%%%%%%%%%%%%%%%%%%%%%%%%%%%%%%%%%%%%%%%%%%%%%%%%%%%%%%%
%Resolve Velocity Vectors in Blade Axes
blade_wt=62; %lb
omega=Vtip/R_bld;
Vax=-Vclimb*cos(-alpha_mast_rad)-Vfwd_fps*sin(-alpha_mast_rad);
Vinp=Vfwd_fps*cos(-alpha_mast_rad)+Vclimb*sin(-alpha_mast_rad);

T_GW_ratio=T_start*num_rot/GW;

if T_GW_ratio>=0.1
    T_GW_ratio=T_GW_ratio;
else
    T_GW_ratio=.1;
end

vo_hov=sqrt(GW*T_GW_ratio/num_rot/(2*rho*pi*R_bld^2));
v_ind=sqrt(-(Vfwd_fps/vo_hov)^2)/2+sqrt((Vfwd_fps/vo_hov)^4/4+1))*vo_hov;

if abs(tiploss)>0
    inflow_ratio=(Vax+v_ind)/Vtip;
    %tiploss=inflow_ratio/num_blds*sqrt(1+inflow_ratio^2) %Prandtl (inflow based)
    %tiploss=1-.5*(pi*solidity/num_blds) %Multiple Authors
    %tiploss=3.56*solidity/num_blds %Sissingh
    tiploss=1.98*(sqrt((GW*T_GW_ratio/num_rot)/(rho*pi*R_bld^2*Vtip^2))/num_blds));
%Wald
else
    tiploss=0;
end

for z=1:num_blds
    psi_count=(z-1)*360/num_blds;

    for i=1:(360/psi_int)
        psi_bld(i)=psi_count;
        psi_count=psi_bld(i)+psi_int;
        beta(i)=ao*d2r-als*d2r*cos(psi_bld(i)*d2r)-bls*d2r*sin(psi_bld(i)*d2r);
        beta_dot(i)=omega*(als*d2r*sin(psi_bld(i)*d2r)-bls*d2r*cos(psi_bld(i)*d2r));
        for j=1:(1/r_int)+1
            X(j,i)= R_bld*r_nondim(j)*cos(psi_bld(i)*d2r);
            Y(j,i)= R_bld*r_nondim(j)*sin(psi_bld(i)*d2r);
            V_ax_tot(j,i)=Vax+v_ind+r_nondim(j)*R_bld*beta_dot(i)-
            Vfwd_fps*beta(i)*cos(psi_bld(i)*d2r);
            Vb_perp(i)=Vinp*sin(psi_bld(i)*d2r);
            U_perp(j,i)=Vtip*r_nondim(j)+Vb_perp(i);
            phi(j,i)=atan2(V_ax_tot(j,i),U_perp(j,i));

theta(j,i)=theta_o*d2r+theta_lat*d2r*cos(psi_bld(i)*d2r)+theta_long*d2r*sin(psi_bld(i)*d2r)+twist(j)*
d2r;

        alpha_bld(j,i)=theta(j,i)-phi(j,i);

        if Compressibility==1
            mach(j,i)=sqrt(U_perp(j,i)^2+V_ax_tot(j,i)^2)/a_amb;
        elseif Compressibility==0
            mach(j,i)=0;
        end

        if (airfoil(j)==1)
            [cl(j,i),cd(j,i),cm(j,i)]=naca0012(alpha_bld(j,i)*r2d,mach(j,i));
        end

        if Vfwd_fps>0
            V_ax_tot(j,i)=V_ax_tot(j,i);
        else
            V_ax_tot(j,i)=Vax/2+(num_blds*chord(j)/12/(pi*R_bld)*cl_alpha_rad*omega*R_bld/16)*(-
            1+sqrt(1+2*(theta(j)*r_nondim(j)*omega*R_bld-
            Vax)/(4*Vax^2/(num_blds*chord(j)/12*cl_alpha_rad*omega*R_bld)+Vax+(num_blds*chord(j)/12/(pi*R_bld))*c
            l_alpha_rad*omega*R_bld/16)));
        end

%Calculate differential forces and moments
        I_pitch(j)=(chord(j)/12)^2*blade_wt/(32.2*1/r_int);

```



```

dM_pitch_TR(j,i)=-I_pitch(j)*omega^2*sin(2*theta(j,i))/2;
dM_bld(j,i)=.5*rho*R_bld*chord(j)^2/12*U_perp(j,i)^2*cm(j,i);
dL_bld(j,i)=.5*rho*R_bld*chord(j)/12*U_perp(j,i)^2*cl(j,i);
dPLL_bld(j,i)=(dM_bld(j,i)+dM_pitch_TR(j,i))/(pitch_link_arm/12);
dD_pro_bld(j,i)=.5*rho*R_bld*chord(j)/12*U_perp(j,i)^2*cd(j,i);
dD_ind_bld(j,i)=dL_bld(j,i)*sin(phi(j,i));
dT(j,i)=cos(phi(j,i))*dL_bld(j,i)-sin(phi(j,i))*dD_pro_bld(j,i);
dM_long(j,i)=dT(j,i)*R_bld*cos(psi_bld(i)*d2r)*r_nondim(j);
dM_lat(j,i)=dT(j,i)*R_bld*sin(psi_bld(i)*d2r)*r_nondim(j);
dD_inplane(j,i)=dD_pro_bld(j,i)*cos(phi(j,i))+dD_ind_bld(j,i);
dHforce(j,i)=dD_inplane(j,i)*sin(psi_bld(i)*d2r);
dYforce(j,i)=dD_inplane(j,i)*cos(psi_bld(i)*d2r);
dQ(j,i)=dD_inplane(j,i)*R_bld*r_nondim(j);
dQpro(j,i)=dD_pro_bld(j,i)*cos(phi(j,i))*R_bld*r_nondim(j);
dQind(j,i)=dD_ind_bld(j,i)*R_bld*r_nondim(j);

end
end
%Integrate to find average forces and moments
L(z)=radtrap2D_int(dL_bld,r_int,psi_int,root_cutout,tiploss);
T(z)=radtrap2D_int(dT,r_int,psi_int,root_cutout,tiploss);
M_bld=TRradtrap2D_int(dM_bld,r_int,psi_int,root_cutout);
PLL_bld=TRradtrap2D_int(dPLL_bld,r_int,psi_int,root_cutout);
M_TR_bld=TRradtrap2D_int(dM_pitch_TR,r_int,psi_int,0);
D_pro_bld(z)=radtrap2D_int(dD_pro_bld,r_int,psi_int,0,0);
D_ind_bld(z)=radtrap2D_int(dD_ind_bld,r_int,psi_int,0,tiploss);
M_long_bld(z)=radtrap2D_int(dM_long,r_int,psi_int,0,tiploss);
M_lat_bld(z)=radtrap2D_int(dM_lat,r_int,psi_int,0,tiploss);
D_inplane(z)=radtrap2D_int(dD_inplane,r_int,psi_int,0,0);
Hforce(z)=radtrap2D_int(dHforce,r_int,psi_int,0,0);
Yforce(z)=radtrap2D_int(dYforce,r_int,psi_int,0,0);
Q(z)=radtrap2D_int(dQ,r_int,psi_int,0,0);
Qpro(z)=radtrap2D_int(dQpro,r_int,psi_int,0,0);
Qind(z)=radtrap2D_int(dQind,r_int,psi_int,0,0);

end

%Sum individual blade contributions
M_long=sum(M_long_bld(:));
M_lat=sum(M_lat_bld(:));
L=sum(L(:));
T=sum(T(:));
D_pro_bld=sum(D_pro_bld(:));
D_ind_bld=sum(D_ind_bld(:));
D_inplane=sum(D_inplane(:));
Hforce=sum(Hforce(:));
Yforce=sum(Yforce(:));
Q=sum(Q(:));
Qpro=sum(Qpro(:));
Qind=sum(Qind(:));

end

```

```

%%

```

```
function [cl,cd,cm]=naca0012(aoa,mach)
mach_ref=[0 0.2 0.3 0.4 0.5 0.6 0.7 0.75 0.8 0.9 1];
```

[illegible]

cd_0012=[0.022	0.022	0.022	0.022	0.022	0.022	0.022	0.022	0.022	0.022	0.022;
0.062	0.062	0.062	0.062	0.062	0.062	0.062	0.062	0.062	0.062	0.062;
0.132	0.132	0.132	0.132	0.132	0.132	0.132	0.132	0.132	0.132	0.132;
0.242	0.242	0.242	0.242	0.242	0.242	0.242	0.242	0.242	0.242	0.242;
0.302	0.302	0.302	0.302	0.302	0.302	0.302	0.302	0.302	0.302	0.302;
1.042	1.042	1.042	1.042	1.042	1.042	1.042	1.042	1.042	1.042	1.042;
1.652	1.652	1.652	1.652	1.652	1.652	1.652	1.652	1.652	1.652	1.652;
1.852	1.852	1.852	1.852	1.852	1.852	1.852	1.852	1.852	1.852	1.852;
2.022	2.022	2.022	2.022	2.022	2.022	2.022	2.022	2.022	2.022	2.022;
2.022	2.022	2.022	2.022	2.022	2.022	2.022	2.022	2.022	2.022	2.022;
1.962	1.962	1.962	1.962	1.962	1.962	1.962	1.962	1.962	1.962	1.962;
1.842	1.842	1.842	1.842	1.842	1.842	1.842	1.842	1.842	1.842	1.842;
1.662	1.662	1.662	1.662	1.662	1.662	1.662	1.662	1.662	1.662	1.662;
1.392	1.392	1.392	1.392	1.392	1.392	1.392	1.392	1.392	1.392	1.392;
0.562	0.562	0.562	0.562	0.562	0.562	0.562	0.562	0.562	0.562	0.562;
0.332	0.332	0.332	0.332	0.332	0.332	0.332	0.332	0.332	0.332	0.332;
0.155	0.155	0.181	0.207	0.235	0.257	0.274	0.292	0.305	0.342	0.342;
0.102	0.102	0.148	0.181	0.209	0.233	0.252	0.271	0.282	0.298	0.298;
0.038	0.038	0.099	0.146	0.18	0.212	0.233	0.249	0.26	0.293	0.293;
0.0264	0.0264	0.0455	0.094	0.148	0.191	0.216	0.231	0.239	0.272	0.292;
0.022	0.022	0.03	0.06	0.111	0.164	0.198	0.211	0.22	0.252	0.291;
0.0196	0.0196	0.0232	0.038	0.078	0.135	0.17	0.192	0.202	0.232	0.275;
0.0174	0.0174	0.0189	0.0259	0.053	0.105	0.145	0.176	0.186	0.213	0.254;
0.0154	0.0154	0.0159	0.0187	0.0351	0.077	0.122	0.159	0.172	0.199	0.232;
0.0138	0.0138	0.0138	0.0147	0.022	0.053	0.101	0.14	0.155	0.183	0.214;

```

0.0122 0.0122 0.0122 0.0123 0.0141 0.035 0.082 0.111 0.139 0.169 0.192;
0.011 0.011 0.011 0.011 0.011 0.0212 0.0615 0.082 0.12 0.14 0.17;
0.01 0.01 0.01 0.01 0.01 0.0132 0.038 0.054 0.088 0.111 0.14;
0.0093 0.0093 0.0093 0.0093 0.0093 0.01 0.0167 0.03 0.0575 0.095 0.112;
0.0088 0.0088 0.0088 0.0088 0.0088 0.009 0.0102 0.0175 0.0355 0.086 0.102;
0.0085 0.0085 0.0085 0.0085 0.0085 0.0085 0.0086 0.0117 0.024 0.081 0.098;
0.0083 0.0083 0.0083 0.0083 0.0083 0.0083 0.0083 0.0091 0.0175 0.078 0.096;
0.008 0.008 0.008 0.008 0.008 0.008 0.008 0.008 0.0137 0.078 0.095;
0.0083 0.0083 0.0083 0.0083 0.0083 0.0083 0.0083 0.0091 0.0175 0.078 0.096;
0.0085 0.0085 0.0085 0.0085 0.0085 0.0085 0.0086 0.0117 0.024 0.081 0.098;
0.0088 0.0088 0.0088 0.0088 0.0088 0.009 0.0102 0.0175 0.0355 0.086 0.102;
0.0093 0.0093 0.0093 0.0093 0.0093 0.01 0.0167 0.03 0.0575 0.095 0.112;
0.01 0.01 0.01 0.01 0.01 0.0132 0.038 0.054 0.088 0.111 0.14;
0.011 0.011 0.011 0.011 0.011 0.0212 0.0615 0.082 0.12 0.14 0.17;
0.0122 0.0122 0.0122 0.0123 0.0141 0.035 0.082 0.111 0.139 0.169 0.192;
0.0138 0.0138 0.0138 0.0147 0.022 0.053 0.101 0.14 0.155 0.183 0.214;
0.0154 0.0154 0.0159 0.0187 0.0351 0.077 0.122 0.159 0.172 0.199 0.232;
0.0174 0.0174 0.0189 0.0259 0.053 0.105 0.145 0.176 0.186 0.213 0.254;
0.0196 0.0196 0.0232 0.038 0.078 0.135 0.17 0.192 0.202 0.232 0.275;
0.022 0.022 0.03 0.06 0.111 0.164 0.198 0.211 0.22 0.252 0.291;
0.0264 0.0264 0.0455 0.094 0.148 0.191 0.216 0.231 0.239 0.272 0.292;
0.038 0.038 0.099 0.146 0.18 0.212 0.233 0.249 0.26 0.293 0.293;
0.102 0.102 0.148 0.181 0.209 0.233 0.252 0.271 0.282 0.298 0.298;
0.155 0.155 0.181 0.207 0.235 0.257 0.274 0.292 0.305 0.342 0.342;
0.332 0.332 0.332 0.332 0.332 0.332 0.332 0.332 0.332 0.332 0.332;
0.562 0.562 0.562 0.562 0.562 0.562 0.562 0.562 0.562 0.562 0.562;
1.392 1.392 1.392 1.392 1.392 1.392 1.392 1.392 1.392 1.392 1.392;
1.662 1.662 1.662 1.662 1.662 1.662 1.662 1.662 1.662 1.662 1.662;
1.842 1.842 1.842 1.842 1.842 1.842 1.842 1.842 1.842 1.842 1.842;
1.962 1.962 1.962 1.962 1.962 1.962 1.962 1.962 1.962 1.962 1.962;
2.022 2.022 2.022 2.022 2.022 2.022 2.022 2.022 2.022 2.022 2.022;
2.022 2.022 2.022 2.022 2.022 2.022 2.022 2.022 2.022 2.022 2.022;
1.852 1.852 1.852 1.852 1.852 1.852 1.852 1.852 1.852 1.852 1.852;
1.652 1.652 1.652 1.652 1.652 1.652 1.652 1.652 1.652 1.652 1.652;
1.042 1.042 1.042 1.042 1.042 1.042 1.042 1.042 1.042 1.042 1.042;
0.302 0.302 0.302 0.302 0.302 0.302 0.302 0.302 0.302 0.302 0.302;
0.242 0.242 0.242 0.242 0.242 0.242 0.242 0.242 0.242 0.242 0.242;
0.132 0.132 0.132 0.132 0.132 0.132 0.132 0.132 0.132 0.132 0.132;
0.062 0.062 0.062 0.062 0.062 0.062 0.062 0.062 0.062 0.062 0.062;
0.022 0.022 0.022 0.022 0.022 0.022 0.022 0.022 0.022 0.022 0.022];

```

```

alpha_cm_ref=[-180 -170 -165 -160 -135 -90 -30 -23 -16 -15 -14 -13 -12 -11 -10 -9 -8 -7 -6 -4 -3 -2 -
1 0 1 2 3 4 6 7 8 9 10 11 12 13 14 15 16 23 30 90 135 160 165 170 180];

```

```

cm_0012=[0 0 0 0 0 0 0 0 0 0 0 0;
0.4 0.4 0.4 0.4 0.4 0.4 0.4 0.4 0.4 0.4 0.4;
0.3 0.3 0.3 0.3 0.3 0.3 0.3 0.3 0.3 0.3 0.3;
0.3 0.3 0.3 0.3 0.3 0.3 0.3 0.3 0.3 0.3 0.3;
0.5 0.5 0.5 0.5 0.5 0.5 0.5 0.5 0.5 0.5 0.5;
0.5 0.5 0.5 0.5 0.5 0.5 0.5 0.5 0.5 0.5 0.5;
0.174 0.174 0.184 0.196 0.214 0.235 0.25 0.264 0.277 0.298 0.319;
0.112 0.112 0.118 0.128 0.144 0.157 0.171 0.183 0.206 0.232 0.258;
0.073 0.073 0.078 0.086 0.097 0.108 0.117 0.137 0.176 0.2 0.224;
0.054 0.054 0.065 0.073 0.084 0.097 0.111 0.133 0.173 0.195 0.217;
0.027 0.027 0.027 0.054 0.068 0.086 0.103 0.127 0.167 0.189 0.211;
-0.0015 -0.0015 -0.0015 0.025 0.05 0.074 0.093 0.122 0.163 0.184 0.205;
0.002 0.002 0.002 0.002 0.03 0.06 0.083 0.116 0.157 0.176 0.195;
-0.003 -0.003 -0.003 -0.003 0.014 0.046 0.074 0.108 0.149 0.17 0.191;
-0.0015 -0.0015 -0.0015 -0.0015 0.002 0.032 0.065 0.1 0.142 0.163 0.184;
-0.003 -0.003 -0.003 -0.003 -0.003 0.016 0.054 0.089 0.132 0.154 0.176;
-0.004 -0.004 -0.004 -0.004 -0.004 0.005 0.041 0.082 0.123 0.145 0.167;
-0.004 -0.004 -0.004 -0.004 -0.004 -0.004 0.0275 0.072 0.1125 0.136 0.1595;
-0.003 -0.003 -0.003 -0.003 -0.003 -0.003 0.016 0.0625 0.1 0.125 0.15;
0.005 0.005 0.005 0.005 0.005 0.005 0.005 0.04 0.076 0.102 0.128;
-0.0025 -0.0025 -0.0025 -0.0025 -0.0025 -0.0025 -0.0025 0.026 0.0665 0.087 0.1075;
0.013 0.013 0.013 0.013 0.013 0.013 0.013 0.013 0.053 0.07 0.087;
0.0035 0.0035 0.0035 0.0035 0.0035 0.0035 0.0035 0.0035 0.033 0.045 0.057;
0 0 0 0 0 0 0 0 0 0 0;
-0.0035 -0.0035 -0.0035 -0.0035 -0.0035 -0.0035 -0.0035 -0.0035 -0.033 -0.045 -0.057;
-0.013 -0.013 -0.013 -0.013 -0.013 -0.013 -0.013 -0.013 -0.053 -0.07 -0.087;
0.0025 0.0025 0.0025 0.0025 0.0025 0.0025 0.0025 -0.026 -0.0665 -0.087 -0.1075;
-0.005 -0.005 -0.005 -0.005 -0.005 -0.005 -0.005 -0.04 -0.076 -0.102 -0.128;
0.003 0.003 0.003 0.003 0.003 0.003 0.003 -0.016 -0.0625 -0.1 -0.125 -0.15;
0.004 0.004 0.004 0.004 0.004 0.004 -0.0275 -0.072 -0.1125 -0.136 -0.1595;
0.004 0.004 0.004 0.004 0.004 -0.005 -0.041 -0.082 -0.123 -0.145 -0.167;
0.003 0.003 0.003 0.003 0.003 -0.016 -0.054 -0.089 -0.132 -0.154 -0.176;

```

```

0.0015 0.0015 0.0015 0.0015 -0.002 -0.032 -0.065 -0.1 -0.142 -0.163 -0.184;
0.003 0.003 0.003 0.003 -0.014 -0.046 -0.074 -0.108 -0.149 -0.17 -0.191;
-0.002 -0.002 -0.002 -0.002 -0.03 -0.06 -0.083 -0.116 -0.157 -0.176 -0.195;
0.0015 0.0015 0.0015 -0.025 -0.05 -0.074 -0.093 -0.122 -0.163 -0.184 -0.205;
-0.027 -0.027 -0.027 -0.054 -0.068 -0.086 -0.103 -0.127 -0.167 -0.189 -0.211;
-0.054 -0.054 -0.065 -0.073 -0.084 -0.097 -0.111 -0.133 -0.173 -0.195 -0.217;
-0.073 -0.073 -0.078 -0.086 -0.097 -0.108 -0.117 -0.137 -0.176 -0.2 -0.224;
-0.112 -0.112 -0.118 -0.128 -0.144 -0.157 -0.171 -0.183 -0.206 -0.232 -0.258;
-0.174 -0.174 -0.184 -0.196 -0.214 -0.235 -0.25 -0.264 -0.277 -0.298 -0.319;
-0.5 -0.5 -0.5 -0.5 -0.5 -0.5 -0.5 -0.5 -0.5 -0.5 -0.5;
-0.5 -0.5 -0.5 -0.5 -0.5 -0.5 -0.5 -0.5 -0.5 -0.5 -0.5;
-0.3 -0.3 -0.3 -0.3 -0.3 -0.3 -0.3 -0.3 -0.3 -0.3 -0.3;
-0.3 -0.3 -0.3 -0.3 -0.3 -0.3 -0.3 -0.3 -0.3 -0.3 -0.3;
-0.4 -0.4 -0.4 -0.4 -0.4 -0.4 -0.4 -0.4 -0.4 -0.4 -0.4;
0 0 0 0 0 0 0 0 0 0 0];

```

```

cl=interp2(mach_ref,alpha_cl_ref,cl_0012,mach,aoa);
cd=interp2(mach_ref,alpha_cd_ref,cd_0012,mach,aoa);
cm=interp2(mach_ref,alpha_cm_ref,cm_0012,mach,aoa);

```

## 2DPIM

```

function [rad_int]=radtrap2D_int(array,dr,dpsi,root_cutout,tiploss)

for j=1:360/dpsi
    for i=(1+round(root_cutout/dr)):1/dr+1

        blade(i-round(root_cutout/dr),j)=array(i,j);
    end
    bld_int(j)=(2*sum(blade(:,j))-blade(1,j)-(1+tiploss/dr)*blade(1/dr+1-
round(root_cutout/dr),j))*dr/2;
end
    rad_int=(2*sum(bld_int(:))-bld_int(1)-bld_int(360/dpsi))*dpsi*pi/180/2/(2*pi);
end

```

## REFERENCES

1. Abbott, Ira H. and Albert E. Von Doenhoff. Theory of Wing Sections. Mineola: Dover Publications, 1959.
2. Gessow, Alfred and Garry C. Myers. Aerodynamics of the Helicopter. New York: Frederick Ungar Publishing Co., 1967.
3. Lynn, Robert R. and M. Jan Drees. Promise of Compounding. Fort Worth: Bell Helicopter Company, 1966.
4. McCloud III, John L., James C. Biggers and Robert H. Stroub. An Investigation of Full-Scale Helicopter Rotors at High Advance Ratios and Advancing Tip Mach Numbers. Washington D.C.: NASA, 1968.
5. Palm III, William J. Introduction to MATLAB 7 for Engineers. New York: McGraw Hill, 2004.
6. Prouty, Raymond W. Helicopter Performance, Stability, and Control. Malabar: Robert E. Krieger Publishing Company, 1990.
7. Stepniewski, W. Z. and C. N. Keys. Rotary-Wing Aerodynamics. New York: Dover Publications, 1984.

## BIOGRAPHICAL INFORMATION

Cory Hitte was born in Dayton, Ohio on April 18, 1986. Cory spent his youth living on multiple USAF bases where his father was a B-1 bomber Captain and T-38 Instructor. After finishing high school, Cory attended Texas A&M University where he received a B.S. in Aerospace Engineering. Cory was hired by Bell Helicopter (Textron) in 2009 as a member of the Conceptual Design group tasked with future product development and competitor analysis. During his time at Bell, Cory pursued a M.S. in Aerospace Engineering from the University of Texas at Arlington. In his free time, Cory enjoys basketball, running, and spending time with his wife, Lauren, and their dogs.